The Canadian Journal of Chemical Engineering

formerly

CANADIAN JOURNAL OF TECHNOLOGY

CONTENTS

Photograph taken at C-I-L Central Research Laboratory, McMasterville, Que.

POLYMERIC PRECISION

This is an ebulliometer—being assembled by the master glass-blower on his own lathe at our Central Research Laboratory.

The ebulliometer uses two vapor lift pumps such as those found in electric coffee percolators. One circulates a polymer solution while the other circulates boiling solvent—each liquid stream is directed over a temperature detector so sensitive that a difference of one-millionth of 1°C. may be sensed. This device allows the measurement of high molecular weights related to the physical properties of polymers.

Such C-I-L research contributes to higher standards of performance in the plastics industry . . . to new and better plastic products . . . and—through better technical service—to greater success in the application of these new materials to modern living.

C-I-L

CANADIAN INDUSTRIES LIMITED

Serving Canadians Through Chemistry

Agricultural Chemicals • Ammunition • Coated Fabrics • Industrial Chemicals • Commercial Explosives • Paints • Plastics • Textile Fibres

The Canadian Journal of Chemical Engineering

formerly

Canadian Journal of Technology

Published by The Chemical Institute of Canada

VOLUME 39 APRIL, 1961 NUMBER 2

Authorized as second class mail, Post Office Department, Ottawa. Printed in Canada

Manuscripts for publication should be submitted to the Editor: Dr. A. Cholette, Faculty of Science, Laval University, Boulevard de l'Entente, Quebec, Que. (Instructions to authors are on the next page).

Editorial, Production and Circulation Offices: 48 Rideau Street, Ottawa 2, Ont.

Advertising Office: C. N. McCuaig, manager of advertising sales, *The Canadian Journal of Chemical Engineering*, Room 601, 217 Bay Street, Toronto, Ont. Telephone—EMpire 3-3871.

Plates and Advertising Copy: Send to *The Canadian Journal of Chemical Engineering*, 48 Rideau Street, Ottawa 2, Ont.

Subscription Rates: In Canada—$6.00 per year and $1.25 per single copy; U.S. and U.K.—$7.00, Foreign—$7.50.

Change of Address: Advise Circulation Department in advance of change of address, providing old as well as new address. Enclose address label if possible.

The Canadian Journal of Chemical Engineering is published by The Chemical Institute of Canada every two months.

The Canadian Journal of Chemical Engineering

INSTRUCTIONS TO AUTHORS

Manuscript Requirements for Articles

1. The manuscript should be in English or French.
2. The original and two copies of the manuscript should be supplied. These are to be on 8½ x 11 inch sheets, typewritten, and double spaced. Each page should be numbered.
3. Symbols should conform to American Standards Association. An abridged set of acceptable symbols is found in the third edition of Perry's Chemical Engineers' Handbook. Greek letters and subscripts and superscripts should be carefully made.
4. Abstracts of not more than 200 words in English indicating the scope of the work and the principal findings should accompany all technical papers.
5. References should be listed in the order in which they occur in the paper, after the text, using the form shown here: "Othmer, D. F., Jacobs, Jr., J. J., and Levy, J. F., Ind. Eng. Chem. **34**, 286 (1942). Abbreviations of journal names should conform to the "List of Periodicals Abstracted by Chemical Abstracts". Abbreviations of the common journals are to be found in Perry's Handbook also. All references should be carefully checked with the original article.
6. Tables should be numbered in Arabic numerals. They should have brief descriptive titles and should be appended to the paper. Column headings should be brief. Tables should contain a minimum of descriptive material.
7. All figures should be numbered from 1 up, in Arabic numerals. Drawings should be carefully made with India ink on white drawing paper or tracing linen. All lines should be of sufficient thickness to reproduce well, especially if the figure is to be reduced. Letters and numerals should be carefully and neatly made, with a stencil. Generally speaking, originals should not be more than twice the size of the desired reproduction; final engravings being 3¼ in. or 7 in. wide depending on whether one column or two is used. For further details ask the Editor for the Guide for Drawings.
8. Photographs should be made on glossy paper with strong contrasts. Photographs or groups of photographs should not be larger than three times the size of the desired reproduction.
9. All tables and figures should be referred to in the text.

Submission of Manuscripts

1. The three copies of the manuscript, including figures and tables, should be sent directly to:
   DR. A. CHOLETTE, editor,
   The Canadian Journal of Chemical Engineering,
   Faculty of Science, Laval University,
   Boulevard de l'Entente,
   Quebec, Que.
2. The authors addresses and titles should be submitted with the manuscript.
3. The author may suggest names of reviewers for his article, but the selection of the reviewers will be the responsibility of the editor. Each paper or article is to be reviewed by two chemical engineers familiar with the topic. Reviewers will remain anonymous.
4. All correspondence regarding reviews should be directed to the editor.

Reprints

1. At least 50 free "tear sheets" of each paper will be supplied.
2. Additional reprints may be purchased at cost. An estimated cost of reprints, with an attached order form, will be sent to the author with the galley proofs.
3. Orders for reprints must be made before the paper has appeared in the Journal.

Communications, Letters and Notes to the Editor

Short papers, as described below, will be considered for publication in this Journal. Their total length should be such that they will not occupy more than one page of the Journal.

Communications

A communication is a prompt preliminary report of observations made which are judged to be sufficiently important to warrant expedited publication. It usually calls for a more expanded paper in which the original matter is republished with more details.

Letters

A letter consists of comments or remarks submitted by readers or authors in connection with previously published material. It may deal with various forms of discussion arising out of a publication or it may simply report and correct inadvertent errors.

Notes

A note is a short paper which describes a piece of work not sufficiently important or complete to make it worth a full article. It may refer to a study or piece of research which, while it is not finished and may not be finished, offers interesting aspects or facts. As in the case of an article a note is a final publication.

* * *

Solid-Liquid Equilibria in Wax Crystallization[1]

R. M. BUTLER[2] and D. M. MacLEOD[2]

The equilibria obtained during the crystallization of waxes has been studied theoretically and it has been found that the degree of separation between normal paraffins may be predicted, if it is assumed that the solid is an ideal solution. Results predicted from the theoretical equations have been compared with mass spectrometer analyses of recrystallized waxes and surprisingly close agreement has been found.

It has also been shown that ketone solvents have essentially the same selectivity for recrystallizing waxes as n-hexane. The reason for this is that the activity coefficients for various n-paraffins in a ketone solution are nearly identical even though they are all much higher than in the hydrocarbon solution.

The separation between normal paraffins in conventional single stage wax recrystallization is not very sharp. This may be improved by the use of a number of stages in a countercurrent cascade. Experimental results with such a cascade are in agreement with the theoretical predictions.

The presence of non n-paraffinic components in some waxes can cause the formation of eutectic mixtures. This affects the separation in a manner analogous to that of hetero-azeotropes in some distillation processes.

The crystallization of waxes from their melts has also been studied both theoretically and experimentally. When mixtures of similar molecular weight n-paraffins, such as n-$C_{21}H_{44}$ and n-$C_{23}H_{48}$ are cooled, a solid solution is formed. This is also found with mixtures of similar recrystallized waxes. On the other hand, mixtures of n-paraffins of widely different molecular weight, such as n-$C_{20}H_{42}$ and n-$C_{32}H_{66}$, or hydrocarbons of different structure, such as n-paraffins and iso-paraffins, form separate crystals and a eutectic. Similar results are found with mixtures of commercial waxes of widely different melting point and type.

This paper is concerned with a study of the equilibrium between hydrocarbon waxes and their solutions or melts. The results may be applied in the field of wax separation and also of wax quality.

In the field of wax quality, the findings which are to be described are concerned with the solidification of waxes and wax blends. Since waxes are almost invariably applied in the liquid state and used in the solid state, this transition is of particular interest. It has been shown that, while blends of similar paraffin waxes crystallize in the form of mixed crystals, blends of dissimilar waxes crystallize as mixtures of crystals of different types. It is thought that the special properties of many practical blends may be explained on this basis.

In wax recrystallization, a method has been developed which allows one to calculate the composition of the solid and liquid phases which are in equilibrium. It is thus possible to estimate the "sharpness" of the separation which is obtained in recrystallization plants. An insight is also developed into the role of the solvent in recrystallization and considerable help is obtained in answering such questions as; "How does the sharpness of separation depend on the type and quantity of solvent which is employed?"

In the paper, an attempt has been made to present a parallel discussion of the theory of wax recrystallization, together with the experimental work which has been suggested by that theory. It is inevitable that the complexity of the composition of actual waxes makes any practical theory appear somewhat oversimplified. However, it is believed that the simple mathematical models which are discussed, describe the behaviour of actual waxes and wax blends qualitatively, and in many cases, quantitatively. Thus, for example, solid solutions of waxes are assumed to behave as ideal solid solutions. Although this is probably only rarely, if ever, exactly true, in most cases the similarities to the behavior of actual solid solutions are far more striking than the differences.

Theory

(1) The Equilibrium Between an Ideal Solid Solution and an Ideal Liquid Solution

Consider any component i which is present both in the liquid and solid phase. Since these phases are in equilibrium, it follows that the fugacity of the component will be the same in both.

i.e., $$Y_i P_{si} = X_i P_{li} \quad \ldots\ldots\ldots\ldots\ldots\ldots (1)$$

where Y_i is the mole fraction of i in the solid.
X_i is the mole fraction of i in the liquid.
P_{si} is the vapor pressure of pure solid i at the temperature of the system.
P_{li} is the vapor pressure of pure liquid i at the temperature of the system.

Equation (1) will be satisfied for each component of the system and will be true in the case where the liquid is a melt and also when a solvent is present.

The variation of the vapor pressures of pure solid and liquid i with temperature may be expressed by means of the Clausius—Clapeyron equation.

$$\frac{d \log_e P_{si}}{dT} = \frac{L_{si}}{RT^2} \quad \ldots\ldots\ldots\ldots\ldots\ldots (2)$$

[1]*Manuscript received June 14; accepted November 19, 1960.*
[2]*Research Department, Imperial Oil Limited, Sarnia, Ont.*
Contribution from the Research Department, Imperial Oil Limited, Sarnia, Ont.
Based on a paper presented to the C.I.C. 43rd Annual Conference, Ottawa, Ont., June 13-15, 1960.

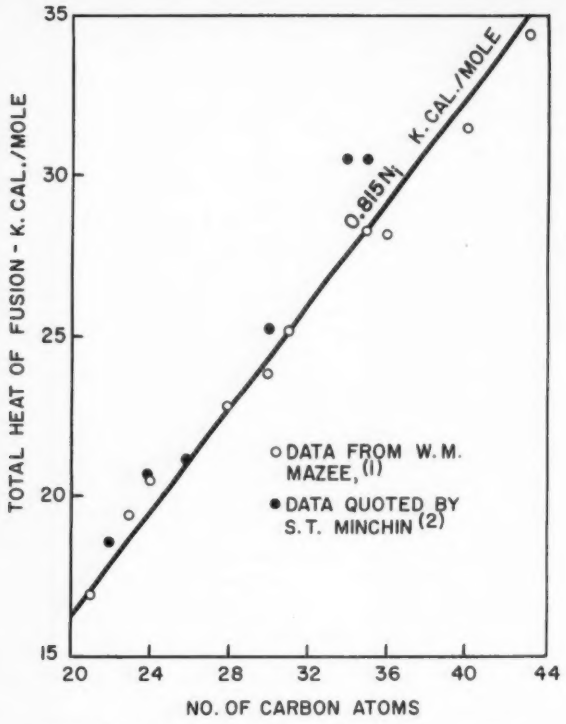

Figure 1—Total latent heat of fusion of n-paraffins.

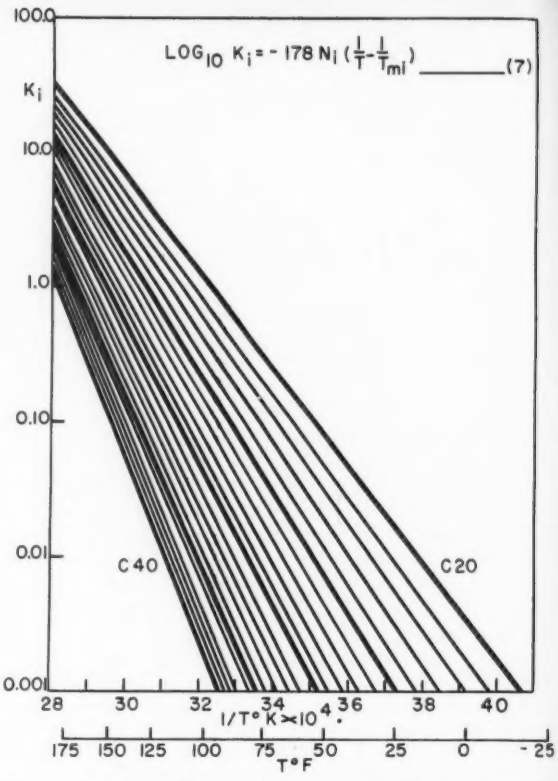

Figure 2—Equilibrium ratios for n-paraffin having from 20 to 40 carbon atoms.

and $$\frac{d \log_e P_{li}}{dT} = \frac{L_{li}}{RT^2}$$

where T is the absolute temperature.
R is the gas constant.
L_{si} is the latent heat of sublimation of i.
L_{li} is the latent heat of evaporation of liquid i.

and

Equations (1) and (2) may be combined to give:

$$\frac{d \log_e Ki}{dT} = \frac{d \log_e Xi/Yi}{dT} = \frac{d \log_e P_{si}/P_{li}}{dT} = \frac{L_{si} - L_{li}}{RT^2} = \frac{L_{Fi}}{RT^2}$$

or $$\frac{d \log_e Ki}{dT} = \frac{L_{Fi}}{RT^2} \quad \ldots\ldots(3)$$

where $K_i = X_i/Y_i$ the equilibrium ratio for component i.

and L_{Fi} is the latent heat of fusion of component i.

It should be noted that at the melting point of component i, T_{mi}, Equation (1) shows that,

$$X_i = Y_i \text{ or } K_i = 1 \text{ at } T_{mi} \quad \ldots\ldots(4)$$

since $P_{si} = P_{li}$

Equation (3) may be integrated if L_{Fi} is assumed constant and the integration constant may be obtained from (4) with the result,

$$\log_e K_i = \frac{-L_{Fi}}{R}\left(\frac{1}{T} - \frac{1}{T_{mi}}\right) \quad \ldots\ldots(5)$$

Equation (5) allows the equilibrium ratio for any temperature to be calculated from a knowledge of the melting point and latent heat of fusion of the component.

Measurements of the latent heats of fusion of n-paraffins are relatively few. The most complete set of measurements appear to be those of W. M. Mazee[1], together with those quoted by S. T. Minchin[2]. In Figure 1, the total latent heat of fusion (including the heat of transition which occurs just below the melting point) has been plotted against the number of carbon atoms for normal paraffins. Over the range of most interest (20 to 35 carbon atoms), the latent heat of fusion may be represented by the equation,

$$L_{Fi} = 0.815\, N_i \quad \ldots\ldots(6)$$

where L_{Fi} is in K cal. per g. mole.

and N_i is the number of carbon atoms per molecule.

Substituting Equation (6) into Equation (5) leads to the result:

$$\log_{10} K_i = -178\, N_i \left(\frac{1}{T} - \frac{1}{T_{mi}}\right) \quad \ldots\ldots(7)$$

where T and T_{mi} are both to be expressed in °K.

Values of K_i for each component may be calculated from Equation (7) or read from Figure 2; these values may be used in calculations analogous to those used for hydrocarbon vapor liquid equilibria. Reference will be made to Equation (7) further on in this paper.

(2) Equilibrium Between an Ideal Liquid Solution and Crystalline Phases When No Mixed Crystals are Formed

In the previous section the solid liquid equilibrium of a number of components which formed both ideal solid and liquid solutions was described. The presence of a solvent in the liquid made no difference to the theory. In this section, the other idealized case will be considered in which, although the liquid solution is ideal, there is no miscibility in the solid phase. Each component forms separate crystals.

In this case, the fugacity of each component in the equilibrium mixture is equal to the vapor pressure of the pure solid (provided

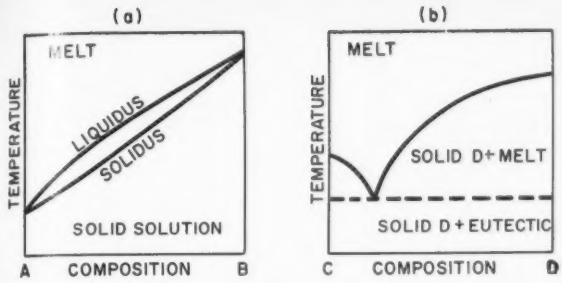

Figure 3—Types of solid-liquid equilibria in binary systems.

that enough of the component is present for a solid phase to form).

Equation (1) becomes,

$$P_{si} = X_i P_{li} \quad \ldots\ldots\ldots\ldots\ldots\ldots\ldots\ldots\ldots\ldots (8)$$

where i now refers to any component which is present in sufficient quantity to form a solid phase.

A similar argument to the previous one results in the following equation,

$$\log_{10} X_i = -178\, N_i \left(\frac{1}{T} - \frac{1}{T_{mi}}\right) \quad \ldots\ldots\ldots\ldots\ldots\ldots\ldots\ldots (9)$$

for all components which will be present as a solid. If an insufficient quantity of one component is present, then, of course, the mole fraction of that component in the solution will be less than that given by Equation (9) and none of the material will be present in the solid.

The Crystallization of Wax Hydrocarbons from the Melt

On crystallization, mixtures of compounds may form either mixed crystals (solid solutions) or separate crystals. The temperature composition diagram shown in Figure 3(a) is typical of that found with solid solutions. The upper "liquidus" curve gives the initial temperature of solidification, and the lower "solidus" curve the final temperature of solidification. The simplest type of diagram for the formation of separate crystals of the pure components is shown in Figure 3(b). The melting point of each pure component is depressed by the addition of the other, and the melting point curves meet at a eutectic point. Any mixture of the two components, other than one of eutectic composition, exhibits an initial freezing point at which one pure component begins to crystallize, and a final solidification point which is the eutectic temperature. Another type, in which the solid components are soluble in each other to a limited degree, is also found. However, the present work has been confined to a consideration of the two cases mentioned.

(1) Solid Solutions

It has been shown by W. M. Mazee[1] that n-paraffins which have nearly the same molecular weights (n-$C_{21}H_{44}$ and n-$C_{23}H_{48}$) will form a solid solution on crystallization. The melting point data for mixtures are shown in Figure 4. Figure 5 shows the cooling curve obtained by Mazee for a mixture of 50 mol.% n-$C_{21}H_{44}$ and 50 ml.% n-$C_{23}H_{48}$, from which the initial and final temperatures of solidification can be obtained.

If the solid wax is considered as an ideal solid solution of n-paraffins, and the melt as an ideal liquid solution, then Equation (7) may be applied for each component and the theoretical initial and final melting points can be calculated. K_i, the ratio of mol fractions of liquid and solid phases, can be obtained for each component at a given temperature. At the temperature at which liquid first appears in the solid wax, the sum of the mol fractions of the components present in the liquid state will be equal to unity. This temperature is found by calculating the sum of the mol fractions in the liquid state at several temperatures, and interpolating to obtain the temperature at which the sum is equal to unity.*

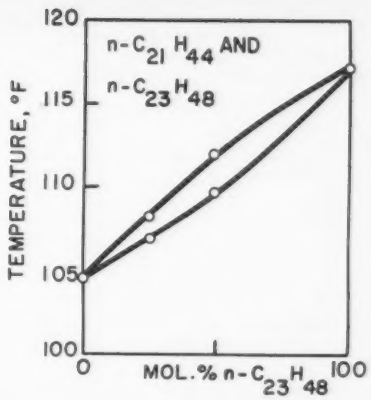

Figure 4—Temperature-composition diagram for mixtures of $nC_{21}H_{44}$ and $nC_{23}H_{48}$.

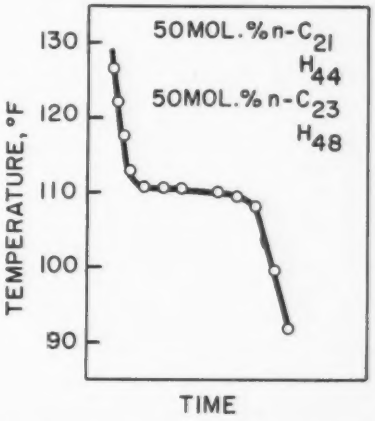

Figure 5—Cooling curve for a mixture of $C_{21}H_{44}$ and $nC_{23}H_{48}$.

Similarly, the point at which solidification begins may be found by employing $1/K_i$, the ratio of mol fractions of a component in the solid and liquid phases, to obtain the sum of the mol fractions of the components in the solid phase. The required temperature is that at which this sum is equal to unity.

The initial solidification point is the temperature at which solid first appears on cooling, and the initial melting point is that at which liquid is first formed on heating. These points are frequently referred to as initial and final melting points. Calculated results are compared with Mazee's experimental melting points in Table 1.

TABLE 1

COMPARISON OF CALCULATED AND EXPERIMENTAL MELTING POINTS

Mixture	Calculated Melting Point		Experimental Melting Point	
	Initial	Final	Initial	Final
50:50 $C_{21}H_{44}$:$C_{23}H_{48}$	111.5 °F.	110.5 °F.	111.9 °F.	109.6 °F.
80:20 $C_{21}H_{44}$:$C_{23}H_{48}$	107.5 °F.	106.0 °F.	108.0 °F.	106.9 °F.

These results show a good check between theoretical and experimental values.

*This method is similar to the normal procedure for the calculation of bubble points and dew points of hydrocarbon mixtures.

TABLE 2

COMPARISON OF CALCULATED AND EXPERIMENTAL MELTING POINTS FOR WAX C.C.9.

Wax	Calculated Melting Point		Experimental Melting Point		Mole Avge. M.P.
	Initial	Final	Initial	Final	
C.C.9	146.3 °F.	140.5 °F.	143.5 °F.	139.5 °F.	143.4

An experimental recrystallized wax designated, for laboratory purposes, as C.C.9, was subjected to mass spectrometer analysis, and found to consist of 99% normal paraffins, ranging from $C_{20}H_{42}$ to $C_{34}H_{70}$. The initial and final melting points of this complex mixture have been calculated by the above method, assuming that the components form a solid solution. A cooling curve was also obtained for wax C.C.9, as shown in Figure 6, and the experimental initial and final melting points were noted. The results are shown in Table 2.

It is difficult to read the initial and final melting points from Figure 6 accurately. The theoretical predictions, however, appear to be quite reasonable, both in actual temperatures and in the difference between initial and final melting points. Limitations of the theoretical method are mainly the lack of exact data for heats of fusions, and the possibility that the compounds do not form a continuous solid solution.

In general, n-paraffins which form solid solutions follow the Rule of Küster[3], which states that the solidifying point of an isomorphous mixture lies on a straight line joining the melting points of the components, when the melting point is plotted against mol.% composition. In Table 2, the mole average melting point may be seen to agree fairly closely with the experimental initial melting point. This is, of course, essentially the same as the "ASTM Melting Point (D87-57)".

It is concluded that the n-paraffins in some recrystallized waxes and mixtures of waxes may be considered as forming

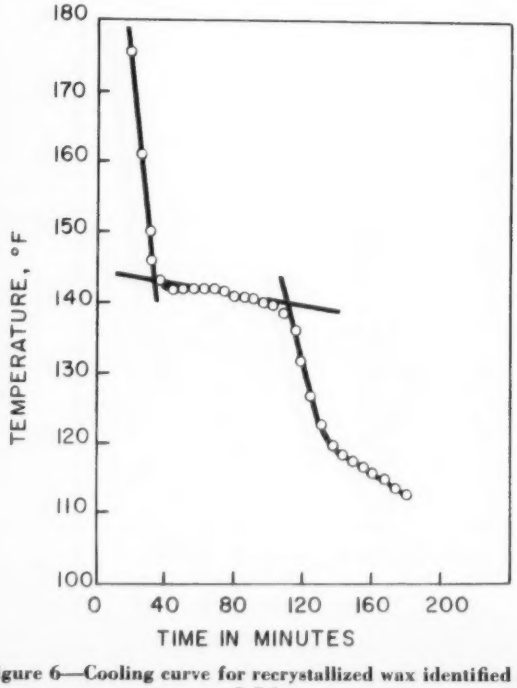

Figure 6—Cooling curve for recrystallized wax identified as C.C.9.

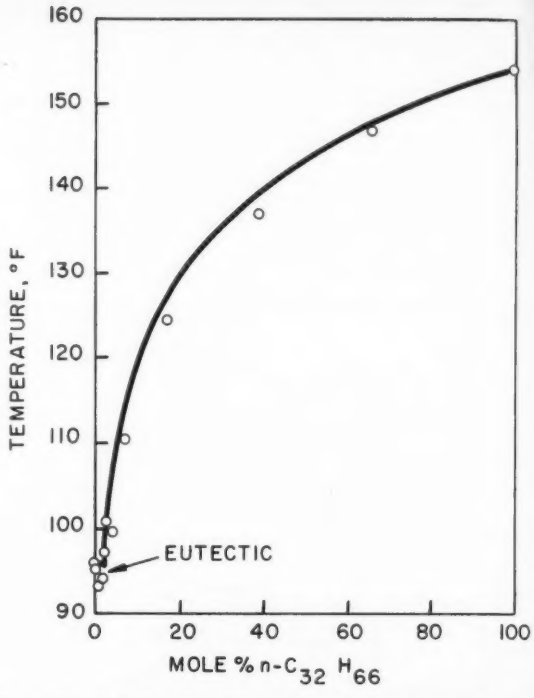

Figure 7—Calculated melting point lines and experimental points for mixtures of n-$C_{20}H_{42}$ and n-$C_{32}H_{66}$.

solid solutions. This is shown by comparison with mixtures of pure n-paraffins of similar molecular weight, and by the closeness of experimental melting point data to figures calculated from the assumption that the mixtures form solid solutions.

(2) **Separate Crystals**

It is known that some n-paraffins of widely different molecular weights will crystallize from a mixture to form separate crystals. (Mazee, loc. cit.). This type of behavior has now been found with mixtures of n-$C_{20}H_{42}$ and n-$C_{32}H_{66}$. The melting point — composition diagram for these compounds, given in Figure 7, shows that the melting points of the mixtures do not lie near the straight line joining those of the components. A eutectic is formed containing a very low percentage of the high molecular weight component.

The cooling curves of these mixtures confirm that separate crystals are formed. This is shown in Figure 8 for the n-paraffin

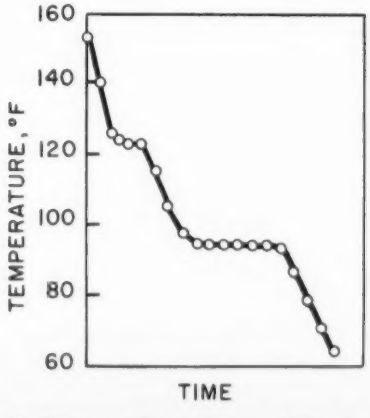

Figure 8—Cooling curve for a mixture of 35 mole % n-$C_{32}H_{66}$ and 65 mole% n-$C_{20}H_{42}$.

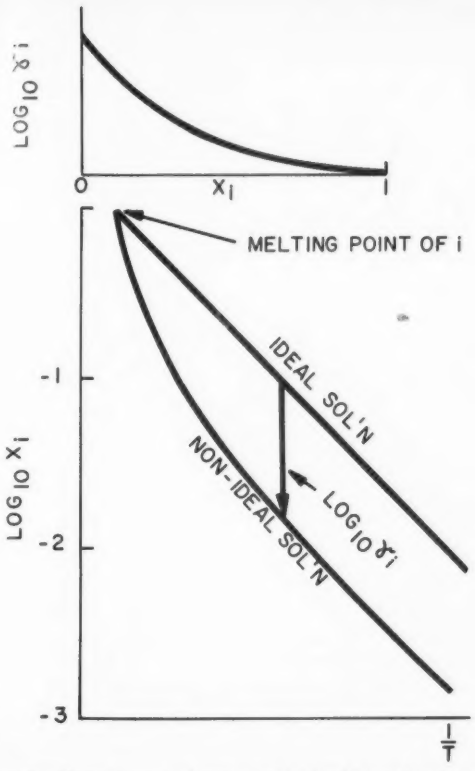

Figure 9—Upper curve shows a typical relationship between activity coefficient and concentration for a constant temperature. The lower part of the figure shows the type of curve to be expected for the solubility of a solid if the activity coefficients are approximately independent of temperature.

mixture. When the mixtures are cooled, high melting material crystallizes first, followed by complete crystallization at the eutectic temperature. A cooling curve showing the low molecular weight component crystallizing first has not been given because the eutectic composition is so close to that of the pure low melting component. However, it can be seen that the eutectic temperature is lower than the melting point of either component, confirming that the phase diagram is of type (b) in Figure 3.

In mixtures of this type, the melting point of one component is lowered by the addition of the other. If pure material crystallizes out, then the melting point lines can be calculated by considering the mixture as one solid component being dissolved in the other component which is liquid. Each component is, in turn, considered to be the solid. The temperature required to completely dissolve that mol fraction of solid which is present is then determined. This is done using Equation (9). Two solubility (or melting point) curves are obtained and are drawn to intersect. Lines calculated in this manner are compared with the data for n-$C_{20}H_{42}$/n-$C_{32}H_{66}$ mixtures in Figure 7. Good agreement was found over the whole range of composition, although the calculated eutectic temperature was slightly higher than that found experimentally.

The agreement between experimental and theoretical data shows that separate crystals and a eutectic are being formed. However, it is not possible to calculate the melting points of mixtures of recrystallized waxes in this way because of their complex nature.

Further data, published by Mazee, have shown that isoparaffins and n-paraffins of the same melting point form separate crystals and eutectic. The hydrocarbons used were 13-methyl pentacosane ($C_{26}H_{54}$) and n-$C_{24}H_{50}$. From this, it may be deduced that n-paraffin waxes form separate crystals when mixed

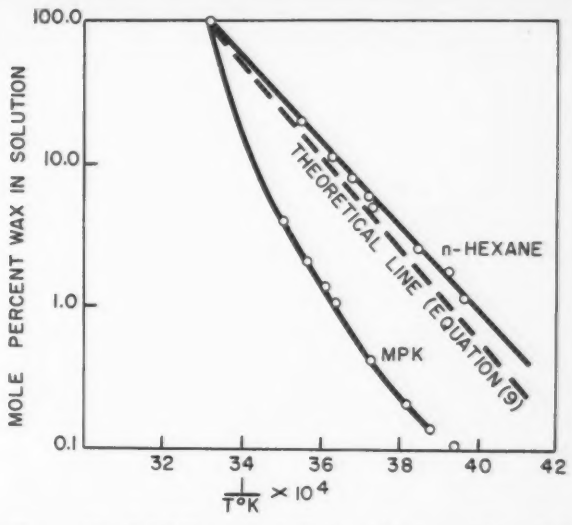

Figure 10—Solubility of n-$C_{18}H_{38}$ in n-hexane and methyl n-propyl ketone.

with microcrystalline wax. This is difficult to determine because microcrystalline waxes are themselves complex mixtures and show cooling curves which are difficult to interpret.

The Crystallization of Wax Hydrocarbons from Solvents

(1) The Solubility of *n*-Paraffins in Methyl *n*-Propyl Ketone and in *n*-Hexane

In the previous section, it was shown that the solubility of a pure n-paraffin, *i*, could be represented by the equation,

$$\log_{10} X_i = -178\, N_i \left(\frac{1}{T} - \frac{1}{T_{mi}}\right) \quad \ldots\ldots\ldots\ldots\ldots\ldots (9)$$

provided that the solution was ideal.

If the solvent is such that there are positive deviations from Raoult's law, the solubility will be less. Thus, if the fugacity of *i* in solution is taken as $\gamma i X_i P_i$, the following equation may be derived:

$$\log_{10} X_i = -178\, N_i \left(\frac{1}{T} - \frac{1}{T_{mi}}\right) - \log_{10} \gamma i \ldots\ldots (10)$$

where γi is the activity coefficient of *i* in solution.

There is a considerable quantity of published work on the subject of non-ideality of solutions from the point of view of vapor liquid equilibrium[4]. It is found that activity coefficients vary greatly with concentration and to a much smaller extent with temperature. In the majority of cases, it is found that activity coefficients vary with concentration in the manner shown in Figure 9. Assuming this to be the case, then one would expect the solubility of a pure n-paraffin in a non-ideal solvent to vary with temperature in the manner shown in the lower part of Figure 9. In this diagram, the logarithm of the solubility of the hydrocarbon has been plotted against the reciprocal absolute temperature for both an ideal solution and for a solution in which the degree of non-ideality (activity coefficient) varies in the manner shown in the upper part of Figure 9.

The following points should be noted:

1. The solubility curves both start at the melting point and the solubility decreases with temperature.
2. On the scales used, the ideal solution gives a straight line, whereas the non-ideal solution gives a curved one.
3. At low solubilities the non-ideal solution line becomes parallel to the ideal solution line. The physical reason for this is that in these very dilute solutions each wax molecule is surrounded by solvent molecules. Slight

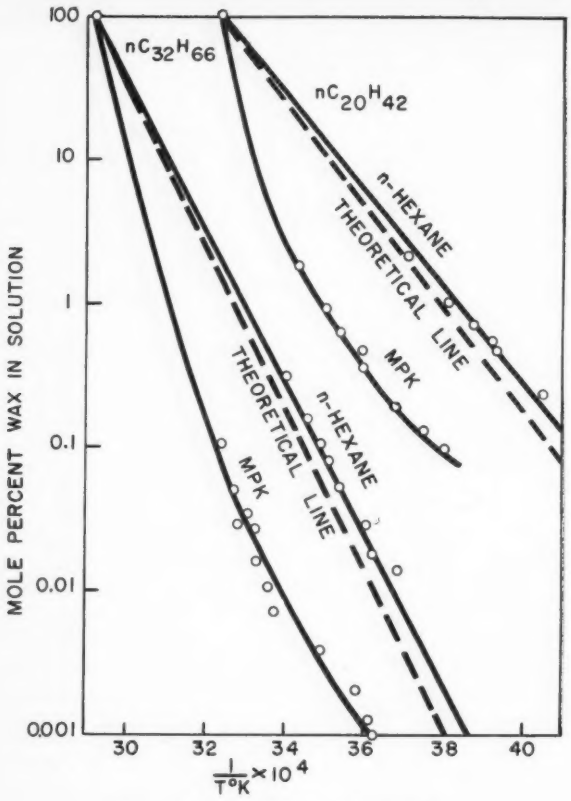

Figure 11—Solubility of n-paraffins.

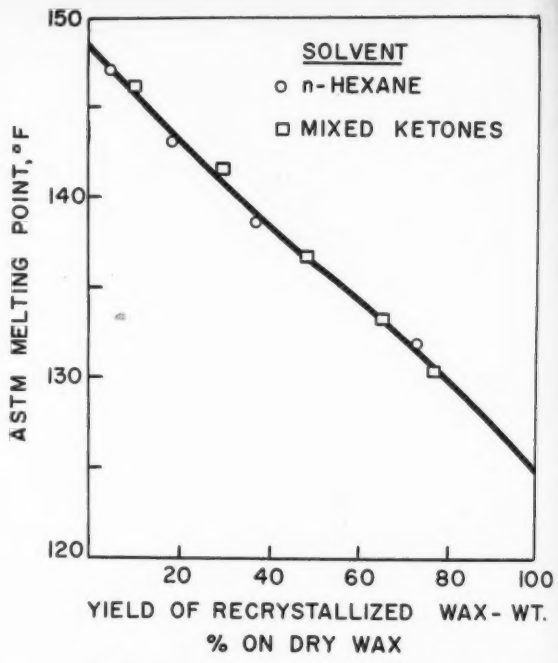

Figure 12—The single stage recrystallization of light slack wax using n-hexane and mixed ketones as solvents. The dilution ratio was 6 volumes of solvent to 1 of feed. Solvent wash to feed ratio was also 6. Filtration temperature was varied from 0°F. to 54°F. for n-hexane experiments and from 40°F. to 90°F. for the ketone solvents.

changes in the concentration of the solution have practically no effect on the environment of the wax molecules and the deviation from ideality remains constant.

Experimental curves for the solubility of pure n-$C_{18}H_{38}$, n-$C_{20}H_{42}$ and n-$C_{32}H_{66}$ in methyl n-propyl ketone and in n-hexane are shown in Figures 10 and 11.

In addition lines have been drawn for the solubility of the waxes in an ideal solution. These lines fall very close to the lines for n-hexane indicating that these solutions are almost ideal. The small differences between the pairs of lines are probably the result of a combination of small deviations from ideality, together with errors in the latent heat correlation used in deriving Equation (9).

This is significant since it shows that the solvent is no more selective for separating the two components than if it formed ideal solutions. Thus, for example, at 40°F. the solubilities of the waxes in MPK are lower than the ideal solubilities by a factor of 13. The ratio of the solubilities has not changed. The solvent does not possess any abnormal solvency for the low melting point material compared to its solvency for the high melting material. From the point of view of equilibrium, the main difference between using ketones, such as MPK and n-hexane for the separation of waxes by recrystallization is that higher temperatures must be used with MPK. There is, of course, a practical advantage in using ketones in that the slurries are more easily filtered.

TABLE 3

ACTIVITY COEFFICIENTS OF N-PARAFFINS IN VERY DILUTE SOLUTIONS IN MPK

Temperature		n-$C_{18}H_{38}$	n-$C_{20}H_{42}$	n-$C_{32}H_{66}$
°K.	°F.			
278	40	—	13	13
270	26	10	13	10

(2) Degree of Separation Obtained by Recrystallization

In commercial wax recrystallization plants, such as the one in Sarnia, wax is fractionated by dissolving it in a solvent, chilling the mixture until part of the wax separates, filtering the resultant slurry and washing the filter cake[5]. It is of interest to be able to predict the degree of separation between wax hydrocarbons which is obtained in such operations. In this section it will be shown how this degree of separation may be predicted if the assumption is made that the solid is an ideal solution. Although it has already been shown that mixtures of widely different n-paraffins, such as n-$C_{20}H_{42}$ and n-$C_{32}H_{66}$ do not form solid solutions, it seems likely that when a whole range of adjacent n-paraffins are present, they do form solid solutions. This view has also been expressed by W. M. Mazee[6]. It will also be shown that a theory based on this assumption predicts results which are fairly close to those found in practice.

The following theory may also be applied when the solvent does not form ideal solutions with the hydrocarbons (i.e., with such solvents as ketones). In order to do this, it is necessary to make the assumption that in any particular solution the activity coefficients for all the n-paraffins have the same value. This assumption has been proposed in the literature for members of homologous series which are present in a non-ideal solution[7] and has been used in correlations of vapor liquid equilibrium data for extractive distillation of hydrocarbon mixtures[8]. The data presented in the previous section on the solubility of pure n-paraffins in MPK is direct evidence in favor of this assumption since it was shown that the activity coefficients for two different pure hydrocarbons in very dilute solutions were practically the

same at a given temperature. More evidence in favor of this assumption is given in Figure 12, where the melting point of recrystallized wax has been plotted against the dry wax yield for a typical light slack wax recrystallized from n-hexane and from a mixed ketone solvent. It may be seen that the points for the two solvents fall very close to the same smooth curve (all points lie within 0.5°F. of the curve). The fact that essentially the same melting point is obtained for the same yield indicates that the selectivity of the two solvents for the separation of waxes is nearly the same. This indicates that in any particular solution the activity coefficients of all the wax components are approximately equal.

Although the equilibrium constants in a system in which the liquid solution is non-ideal will be less than those given by Equation (5), the ratio between the values for any two particular components will be the same as for the case of an ideal solution. The reason for this is that the effect of the two activity coefficient terms cancel if the values are the same. The ratio of two equilibrium constants is termed a separation factor and is analogous to the term relative volatility which is used in distillation technology. These may be obtained by calculating values of K from Equation 7 (or alternatively read from Figure 2), and dividing each by the value obtained for the reference component. As will be seen, it is most convenient to employ the component which is equally divided in quantity between the solid and the liquid as the reference component.

For example, consider a separation in which the mole fractions of the various components in the liquid are represented by X_1, X_2.....etc. and the corresponding mole fractions in the solid are Y_1, Y_2, etc. Let the suffix R refer to the reference component. Then the separation factor for component i with respect to component R is given by,

$$\beta_{iR} = \frac{K_i}{K_R} = \frac{X_i}{Y_i}\frac{Y_R}{X_R} \quad \ldots\ldots\ldots\ldots\ldots\ldots (11)$$

Suppose D is the total number of moles in the liquid and S is the total number of moles in the solid. Then the number of moles of i and R in the liquid are given by,

$$D_i = DX_i \text{ and } D_R = DX_R \quad \ldots\ldots\ldots\ldots\ldots\ldots (12)$$

Similarly $S_i = SY_i$ and $S_R = SY_R$
Hence it follows that

$$\beta_{iR} = \frac{D_i}{S_i}\frac{S_R}{D_R} \quad \ldots\ldots\ldots\ldots\ldots\ldots (13)$$

Now if R has been chosen such that $D_R = S_R$ it follows that,

$$\beta_{iR} = \frac{D_i}{S_i} \quad \ldots\ldots\ldots\ldots\ldots\ldots (14)$$

Now the total quantity of component i in the feed is given by,

$$F_i = S_i + D_i \quad \ldots\ldots\ldots\ldots\ldots\ldots (15)$$

The fraction of the component i which appears in the recrystallized product may be obtained by eliminating D_i from Equation (14) and (15) with the result,

$$\frac{S_i}{F_i} = \frac{1}{1 + \beta_{iR}} \quad \ldots\ldots\ldots\ldots\ldots\ldots (16)$$

Equation (16) may be used to calculate the composition of the recrystallized product. An example of its use is given below.

Numerical Example

A mass spectrometer analysis of a deoiled paraffin wax is given in Table 4. Calculate the composition of the product which should be obtained if this wax is recrystallized at 80°F. and the quantity of solvent is such that half of the n-$C_{29}H_{80}$* which is present in the feed appears in the product.

*Ths value was chosen to make the yield comparable with that for which experimental data were available.

TABLE 4

TYPICAL CALCULATION OF SEPARATION BY RECRYSTALLIZATION

Number of Carbon Atoms in Component	c.c.[3] per 100 c.c. Feed	K_i[1] at 80°F.	β_i[2]	$\frac{1}{1+\beta_i}$	c.c. in[4] Product per 100 c.c. of Feed
20	—	0.436	38.0	.0256	—
21	1.2	0.295	25.6	.0376	.0451
22	2.9	0.192	16.7	.0565	.164
23	5.6	0.130	11.4	.0806	.451
24	8.8	0.0862	7.50	.118	1.04
25	11.9	0.0600	5.21	.161	1.91
26	12.9	0.0392	3.41	.227	2.93
27	13.0	0.0278	2.42	.292	3.80
28	10.5	0.0177	1.54	.394	4.14
29	8.5	0.0115	1.0	.500	4.25
30	5.3	0.00803	0.700	.588	3.12
31	3.4	0.00525	0.456	.687	2.34
32	2.1	0.00363	0.326	.755	1.58
33	0.9	0.00251	0.218	.822	0.74

[1]From Equation (7).
[2]By dividing values of K_i by 0.0115 the value for C_{29}.
[3]From M.S. analysis.
[4]By multiplying figures in column (3) by $1/1+\beta_i$.

Solution

The calculation is carried out in Table 4 and the footnotes describe the various arithmetical operations involved.

A mass spectrometer analysis was obtained of a wax which was recrystalized from this feed at 80°F. using a mixture of 50% methyl ethyl ketone and 50% toluene. The results are compared with the theoretical values in Figures 13 and 14.

In Figure 13, the quantity of each of the n-paraffins per 100 c.c. of feed has been plotted against the number of carbon atoms in the n-paraffin. Curves are shown for both the feed and the recrystallized product. The curve for the feed is simply a plot of the mass spectrometer analysis. The curve for the product is the theoretical curve which has just been calculated. The solid circles are experimental points for the product which were obtained from the mass spectrometer analysis of the product together with yield data. The agreement between theory and experiment is surprisingly good when one considers the approximate nature of the theory together with the difficulties inherent in mass spectrometer analysis of mixtures of this type.

The same data are compared in another type of graph in Figure 14. Here the percentage of each component in the feed which appears in the product has been plotted against the number of carbon atoms. The theoretical curve is compared with the experimental points. Again it may be noted that the agreement is fairly satisfactory although there is some tendency for the separation to be slightly sharper than the theoretical.

(3) Predicted Degree of Separation for Typical Wax Recrystallizations

Figure 15 shows calculated curves for the recrystallization of waxes under typical conditions. They should be useful in obtaining a preliminary estimate of the degree of separation in a proposed operation.

(4) The Sharpness of Separation Between Normal Paraffins in Successive Recrystallized Cuts

Figure 16 shows the results of an experiment in which a light slack wax was first recrystallized from a ketone solvent to give a 28% yield of solid wax. The filtrate from this operation was then cooled further to give a 47% yield of a second cut wax. In each case, the cakes were adequately washed to remove entrained liquid.

The separation between normal paraffins is shown in Figure 16. The points in this Figure were obtained from mass spectro-

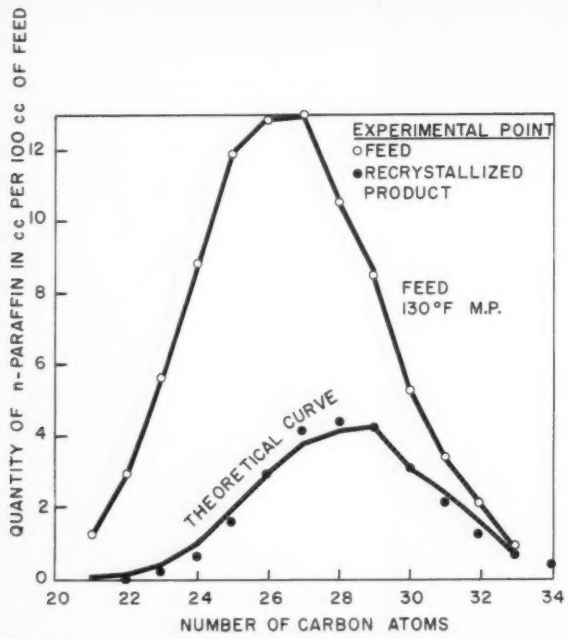

Figure 13—Recrystallization of paraffin wax. Solvent was 50 LV% MEK and 50 LV% toluene. Initial dilution ratio was 6:1 and wash to feed ratio was 2:1.

meter analysis of these waxes, together with yield data. The curves for first and second cut waxes and the residue were calculated from the analysis for the feedstock and Equations (7) and (16). The agreement between the theoretical curves and the experimental points is very satisfactory.

These data show that the separation obtained between successive cuts is not very sharp; there is considerable overlap.

Figure 17 also shows that the separation is not very sharp. In this Figure, the melting point of first cuts has been plotted against the yield. The lower curve is an experimental one; the upper curve is calculated from a mass spectrometer analysis of the feedstock assuming a perfect separation between adjacent normal paraffins. The ASTM melting point for the theoretical separations were taken as being equal to the molar average melting points. The two square points were obtained from the same mass spectrometer analysis, but using a separation calcu-

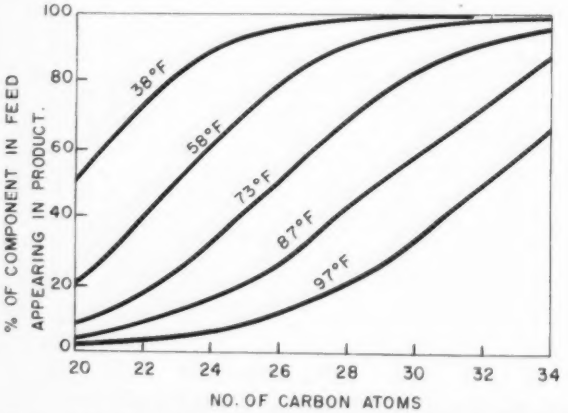

Figure 15—The theoretical separation obtained for typical recrystallization conditions. The indicated temperatures are those used for calculating the various curves. They are approximately the temperatures which would be required for separations using typical ketone solvents.

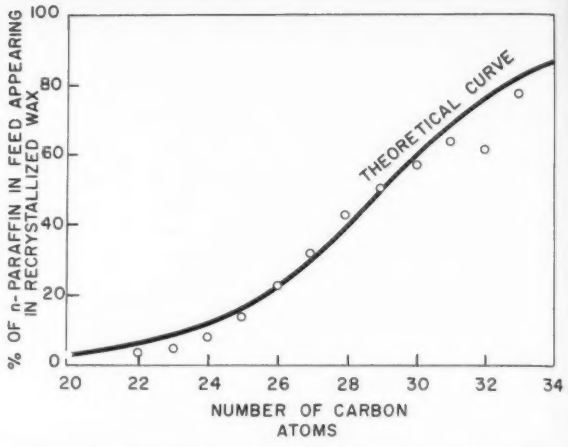

Figure 14—Recrystallization of paraffin wax—same experiment as in Figure 13.

lated by the method described previously. The agreement between these points and the experimental ones is very good.

There is considerable room for improving the sharpness of separation between normal paraffins obtained in wax recrystallization. On the other hand, the separation between normal paraffins and other wax components is comparatively good. There are two main reasons for this:

(1) In any distillate wax the non-normal paraffins and naphthenes have relatively low melting points and as a result relatively high solubilities. (See Equation (9)).

(2) It seems unlikely that the non-normals can form mixed crystals with normal paraffins.

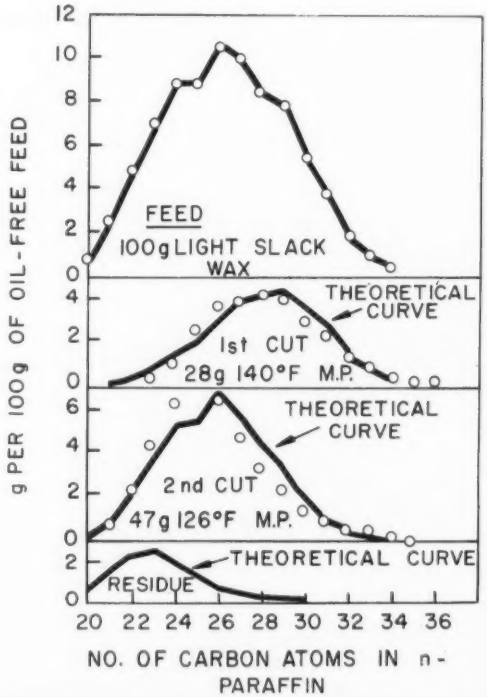

Figure 16—The recrystallization of light slack wax into two cuts and a residue. The experimental points are from mass-spectrometer analyses. The following quantities of non-normal hydrocarbons were also present: Feed 12g.; 1st cut 0.6 g.; 2nd cut 6.6g.; residue 4.8g. (by difference).

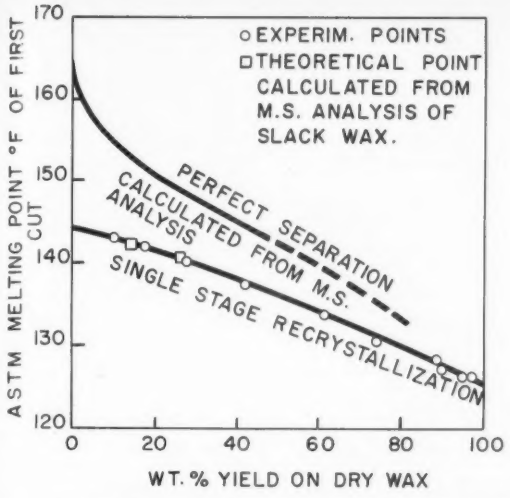

Figure 17—The melting points of first cuts from light slack wax.

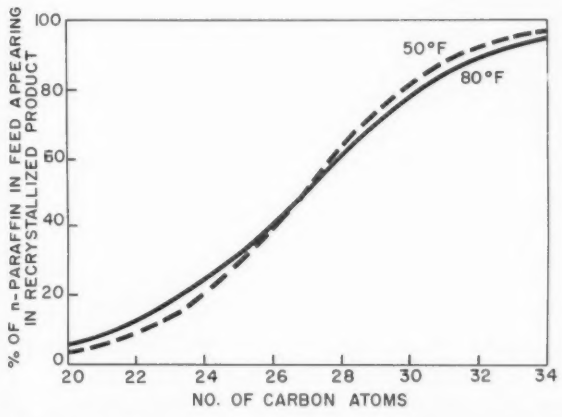

Figure 18—The predicted effect of temperature on the sharpness of separation. In both cases the quantity of solvent is such that 50% of the n-$C_{27}H_{56}$ is dissolved. This means that about three times as much solvent is required for the separation at 50°F. as at 80°F.

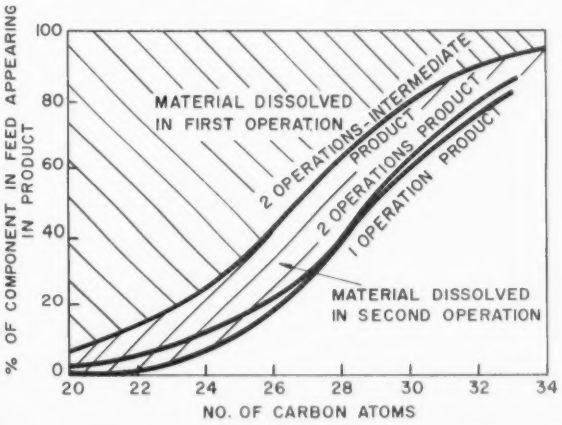

Figure 19—Diagram showing how the sharpness of separation may be increased if the solvent is applied in two separate operations—curves calculated for a temperature of 80°F.

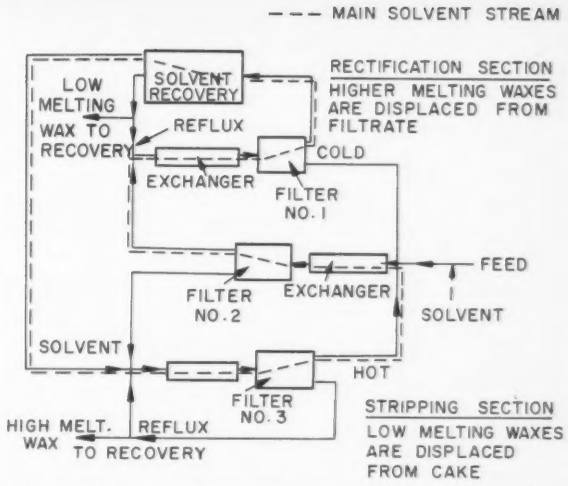

Figure 20 — Countercurrent recrystallization fractionator. Temperatures are adjusted by the scraped exchangers so that the ratio of solid to liquid wax in the slurries is about the same order as the yields.

This means that when such a wax is recrystallized the solid which separates first will be essentially a mixture of pure normal paraffins. As more and more solid separates a point will eventually be reached when separate crystals of non-normals will also form. Thus, while it is possible to separate n-paraffin mixtures containing practically no non-normals from a wax by recrystallization, it is not possible to obtain low melting fractions which are not contaminated with n-paraffins. The problem is analogous to crystallizing a salt from an aqueous solution. The first material which crystallizes is the pure salt, but eventually a eutectic point is reached where a mixture of crystals of salt

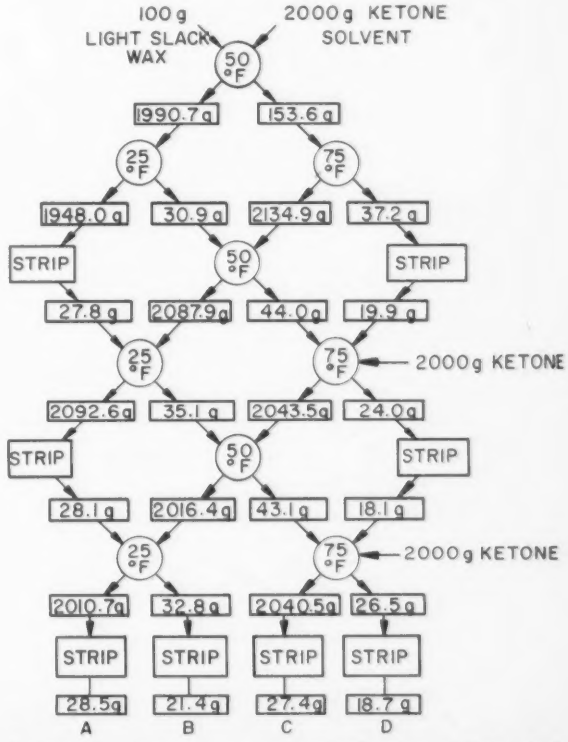

Figure 21—Countercurrent recrystallization of light slack wax at total reflux.

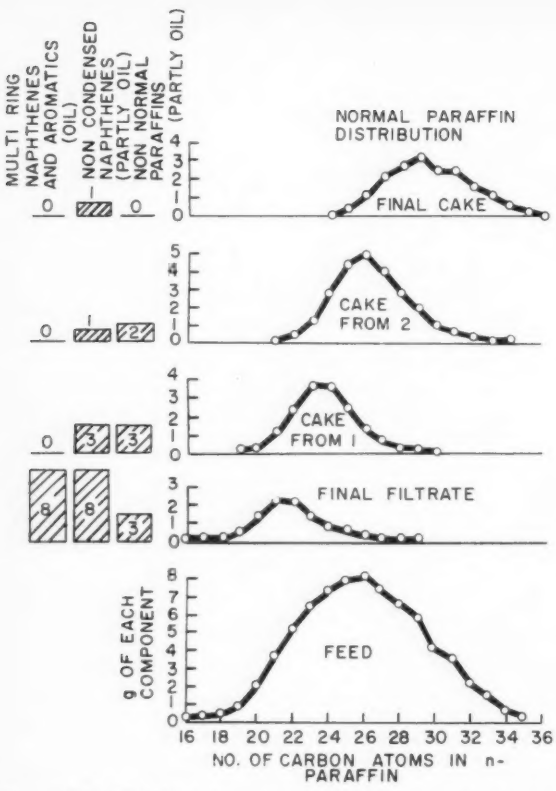

Figure 22—Weight balance for countercurrent three stage wax recrystallization at total reflux. Basis 100 g. of feed.

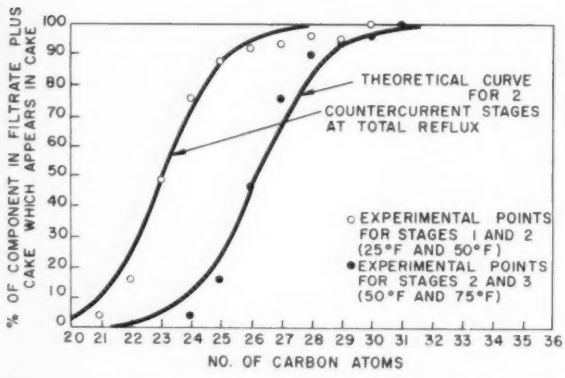

Figure 24—Separation across two countercurrent stages at total reflux.

and water is obtained. It is not possible to carry the process on until only crystals of water are obtained.

The inability to obtain pure non-normal waxes would appear to be a fundamental limitation of the wax recrystallization process.

(5) The Effect of Temperature of Recrystallization Upon the Degree of Separation Between Normal Paraffins

It is possible to crystallize a given yield of wax from a particular feedstock by employing either a relatively large quantity of solvent at a low temperature or a smaller quantity of solvent at a higher temperature. An examination of Equation (7) shows that the selectivity of the solvent should increase as the temperature is lowered. This is analogous to the increase in selectivity which is obtained when the temperature is lowered in solvent extraction. Figure 18 shows that the magnitude of

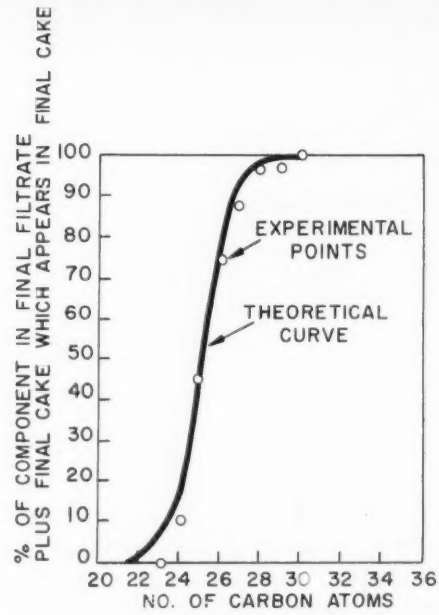

Figure 23—Separation across three countercurrent stages at total reflux. Stage temperatures 25°F.; 50°F.; and 75°F.

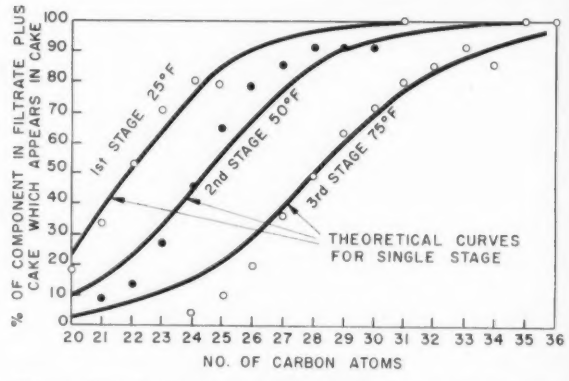

Figure 25—Separation across single stages in countercurrent cascade.

the effect is not very large, however. Other factors such as the minimum solvent requirements for deoiling and the relative filtration properties are of more importance in determining the type and relative quantity of solvent which should be used.

(6) Two Stage Recrystallization

A somewhat more selective separation is predicted if the recrystalliaztion is carried out in two stages.

(1) The recrystallization and filtration of a wide cut.

(2) The recrystallization of the wide cut to product the required narrow cut.

The predicted effect of such an operation upon the degree of separation is compared with that of a normal operation in Figure 19.

(7) Countercurrent Recrystallization

One possible method of increasing the sharpness of separation obtained on recrystallization is to employ a countercurrent cascade of recrystallization stages. A possible arrangement of this type is shown in Figure 20. In this diagram, each stage consists of a scraped exchanger together with a rotary filter. The solvent passes upwards through the cascade and the products

are refluxed at each end. Feed enters at an intermediate stage. A temperature gradient is required across the cascade in order to keep the wax solubility approximately constant.

In order to demonstrate the feasibility of an operation of this type, a simulated three stage continuous countercurrent recrystallization of light paraffin slack was carried out. To simplify the experimental details, the operation was carried out at total reflux. The experimental scheme which was used is shown in Figure 21. In this figure, each circle represents a batch filtration at the temperature shown. Filtrates move downwards to the left and filter cakes downwards to the right. The initial solvent to feed ratio was chosen so that entrainment of liquid in the cake would not be significant. The weights of the various quantities of cake and filtrate are indicated in the narrow rectangles.

Mass spectrometer analysis of samples A, B, C, D, and the feed were obtained. It is believed that the cascade was essentially in equilibrium at this point. Since the operation was at total reflux the quantity and composition of the wax dissolved in the filtrate passing between two stages must be the same as that of the wax in the wax cake passing in the opposite direction between the same two stages. This fact has been made use of in evaluating the results.

The mass spectrometer results are plotted in Figure 22. It may be seen that there is a continual change in composition of the wax from stage to stage. It is of particular interest to note that there is very little overlap between the final cake and the final filtrate. This may also be seen from an examination of Figure 23. In this Figure, the overall separation which is obtained is compared with a theoretical curve predicted from the previously derived equation for the separation factor. The agreement is surprisingly good and should add considerable confidence to the use of this equation.

Similar comparisons for the separation across two of the three stages and across the single steps are shown in Figures 24 and 25. The agreement is considered to be satisfactory.

Acknowledgement

The authors wish to acknowledge the contribution made by members of the Process Research Division of the Esso Research and Engineering Company who carried out the mass spectrometer analyses described in this paper.

References

(1) Mazee, W. M., "Report No. 8975 on the Physico-Chemical Properties of Some Hydrocarbons containing more than 20 Carbon Atoms", January 9, 1943. N.V. de Bataapsche Petroleum Maatschappij Laboratory, Amsterdam. Oil Mission Films Bag 3996, Recl. No. 79, Item No. 130/p. 2504-2578.

(2) Minchin, S. T., J. Inst. Petrol., **34**: 542 (1948).

(3) Partington, J. R., "Advanced Treatise of Physical Chemistry", Vol. III, p. 122 (1952); Küster, Z. Physik. Chem. **5**: 601 (1890).

(4) Carlson, H. C., and Colburn, A. P., Ind. Eng. Chem. **34**: 581 (1942).

(5) Butler, R. M., and Tiedje, J. L., Can. J. Tech. **34**: 455 (1957).

(6) Mazee, W. M., J. Inst. Petrol. **34**: 591 (1948).

(7) Scheibel, E. G., Chem. Eng. Progr. **44**: 927 (1948).

(8) Drickamer, H. G., and Hommel, H. H., Trans Am. Inst. Ch. Engrs. **41**: 607 (1945).

★ ★ ★

Optimum Process Conditions for a Completely Mixed Multistage Reactor[1]

H. KUBOTA[2], *S. NAMKOONG*[2], *T. AKEHATA*[2], *and M. SHINDO*[2]

A graphical method for determining the process conditions which give the minimum volume of reactor at a given outlet conversion is described, and illustrated by application to a multistage fluidized bed reactor for the catalytic oxidation of sulphur dioxide.

The optimum process conditions for practical chemical reactors is of great importance to the chemical engineers. The optimum is usually considered to be the economic optimum, but in this paper it will be defined as the process conditions which give the minimum volume of reactor for a given outlet conversion of a specified reactant. It has been shown by Bilous and Amundson[1] that these conditions are equivalent to the conditions which give the maximum conversion for a fixed volume of reactor. These optimum process conditions may not coincide with the economic optimum but should be a valuable guide to it.

Bilous and Amundson[1] have presented a method for determining the optimum temperature gradient of an ideal reactor in which temperature and concentration can be controlled so as to satisfy the requirement given in Equation (1) for a single reaction at any part of the reactor

$$\frac{\partial v(y,T)}{\partial T} = 0 \qquad (1)$$

In general, this condition can be found graphically from a rate chart as shown in Figure 1, where the broken line marks the "ideal process path".

In practical types of reactors, methods of determining the optimum process conditions have been discussed by Boreskov[2], Konoki[3], and the authors for a multistage adiabatic piston flow reactor and for an autothermic and an externally cooled single stage reactor[4]. This paper outlines a method of obtaining the optimum process conditions for a multistage, completely mixed reactor.

Derivation of Optimum Process Conditions

Assuming continuous flow from stage to stage, complete mixing within each stage, and individual temperature control within each stage, the derivation is as follows.

From the mass balance of a particular component in steady state,

$$v_{Ai}V_i = F_0(y_i - y_{i-1}) \qquad i = 1,2,\ldots n \qquad (2)$$

or

$$V_i/F_0 = (y_i - y_{i-1})/v_{Ai} \qquad (2a)$$

When y_o and y_n are given, the optimum process condition is defined by

$$V/F_0 = \sum_{i=1}^{n} V_i/F_0 = \text{minimum} \qquad (3)$$

therefore,

$$\delta(V/F_0) = \sum_{i=1}^{n} \delta(V_i/F_0) = 0 \qquad (4)$$

At the first stage y_o is fixed, so the change in V_1 caused by a change of y_1 and temperature T_1 is given by

$$\delta(V_1/F_0) = \frac{\partial(V_1/F_0)}{\partial y_1}\delta y_1 + \frac{\partial(V_1/F_0)}{\partial T_1}\delta T_1 \qquad (5)$$

Similarly for the second stage, and so forth,

$$\delta(V_i/F_0) = \frac{\partial(V_i/F_0)}{\partial y_{i-1}}\delta y_{i-1} + \frac{\partial(V_i/F_0)}{\partial y_i}\delta y_i + \frac{\partial(V_i/F_0)}{\partial T_i}\delta T_i \qquad (6)$$

$$i = 2,3,\ldots n-1$$

At the last stage y_n is fixed, so that

$$\delta(V_n/F_0) = \frac{\partial(V_n/F_0)}{\partial y_{n-1}}\delta y_{n-1} + \frac{\partial(V_n/F_0)}{\partial T_n}\delta T_n \qquad (7)$$

Since $y_1, y_2, \ldots y_{n-1}$ and $T_1, T_2, \ldots T_n$ are independent of each other, Equation (4) can be restated as

$$\frac{\partial(V_i/F_0)}{\partial y_i} + \frac{\partial(V_{i+1}/F_0)}{\partial y_i} = 0 \qquad i = 1,2,\ldots n-1 \qquad (8)$$

and

$$\frac{\partial(V_i/F_0)}{\partial T_i} = 0 \qquad i = 1,2,\ldots n \qquad (9)$$

Substituting Equation (2a) into Equation (8) and (9), the following relationship can be stated for the optimum process conditions.

$$\frac{1}{v_{Ai+1}} - \frac{1}{v_{Ai}} = (y_i - y_{i-1})\frac{\partial(1/v_{Ai})}{\partial y_i} \qquad i = 1,2,\ldots n-1 \qquad (10)$$

and

$$\frac{\partial(1/v_{Ai})}{\partial T_i} = 0 \qquad i = 1,2,\ldots n \qquad (11)$$

Equation (11) shows that the relation between y_i and T_i in each stage must be that of the ideal process path.

Now as a special case, assume the same temperature for each stage and that the reaction rate v_A is first order with respect to the concentration of a particular reactant A. Then the following relation can be derived.

[1]*Manuscript received July 16, 1960; accepted December 16, 1960.*
[2]*Tokyo Institute of Technology, Tokyo, Japan.*

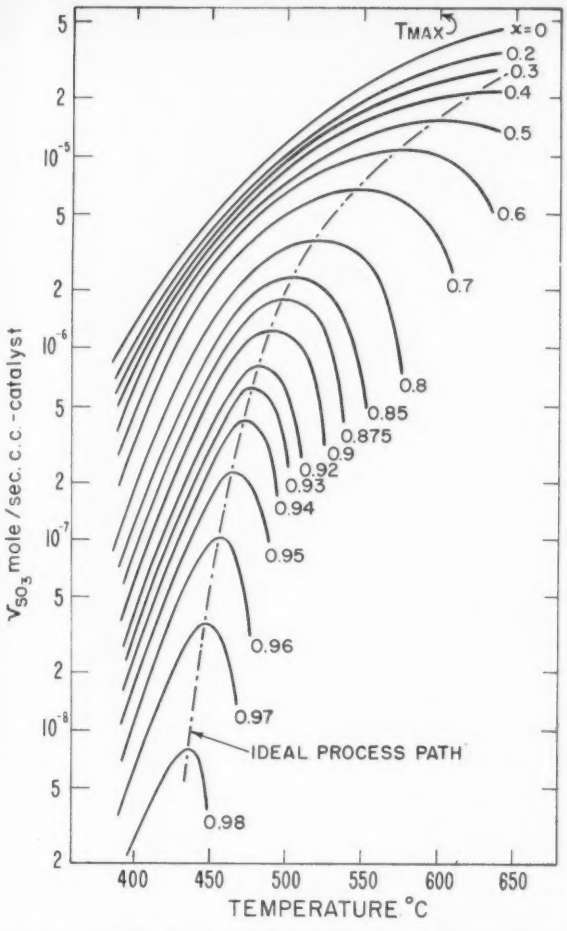

Figure 1—Rate chart of SO_2 oxidation reaction on an industrial vanadium catalyst.

$$y_i = 1 - (1 - y_n)^{i/n} \quad \ldots\ldots(12)$$

$$V_1 = V_2 \ldots\ldots = V_n = V/n \quad \ldots\ldots(13)$$

where y can be replaced directly with the concentration of the reactant A. This relation has been given by Boreskov[5].

Graphical Method

The values of y_i and T_i satisfying the conditions of Equation (10) and (11) are determined easily by a graphical method. $1/v_{A\max}$ which is defined by the ideal process path in Figure 1, is plotted as a function of y as shown in Figure 2. Assume first a value of y_1. From Equation (11) the temperature T_1 has a particular value on the ideal process path, so that point A in Figure 2 is given. The ordinate $\overline{AB}$ is equal to $1/v_{A1}$. From Equation (10),

$$\frac{1}{v_{A1}} + (y_1 - y_0)\frac{\partial(1/v_{A1})}{\partial y_1} = \frac{1}{v_{A2}} \quad \ldots\ldots(14)$$

The tangent of $1/v_{A\max}$ at point A is equal to $\partial(1/v_{A1})/\partial y_1$, thus it is easy to show that $\overline{AD} = (y_1 - y_0)\,\partial(1/v_{A1})/\partial y_1$. Therefore, taking $\overline{AD} = \overline{AE}$, the ordinate $\overline{BE}$ is equal to $1/v_{A2}$. This value of $1/v_{A2}$ locates the point F, and hence the value of y_2. From Figure 1, where $v_{A\max}$ is shown as a function of values of T, the value of T_2 may be obtained. The procedure is continued to the n-th stage so as to obtain the value of y_n.

If this calculated value of y_n does not agree with the desired value, then the calculations are repeated with new assumed values of y_1 until agreement is reached. After y_i and T_i have been obtained, the volume of reactor V_i may be determined by the application of Equation (2a).

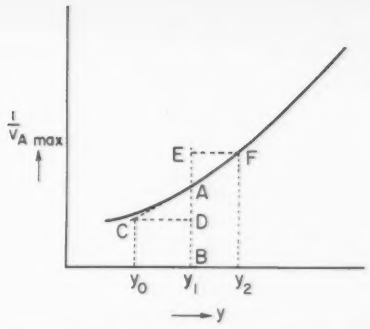

Figure 2—Graphical method for determining the process optimum condition.

Illustrative Calculation

The calculation of the optimum process conditions for sulphur dioxide oxidation in multistage fluidized catalyst bed, is illustrated. In a fluidized bed the assumption of complete mixing may not be entirely correct, but it is a good first approximation.

The rate expression for this reaction on the industrial vanadium catalyst as proposed by the authors[6] is:

under 450°C.,

$$v_{SO_3} = \frac{k\,E_f(p_{O_2} - p_{SO_3}^2/K_p\,p_{SO_2}^2)}{(1 + K_a\,p_{SO_3}/p_{SO_2})^2}$$

above 500°C.,

$$v_{SO_3} = \frac{k\,E_f\,(p_{SO_2}^2 - p_{SO_3}^2/K_p\,p_{O_2})}{(1 + K_b\,p_{SO_2}/p_{O_2}^{0.5})^2}$$

The rate chart calculated from these equations is shown in Figure 1. The following values for the constants were used:

$$k = 2.17 \times 10^3 \exp[-1{,}290/(T + 273)]$$
$$K_a = 1.02 \times 10^{-5} \exp[7{,}025/(T + 273)]$$
$$K_b = 4.39 \times 10^3 \exp[-890/(T + 273)]$$

The catalytic effectiveness factor E_f is assumed to be 1, and the rates at temperatures between 450 ~ 500°C. are interpolated. An inlet composition of reactant gases of 8% SO_2, 12% O_2 and the remainder N_2, and an average pressure of 800mm. Hg are assumed. The desired exit conversion of SO_2 is 97%, and the maximum allowable temperature is 600°C.

When the reactant SO_2 is chosen as the particular component A, the design Equation (2) and the optimum process conditions, Equations (10) and (11), become

$$v_{SO_2i}V_i = -F_0\,z_{SO_20}(x_i - x_{i-1}) \quad \ldots\ldots(15)$$

$$\frac{1}{v_{SO_2i+1}} = \frac{1}{v_{SO_2i}} + (x_i - x_{i-1})\frac{\partial(1/v_{SO_2i})}{\partial x_i} \quad \ldots\ldots(16)$$

and

$$\frac{\partial(1/v_{SO_2i})}{\partial T_i} = 0 \quad \ldots\ldots(17)$$

where v_{SO2} is the change in the moles of the sulphur dioxide per unit time per unit volume of catalyst, and hence V_i in Equation (15) has the dimension of the volume of catalyst.

Values of $v_{SO_2\max}$ are obtained as a function of the conversion x from Figure 1. Calculated values of $1/v_{\max}$ and $\partial(1/v_{\max})/\partial x$ are shown in Table 1.

For a numerical example, consider the case where the number of stages is 3.

TABLE 1

IDEAL PROCESS PATH FOR SULPHUR DIOXIDE OXIDATION

x (%)	T (°C)	$-v_{SO_2max}$*	$-1/v_{max}$	$-\frac{\partial(1/v_{max})}{\partial x}$
0	600	131.04	0.007631	0.0067
0.1	600	118.08	0.008469	0.00905
0.2	600	104.40	0.009579	0.0130
0.3	600	89.64	0.01100	0.0196
0.4	600	74.16	0.01348	0.0316
0.5	598	55.80	0.01792	0.0556
0.6	573.5	39.24	0.02548	0.103
0.7	546	24.66	0.04055	0.212
0.80	519.7	13.39	0.07468	0.565
0.825	513.0	10.93	0.0915	0.800
0.85	505.3	8.64	0.1157	1.20
0.875	496.3	6.59	0.1518	1.99
0.90	488.6	4.464	0.2240	3.81
0.91	484.5	3.636	0.2750	5.33
0.92	480.8	2.934	0.3408	8.23
0.93	477.0	2.268	0.4409	14.9
0.94	471.5	1.512	0.6614	32.0
0.95	464.0	0.828	1.208	80.0
0.96	456.0	0.360	2.778	240
0.97	447.6	0.1228	8.150	960
0.975	442	0.0595	16.80	—

*kg-mole/hr. m³ of catalyst.

As a first trial the first stage conversion, x_1 is assumed to be 0.70. Hence from Table 1, $-1/v_1 = 0.0406$ and $-\partial(1/v_1)/\partial x_1 = 0.212$. For the second stage

$$1/-v_2 = 0.0406 + (0.70)(0.212) = 0.189.$$

From Table 1, the corresponding value of x_2 is 0.889, and $\partial(-1/v_2)/\partial x_2$ is 2.80. For the third stage,

$$1/-v_3 = 0.189 + (0.889 - 0.70)(2.80) = 0.718.$$

The corresponding value for x_3 is 0.94 which is smaller than the desired conversion; and so the calculation must be repeated with a new assumed value for x_1.

After a few trials, x_1 is found to be 0.850. The final results are:

$x_1 = 0.850$, $T_1 = 505.3$, $-1/v_1 = 0.1157$, $-\partial(1/v_1)/\partial x_1 = 1.20$
$-1/v_2 = 0.116 + (0.85)(1.20) = 1.136$
$x_2 = 0.9492$, $T_2 = 456.3$, $-1/v_2 = 1.136$, $-\partial(1/v_2)/\partial x_2 = 70.4$
$-1/v_3 = 1.136 + (0.9492 - 0.85)(70.4) = 8.116$
$x_3 = 0.970$, $T_3 = 447.6$, $-1/v_3 = 7.868$.

The resulting volumes of catalyst become:

$$V_1/F_O = (0.08)(0.1157)(0.850) = 0.007855$$
$$V_2/F_O = (0.08)(1.136)(0.949 - 0.85) = 0.00901$$
$$V_3/F_O = (0.08)(8.150)(0.970 - 0.949) = 0.01355$$
$$V/F_O = 0.007855 + 0.00901 + 0.01355 = 0.0304$$

The calculated results are shown in Table 2 when the number of stages is $n = 1, 2, \ldots 7$. It may be observed that there is a large change in the catalyst volume in going from 1 to 2 stages and increasing the number of stages beyond 5 decreases the catalyst volume very little. For an infinite number of stages, i.e., following the ideal path, the volume of catalyst in V/F_O is 0.0104 m³ of catalyst hr./kg-mol.

Nomenclature

F_O = total moles fed to the first stage of the reactor per unit time
E_f = catalytic effectiveness factor
k = reaction rate constant

TABLE 2

OPTIMUM PROCESS CONDITION IN MULTISTAGE, COMPLETELY-MIXED REACTOR FOR SO_2 OXIDATION

n*	Stage no.	x (%)	T (°C.)	V_i/F_O**	$\Sigma V_i/F_O$**
1	1	97.0	447.6	0.633	0.633
2	1	92.0	480.8	0.0251	
	2	97.0	447.6	0.0326	0.0577
3	1	85.0	505.3	0.00786	
	2	94.9	465.3	0.00901	
	3	97.0	447.6	0.01355	0.0304
4	1	78.0	524.7	0.00407	
	2	92.7	477.3	0.00488	
	3	95.8	457.7	0.00550	
	4	97.0	447.6	0.00796	0.0224
5	1	72.0	540.1	0.00258	
	2	90.0	488.6	0.00326	
	3	94.5	467.8	0.00332	
	4	96.1	455.5	0.00414	
	5	97.0	447.6	0.00548	0.0188
6	1	66.0	557.0	0.00174	
	2	86.5	500.0	0.00224	
	3	93.1	475.4	0.00255	
	4	95.4	462.0	0.00283	
	5	96.4	453.5	0.00350	
	6	97.0	447.6	0.00372	0.0165
7	1	62.5	566.3	0.00141	
	2	84.1	507.6	0.00181	
	3	91.7	481.8	0.00198	
	4	94.5	467.8	0.00194	
	5	95.7	458.9	0.00225	
	6	96.4	453.0	0.00262	
	7	97.0	447.6	0.00332	0.0153

* n; number of stages.
**Unit of V_i/F_O is m.³ hr./kg-mole.

K_a, K_b = adsorption constants
K_p = reaction equilibrium constant
n = number of stage
$p_{O_2}, p_{SO_2}, p_{SO_3}$ = partial pressure of gases
T_i = temperature at i-th stage of reactor
v_{Ai} = reaction rate at i-th stage, defined as the change in moles of a particular component A per unit time per unit volume of reactor
V_i = volume of i-th stage of reactor
x_i = $(F_{AO} - F_{Ai})/F_{AO} = 1 - y_i/z_{AO}$, where F_{AO} is moles of a particular component A fed to the first stage of the reactor per unit time
z_{AO} = mole fraction of a particular component A in feed

References

(1) Bilous, O. and Amundson, N. R., Chem. Eng. Sci., **5,** 81, 115 (1956).
(2) Boreskov, G. K., "Manufacturing of Sulphuric Acid by Catalysis" (in Russian), Soviet Science Academy (1956).
(3) Konoki, K., Chem. Eng. (Japan), **21,** 408, 780 (1957)
(4) Kubota, H., Akehata, T., and Shindo, M., ibid., **23,** 506 (1959).
(5) Boreskov, G. K., and Slinko, M. G., Khim. Prom., Moscow, No. 6, 321 (1957).
(6) Kubota, H., Ishizawa, M., and Shindo, M., Sulphuric Acid, (Japan), **23,** 284 (1959).

★ ★ ★

The Upward Vertical Flow of Oil-Water Mixtures[1]

G. W. GOVIER[2], *G. A. SULLIVAN*[3] *and R. K. WOOD*[4]

The upward vertical flow of oil-water mixtures has been investigated in a 37-ft. length of cellulose acetate butyrate tubing of inside diameter 1.038-in. Flow pattern, holdup and pressure drop data were obtained for water mixtures with 0.936, 20.1 and 150 centipoise oils at superficial water velocities ranging from 0.10 to 10.0 ft./sec.

The oil-water mixtures exhibited a behavior similar to that of air-water mixtures studied previously. The flow patterns observed at constant superficial water velocity with increasing oil-water ratio were: drops of oil in water, slugs of oil in water, froth, and drops of water in oil. Holdup of the phase forming the continuous medium was observed but to a much lesser extent than with the air-water system. Curves of pressure drop versus oil-water ratio exhibited a minimum, a maximum and a second minimum at low water velocities; a single minimum at intermediate water velocities; and a steady increase at superficial water velocities above about 5 ft./sec.

A friction factor based upon the properties and the superficial velocity of the water is correlated with the superficial velocity of the oil and a Reynolds number based on the properties and superficial velocity of the water. This shows that the pressure drop due to friction and other irreversibilities is essentially independent of the viscosity of the oil except under conditions where the oil is the continuous phase.

Growing interest in two-phase flow is evidenced by the recent increase in publications dealing with the horizontal and the vertical flow of gas-liquid, liquid-liquid and liquid-solid mixtures. The flow of both gas-liquid and liquid-liquid mixtures is of importance in petroleum production and transport, while the flow of gas-liquid mixtures is important in chemical reactors, in evaporator design and applications are being encountered in the design of nuclear reactors. The flow of liquid-solid systems is met in certain chemical reactions, in pipeline transport of coal, ores and other solids and is also of considerable interest in nuclear reactor design.

While much attention has been given to the vertical flow of gas-liquid mixtures, little has been devoted to the fundamentally simpler case of liquid-liquid mixtures. This is undoubtedly because of the greater number of applications of the former case as compared with the latter and especially because of the interest of the petroleum industry. Yet, the vertical flow of a gas-liquid mixture is a special case of the flow of two immiscible fluids — and a complex one because of the compressibility of the gas phase.

The work here reported is part of a long term program of research on the vertical flow of immiscible fluids. Previously reported results[1,2,3] and those of many other workers[4,5,6,7,8,9,10,11,12] on the vertical flow of gas-liquid mixtures have shed considerable light on the effects of absolute and relative flow rates, diameter, and liquid properties on the vertical flow phenomenon. A limited amount of data is available on the effect of gas phase density on flow pattern, holdup and pressure drop. This effect is relatively small over gas phase densities encountered to system pressures of 100 p.s.i. or so. With the exception of some data on the steam-water system[13], quantitative data on the effect of higher gas phase densities are not available. Very few data on the vertical flow of liquid-liquid mixtures are available[14]. These deficiencies suggested this study of the flow of mixtures of water and oil with the overall objectives of

(a) determining the nature of the flow pattern and obtaining holdup and pressure drop data and

(b) assessing the effect of the viscosity of the oil phase.

Previous Related Studies

Previous work on the vertical flow of gas-liquid systems and the few studies on the horizontal flow of liquid-liquid systems[15,16,17] have a definite bearing on the liquid-liquid vertical flow problem. This work reveals what might be expected as to flow pattern, the general nature of the holdup phenomenon and the form of the pressure drop — flow rate relationships. The interpretation method developed by the University of Alberta workers suggests a method of analysis of the data.

Flow Patterns

The results reported by different observers of the flow patterns in the vertical flow of gas-liquid mixtures are in good agreement although differences in nomenclature have been employed. Govier, Radford and Dunn[2] compared nomenclature used by other workers and proposed terms related to "pressure drop regimes" defined through inflection points observed in the pressure drop versus gas-liquid ratio curves. Their terms, for increasing gas-liquid ratios, are bubble flow, slug flow, froth flow, ripple flow, film flow and mist flow. All these flow patterns are observed at low superficial liquid velocities — below about 3 ft./sec. — but froth flow is not observed at higher liquid velocities. Similar flow patterns are to be expected for liquid-liquid systems. For the air-water system, Brown, Sullivan and Govier[1] give a correlation of the effect of superficial water velocity, air-water volume ratio, air density and tube diameter on the pressure drop regimes and the flow patterns. The correlation has been tested only to air densities correspond-

[1]*Manuscript received August 16, 1960; accepted January 23, 1961.*
[2]*Professor of Chemical Engineering, Dean of Faculty of Engineering, University of Alberta, Edmonton, Alta.*
[3]*Graduate student, University of Alberta, June 1958; Chemical Engineering Section, Canadian Industries Limited, Montreal, Que. from July 1958.*
[4]*Graduate student, University of Alberta, October 1959; Research Engineer, Canadian Chemical Co. Limited to August 1960; Graduate student, Northwestern University from September 1960.*
Contribution from the Department of Chemical and Petroleum Engineering, University of Alberta, Edmonton, Alta.

ing with system pressures of about 100 p.s.i. and to diameters up to 2½ inches.

Holdup or Slip

The holdup of the liquid phase by the gas phase or the "slip" of the liquid past the gas, has been observed by most workers since Moore and Wilde[9]. The difference in average velocity of the two phases has been called the slip velocity. Related to it is the term holdup ratio which is the ratio of (a)the gas-liquid volume ratio in the supply mixture to (b) the in situ gas-liquid volume ratio. The two quantities are different measures of the same phenomenon and are interrelated[2] through the equation

$$V_S = V_G' - V_L' = V_L'(H_R - 1) \quad \ldots\ldots(1)$$

$$\text{or } H_R = \frac{V_G' - V_L'}{V_L'} + 1 \quad \ldots\ldots(2)$$

While these equations are written for a gas-liquid system similar equations apply to a system of two immiscible liquids.

The slip velocity tends to zero and the holdup ratio to unity as single phase conditions are approached.

For the air-water system holdup ratios have been correlated for each pressure drop regime by the University of Alberta workers[1,2,3] in terms of the air-water volume ratio, the tube diameter, the air density and the average velocity of one of the phases.

Pressure Drop

Many efforts have been made to correlate the pressure drop data obtained in vertical two phase flow studies. With the exception of that of Calvert and Williams[4] which is limited to the annular or film flow pattern, all are empirical. Many of the methods are based upon the use of a Fanning friction factor modified in one way or another to take account of the mixed phases. Poettmann and Carpenter[11] and the University of Alberta workers separated the overall pressure drop into its hydrostatic head and irreversibility components and applied the friction factor concept only to the latter. This seems a proper procedure.

In the University of Alberta method mechanical energy balances applied to each flowing fluid lead to

$$-v_L\left(\frac{\Delta P}{\Delta X}\right) = \frac{1 + R_m}{1 + R_s} + \frac{1}{1 + R_s}\left(\frac{\Delta F}{\Delta X}\right)_L \quad \ldots\ldots(3)$$

$$\text{and } \left(\frac{\Delta F}{\Delta X}\right)_L = \frac{2f_L' V_L^2}{g_c D} \quad \ldots\ldots(4)$$

The superficial friction factor based upon the properties and the velocity of liquid phase has been correlated[1], for the air-water system, in terms of the parameters DV_L (a reduced Reynolds number) and $D^{3.5}V_G$. Gas phase density has been found to have no significant effect over the range 0.092 to 0.552 lbs./cu. ft.

Poettmann and Carpenter's[11] similar approach in 1952 has led to a friction factor defined in terms of the density and the velocity of the flowing mixture. This friction factor was correlated through a modified Reynolds number incorporating the mass velocity of the mixture but no viscosity term.

Experimental Program

The experimental program undertaken involved two phase vertical flow tests with water and each of three different oils. The viscosity, density and interfacial tensions of the oils at or near the average temperature of the tests are presented in Table 1.

The tests were planned to give the maximum information concerning the effect of substituting an oil phase for the air phase of previous air-water tests and to determine the effect of oil phase viscosity on the flow pattern, holdup and pressure drop.

TABLE 1

PROPERTIES OF OILS

Viscosity Centipoise	Density gms. per cm.^{3}	Interfacial Tension oil-water dynes per cm.
0.936 (75°F.)	0.780 (75°F.)	35.3 (68°F.)
20.1 (72°F.)	0.851 (72°F.)	50.2 (68°F.)
150 (76°F.)	0.880 (76°F.)	49.8 (68°F.)

Equipment

A schematic flow diagram of the experimental equipment used is presented in Figure 1. The test section consisted of a 37 ft. length of 1.038 in. i.d. cellulose acetate butyrate transparent tubing. The tubing was equipped with full flow plug valves for holdup measurements and with static pressure drop connections over a 28.37 ft. length.

Piping and storage vessels were aluminum. Oil and water were pumped from their respective reservoirs by 5 h.p. centrifugal pumps and metered by calibrated rotameters. The discharge mixture was passed into a 210 gal. separator for preliminary separation of the oil and water and then the oil layer was passed through a 75 gal. vessel packed with salt for removal of the last traces of water. Pressure drops were measured with 60 in. manometers employing water over carbon tetrachloride or water over mercury as determined by the range required. The manometer lead lines were kept water filled with the aid of small oil-water separators mounted at the static pressure connection to the tube. The temperature of the flowing mixture was measured by a copper-constantan thermocouple inserted at the mid-point of the test section.

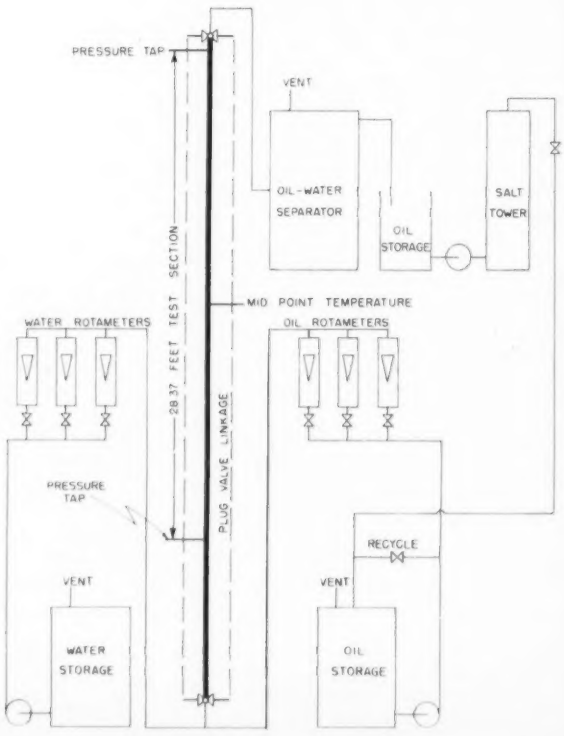

Figure 1—Schematic flow diagram of equipment.

TABLE 2 (Partial)

TYPICAL EXPERIMENTAL DATA 20.1 CENTIPOISE OIL

1 Test Number	2 Water Rate $\frac{ft.^3}{sec.}$	3 Oil Rate $\frac{ft.^3}{sec.}$	4 Discharge Oil-Water Ratio $\frac{ft.^3}{ft.^3}$	5 In Situ Oil-Water Ratio $\frac{ft.^3}{ft.^3}$	6 Pressure Drop $\frac{ft.\ of\ water}{ft.\ of\ tube}$	7 Midpoint Temperature °F.	8 Oil Viscosity Centipoise
308AA	0.000589	—	0	—	1.000	72.4	—
15AA	0.000589	0.000340	0.578	—	0.980	72.0	19.90
22AA	0.000589	0.000340	0.578	0.185	0.978	79.5	17.00
11AA	0.000589	0.000566	0.962	—	0.965	72.0	19.90
25AA	0.000589	0.000754	1.28	0.439	0.956	69.4	21.20
26AA	0.000589	0.000886	1.51	0.499	0.953	70.0	20.90
27AA	0.000589	0.00102	1.72	0.589	0.955	70.2	20.80
24AA	0.000589	0.00126	2.14	—	0.944	70.0	20.90
16AA	0.000589	0.00183	3.11	—	0.928	74.2	18.90
28AA	0.000589	0.00151	2.56	—	0.927	72.0	20.00
218AA	0.000589	0.00242	4.11	1.34	0.913	74.2	18.90
214AA	0.000589	0.00370	6.29	—	0.907	71.2	20.30
52AA	0.000589	0.00415	7.05	3.68	0.905	77.2	19.85
217AA	0.000589	0.00568	9.65	6.13	0.897	78.0	17.50
53AA	0.000589	0.00660	11.21	—	0.899	65.0	23.00
56AA	0.000589	0.00660	11.21	14.90	0.900	65.8	22.85
54AA	0.000589	0.00809	13.72	17.60	0.904	65.4	23.00
204AA	0.000589	0.00847	14.40	14.65	0.912	69.8	21.00
202AA	0.000589	0.00890	15.12	13.75	0.915	78.2	17.40
62AA	0.000589	0.00944	16.02	14.90	0.927	66.8	22.40
57AA	0.000589	0.01020	17.34	16.62	0.927	65.0	23.25

Procedure

The tests on the 0.936 centipoise oil were conducted by G. A. Sullivan and submitted as part of his M. Sc. thesis[18]. These covered seven different water rates ranging to 5.6 ft./sec. The tests on the 20.1 and the 150 centipoise oil were conducted by R. K. Wood and submitted in his M. Sc. thesis[19]. These covered seven different water rates ranging to 10.0 ft./sec. In all tests at each constant water rate the oil rate was varied from zero to the maximum flow allowed by the pumping capacity available.

A test was conducted by first setting a constant water rate on one of the water rotameters and then oil was introduced to the test section by adjusting the appropriate oil rotameter and when steady state conditions prevailed (as indicated by a stable manometer reading) the flow pattern was observed and the pressure drop, mid-point temperature and ambient temperature were recorded.

The in situ oil to water ratio was obtained by simultaneously closing the two plug valves. For the 0.936 and 20.1 centipoise oils, the oil and water were allowed to separate and the volume of each phase was determined by observing the position of the interface in the tube. The same method was used for the 150 centipoise oil at low water velocities but at superficial water velocities above about 1.0 ft./sec. the in situ ratio was obtained

TABLE 3 (Partial)

TYPICAL CALCULATED DATA 20.1 CENTIPOISE OIL

1 Test Number	2 Pressure Drop $\frac{ft.\ of\ water}{ft.\ of\ tube}$	3 Hydrostatic Head Component $\frac{ft.\ of\ water}{ft.\ of\ tube}$	4 Irreversibility Component $\frac{ft.\ of\ water}{ft.\ of\ tube}$	5 Friction Factor	6 Pressure Drop Regime	7 Holdup Ratio
308AA	1.000	1.000	0	—	I	—
15AA	0.980	0.941	0.039	8.55	I	—
22AA	0.978	0.941	0.037	8.11	I	3.12
11AA	0.965	0.924	0.041	11.18	I	—
25AA	0.956	0.914	0.042	13.30	I	1.28
26AA	0.953	0.916	0.037	12.90	I	1.51
27AA	0.955	0.916	0.039	14.72	I	1.72
24AA	0.944	0.909	0.035	15.30	I	—
16AA	0.928	0.881	0.047	26.65	I	—
28AA	0.927	0.890	0.037	18.35	I	—
218AA	0.913	0.872	0.041	29.05	I	3.07
214AA	0.907	0.870	0.037	37.55	I	—
52AA	0.905	0.863	0.042	47.1	I	1.93
217AA	0.897	0.855	0.042	62.1	I	1.57
53AA	0.899	0.855	0.044	74.6	II	—
56AA	0.900	0.855	0.045	76.5	II	0.753
54AA	0.904	0.856	0.048	98.2	II	0.78
204AA	0.912	0.855	0.057	121.9	II	0.983
202AA	0.915	0.855	0.060	134.3	II	1.10
62AA	0.927	0.853	0.074	175.6	II	1.076
57AA	0.927	0.850	0.077	196.3	III	1.041
39AA	0.926	0.854	0.072	196.8	III	0.865

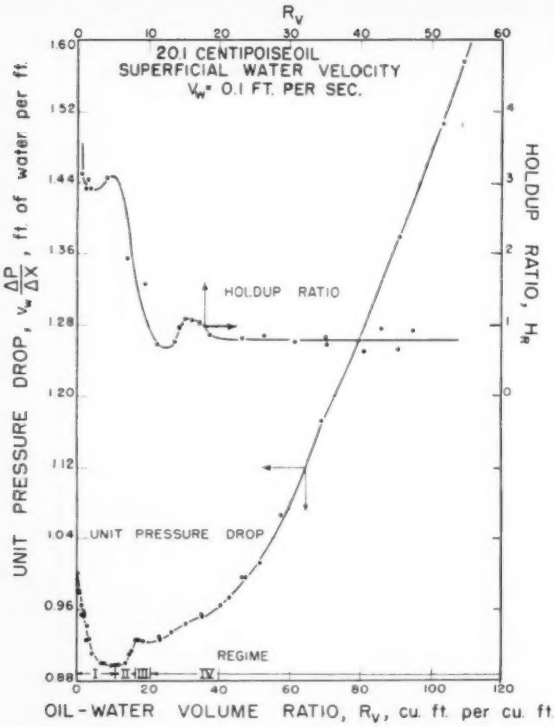

Figure 2—Unit pressure drop and holdup relationships for a superficial water velocity of 0.1 ft./sec.

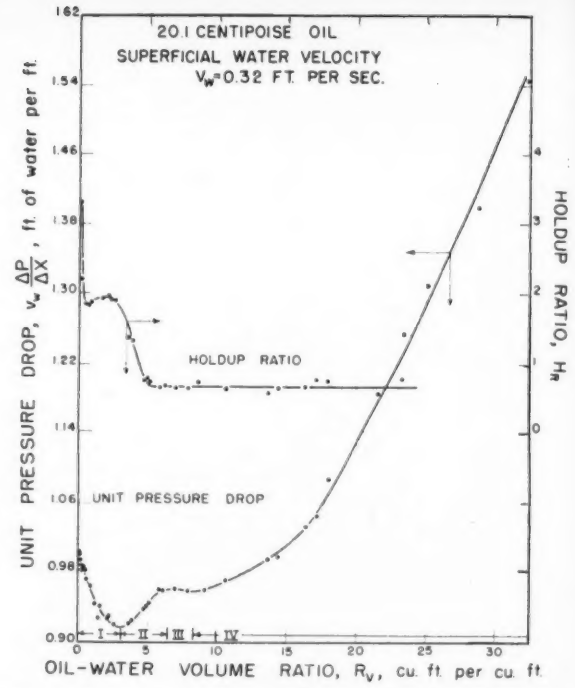

Figure 3—Unit pressure drop and holdup relationships for a superficial water velocity of 0.32 ft./sec.

by draining the tube and weighing the mixture. This was necessary since separation of the two phases took a lengthy time and was incomplete.

Experimental Results

The experimental data are presented in Table 2.* Table 2 (Partial) gives a typical data for the 20.1 centipoise oil. Some 220 individual tests were conducted for the 0.936 centipoise oil[18], 215 for the 20.1 centipoise oil[19] and 135 for the 150 centipoise oil[19].

Calculated results are presented in Table 3.* Table 3 (Partial) gives a sampling of these results for the 20.1 centipoise oil. In Table 3 the hydrostatic head component, irreversibility component, friction factor and holdup ratio were calculated in accordance with the definition of these terms in Equations 2, 3 and 4.

The unit pressure drop and the holdup ratio are shown, for selected superficial water velocities and for the 20.1 centipoise oil, as plots versus the input oil-water volume ratio in Figures 2 to 6. At low superficial water velocities the existence of two minima and a maximum point in the pressure drop curve is clearly evident. This is entirely analogous to the observations which have been made on the air-water system. With increasing superficial water velocity the two minima and the maximum point disappear until ultimately the unit pressure drop increases steadily with oil-water ratio. Similar plots for the other water velocities and the other two oils showed the same general shapes and trends except that no maximum or second minimum point was observed within the 150 centipoise oil. The pressure drop regimes, based upon the definitions of Govier, Radford and Dunn[2] related to the minima and the maximum points are indicated on the figures.

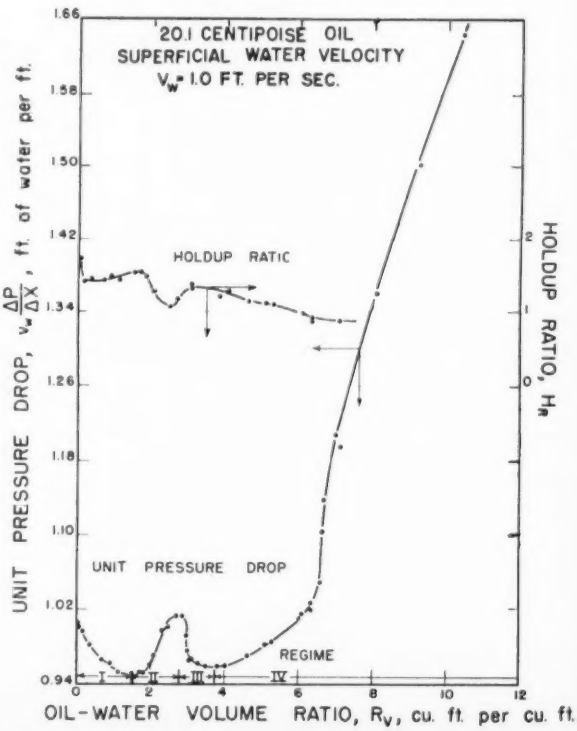

Figure 4—Unit pressure drop and holdup relationships for a superficial water velocity of 1.0 ft./sec.

*Complete experimental data of Table 2 and complete calculated results of Table 3 have been deposited as Document No. 6565 with the ADI Auxiliary Publications Project, Photoduplication Service, Library of Congress, Washington 25, D.C. A copy may be obtained by citing the Document No. and by remitting $5.00 for photoprints, or $2.25 for 35 mm. microfilm. Advance payment is required. Make cheques or money orders payable to: Chief, Photoduplication Service, Library of Congress.

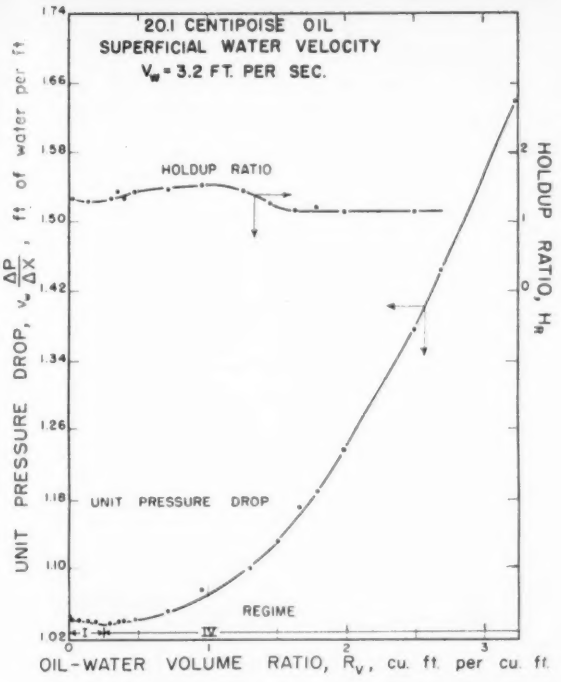

Figure 5—Unit pressure drop and holdup relationships for a superficial water velocity of 3.2 ft./sec.

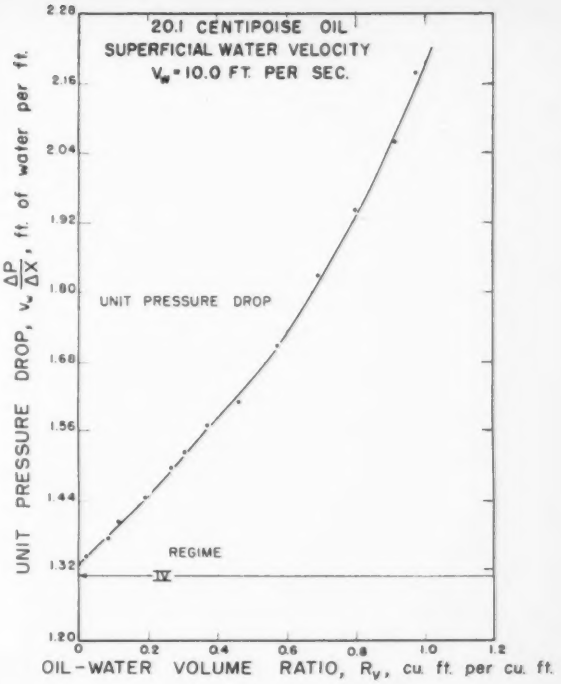

Figure 6—Unit pressure drop and holdup relationships for a superficial water velocity of 10.0 ft./sec.

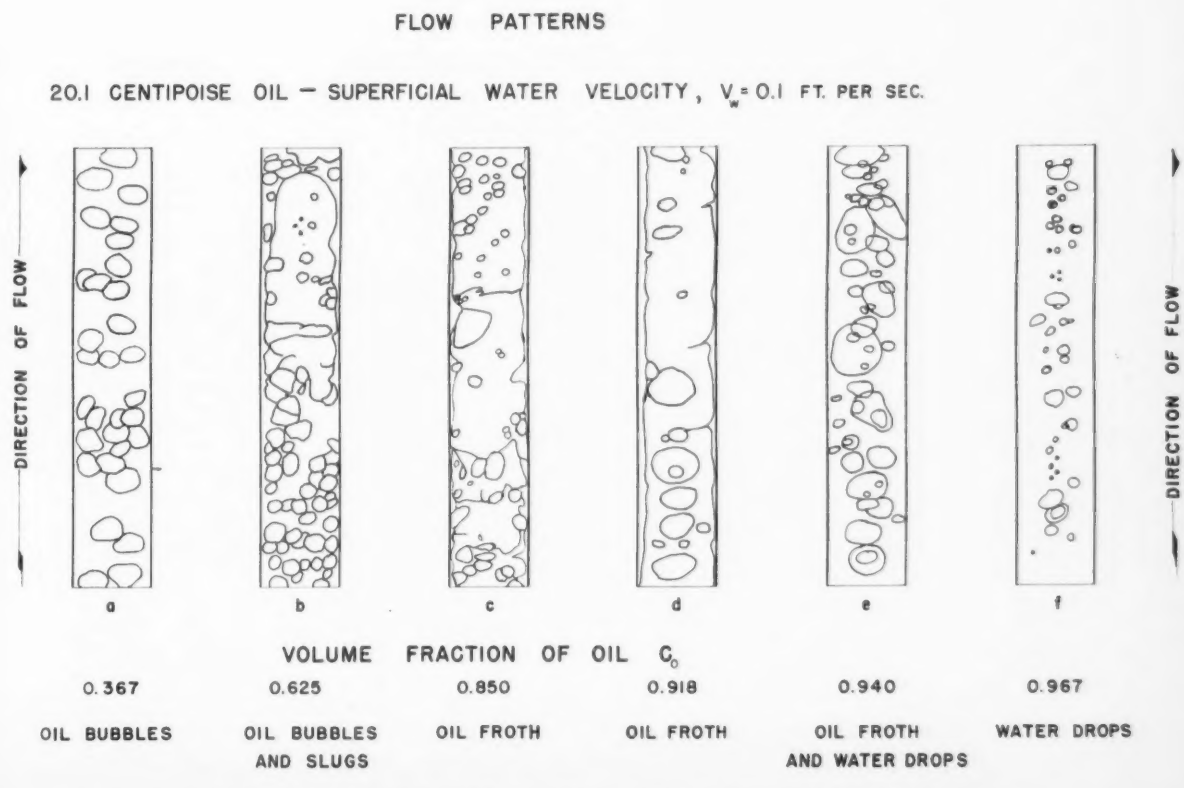

Figure 7—Flow patterns for 20.1 centipoise oil at 0.1 ft./sec. superficial water velocity.

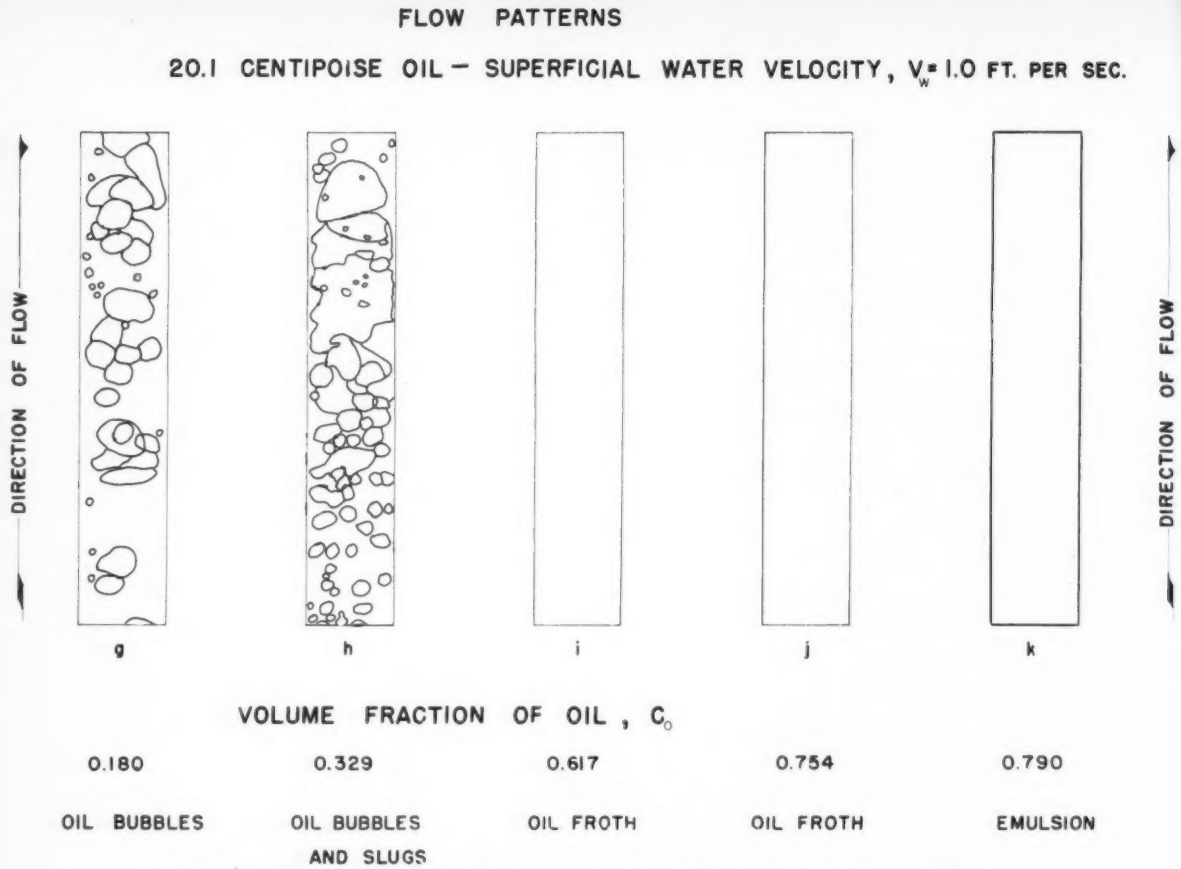

Figure 8—Flow patterns for 20.1 centipoise oil at 1.0 ft./sec. superficial water velocity.

Flow Pattern

The flow patterns observed corresponded, as for the air-water system, with the pressure drop regimes in accordance with the following:

Observed Flow Pattern	Pressure Drop Regime
Bubbles and drops of oil in water	I
Slugs of oil in water	I
Froth of oil and water	II, III
Drops of water in oil	IV

Photographs of the flow pattern were taken for the 0.936 and the 20.1 centipoise oils. The latter were then traced in ink to form the sketches which are reproduced as Figure 7, a series at a superficial water velocity of 0.1 ft./sec.; and Figure 8 a corresponding series at a water velocity of 1.0 ft./sec.

Figure 9 presents for the 20.1 centipoise oil the pressure drop regime boundaries (loci of the first minimum, the maximum and the second minimum points) in terms of the superficial

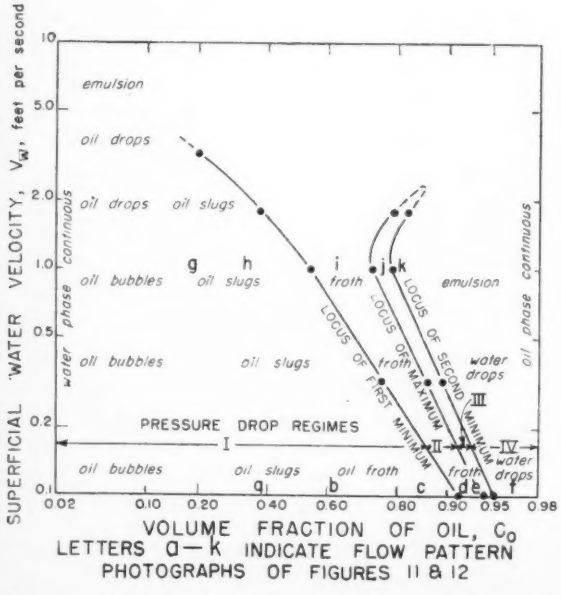

Figure 9—Pressure drop regime boundaries for 20.1 centipoise oil.

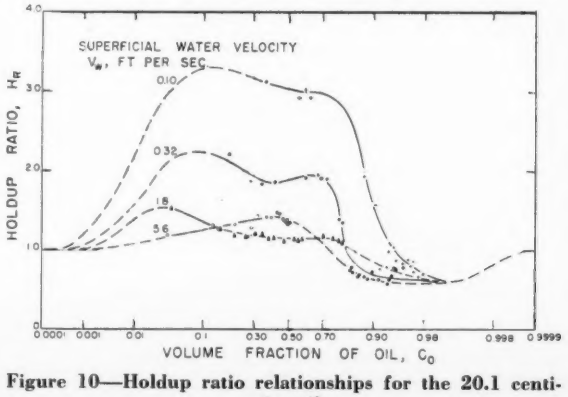

Figure 10—Holdup ratio relationships for the 20.1 centipoise oil.

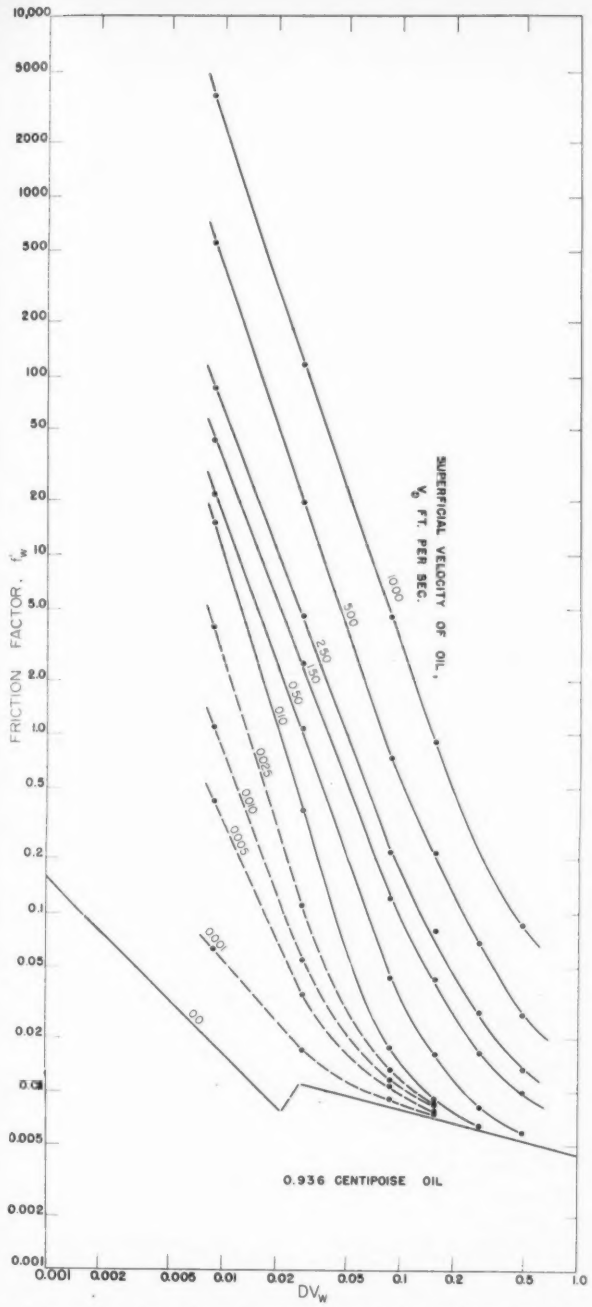

Figure 11—Two phase friction factor relationships for the 0.936 centipoise oil.

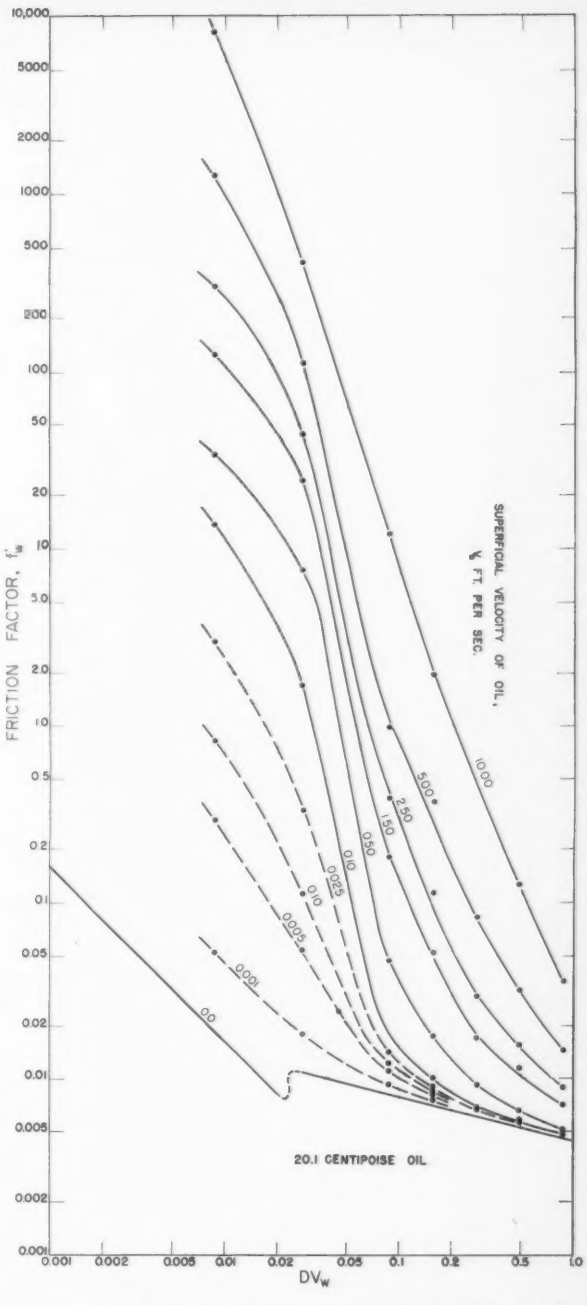

Figure 12—Two phase friction factor relationships for the 20.1 centipoise oil.

velocity of the water and the volume fraction of oil in the input mixture. Located on this figure by the symbol "P" are the conditions corresponding with the tests for which photographs were taken, the pressure drop regimes and the flow patterns. The regime boundaries for the other two oils are similar. The first minimum locus shifts to slightly lower volume fractions of oil with increase in oil viscosity. The second minimum and maximum were not observed with the 150 centipoise oil and extended to somewhat higher superficial water velocities in the case of the 0.936 centipoise oil.

Holdup Ratio

The holdup ratio data shown on Figures 2 to 6 for the 20.1 centipoise oil are summarized in Figure 10 where they are expressed as functions of the volume fraction of oil for each of several superficial water velocities. A similar family of curves was obtained for each of the 0.936 and the 150 centipoise oils with little significant effect of oil viscosity being apparent. It is to be noted that at each water velocity the holdup ratio increases gradually from unity at zero oil fraction, passes through a maximum, then decreases to values less than unity and finally approaches unity as the oil fraction itself does. Maximum holdup ratios are encountered at the minimum superficial water velocity and exceed 3 for a water velocity of 0.10 ft./sec. and a supply mixture oil fraction of 0.05 to 0.50. This corresponds with a "slip-velocity" of about 0.20 ft./sec. or indicates at this

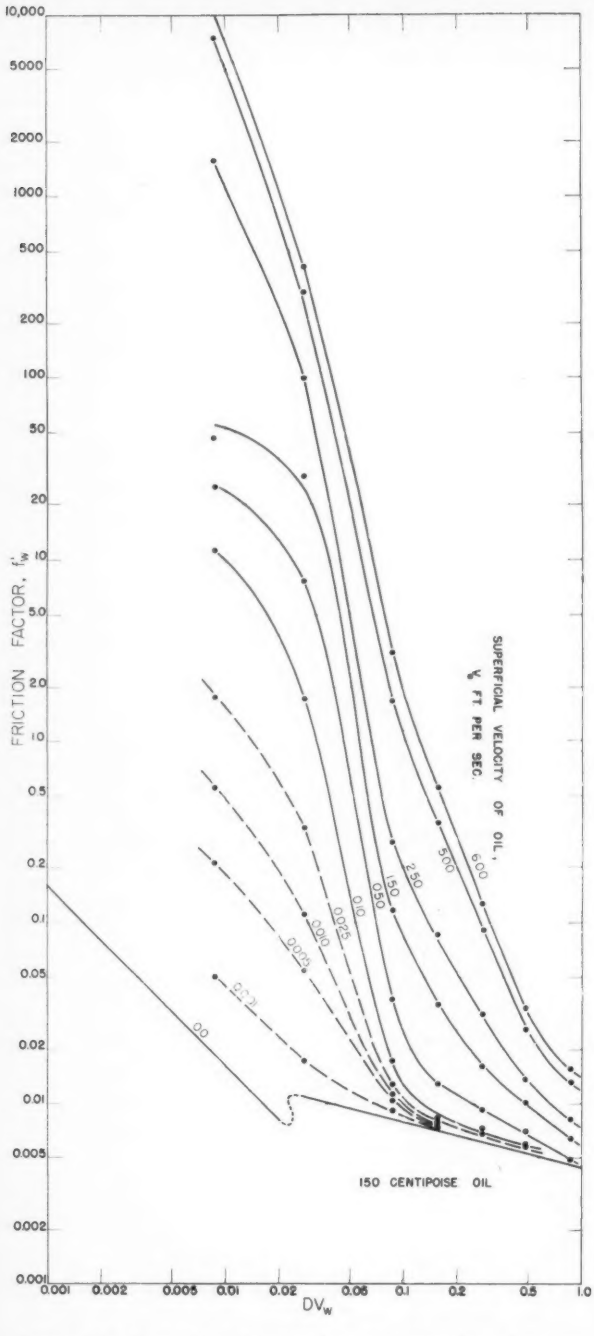

Figure 13—Two phase friction factor relationships for the 150 centipoise oil.

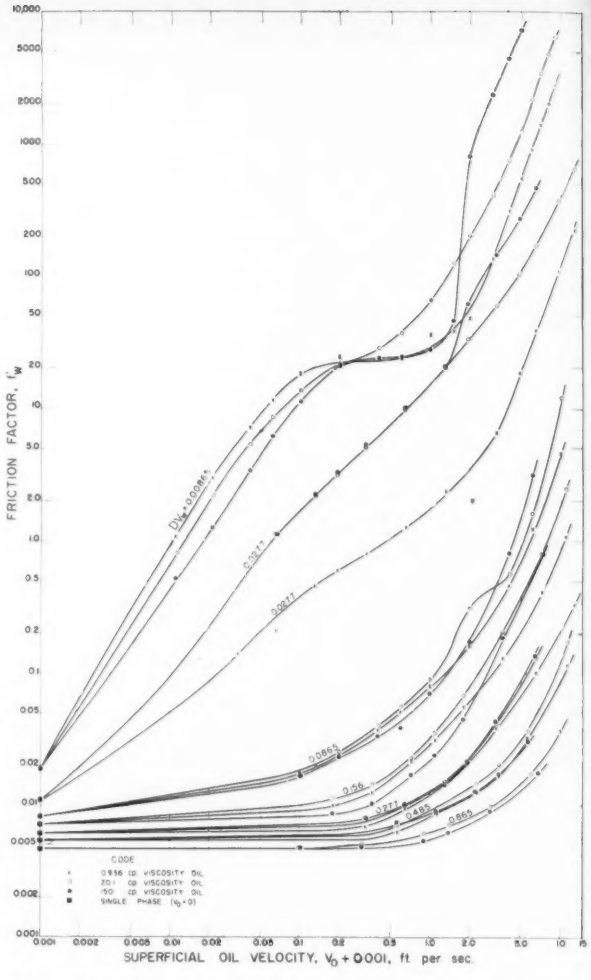

Figure 14—Effect of viscosity on two phase friction factors.

extreme that the average velocity of the oil exceeds that of the water by some 0.2 ft./sec.

Holdup ratios below unity at high volume fractions of oil were clearly observed for the 20.1 and the 150 centipoise oil although not for the 0.936 centipoise oil. This is undoubtedly due to the concentration of the water in the central part of the flow section where the local velocities are higher. The region of rapid decrease in holdup ratio with increasing oil fraction correlates with the transition from a more or less continuous water phase to a more or less continuous oil phase.

Pressure Drop

Figures 11, 12 and 13 show the two phase friction factors, f_W' plotted versus DV_W at different constant superficial oil velocities. The dashed lines on these figures are estimated by interpolation based upon cross plots at constant superficial oil velocity. It is to be noted that while the upper portions of the lines at all water velocities are nearly straight for the 093.6 centipoise oil, an increasing degree of curvature develops with increasing viscosity. This appears to be a very real effect. In all cases the friction factor lines tend toward the single phase line with increase in DV_W.

The effect of the viscosity of the oil phase is best shown in Figure 14 which represents a cross plot of the data of all of Figures 11, 12 and 13. At DV_W values of 0.08 and higher there appears to be no significant effect of oil viscosity below superficial oil velocities of 2 ft./sec. and only a modest effect beyond that. At lower values of DV_W the variation of friction factor with oil viscosity is not entirely systematic but the higher viscosity oils definitely show higher friction factors at oil velocities above 2 ft./sec. as would be expected when the oil becomes the continuous phase. At superficial oil velocities below about 1 ft./sec. the water phase is more or less continuous (bubbles, drops and slugs of oil in water) and no effect of oil viscosity would be expected. No significant effect is observed except at DV_W values of 0.0277 and 0.00865. Whether the effect shown under these two conditions is real is not known. The situation

is somewhat confused also by the difference in interfacial tension between the two high viscosity oils (approximately 50 dynes per cm.) compared with the low viscosity oil (approximately 35 dynes per cm.).

Conclusions

The study of the vertical flow of oil water mixtures reveals that the unit pressure drop versus oil-water ratio curves and the flow patterns are similar to those observed in the vertical flow of gas liquid mixtures, the oil phase behaving as would a high density gas. Holdup ratios are also generally similar but lower in magnitude and trending below unity for the high viscosity oils. Superficial friction factors correlated in terms of the superficial velocities of the two phases indicate no real effect of oil viscosity except under conditions where the oil phase is continuous.

Nomenclature

C_o = volume fraction of oil, dimensionless
D = tube diameter, ft.
f_L' = superficial two phase friction factor based on the liquid or reference phase, dimensionless
f_W' = superficial two phase friction factor based on the water phase, dimensionless
g_c = dimensional conversion factor $\frac{\text{lb. } (m) \text{ ft.}}{\text{lb. } (f) \text{ sec.}^2}$
H_R = holdup ratio, dimensionless
R_m = gas-liquid (or oil-water) mass ratio, lb./lb.
R_t = gas-liquid (or oil-water) volume ratio, cu. ft./cu. ft.
v_L = specific volume of the liquid or reference phase, cu. ft./lb.
v_w = specific volume of water, cu. ft./lb.
V_L = superficial velocity of the liquid or reference phase, based on the total tube cross section, ft./sec.
V_W = superficial water velocity based on the total tube cross section, ft./sec.
V_L' = average liquid phase velocity, ft./sec.
V_G' = average gas phase velocity, ft./sec.
V_o = superficial oil velocity, based on the total tube cross section, ft./sec.
V_S = slip velocity, ft./sec.
$\left(\frac{\Delta P}{\Delta X}\right)$ = unit total pressure drop, lbs./sq. ft./ft. of tube
$\left(\frac{\Delta F}{\Delta X}\right)_L$ = unit head loss due to friction and irreversibilities, ft. of liquid or reference phase/ft. of tube

References

(1) Brown, R. A. S., Sullivan, G. A., and Govier, G. W., Can. J. Chem. Eng., **38,** 62 (1960).
(2) Govier, G. W., Radford, B. A., and Dunn, J. S. C., Can. J. Chem. Eng., **35,** 58 (1957).
(3) Govier, G. W., and Short, W. L., Can. J. Chem. Eng., **36,** 195 (1958).
(4) Calvert, S., and Williams, B., A.I.Ch.E. Journal, **1,** 78 (1955).
(5) Cromer, S., and Huntington, R. L., Trans. Am. Inst. Mining Met. Eng. Petrol Development and Technology, **136,** 79 (1940).
(6) Davis, G. I., Jr., and Weidner, C. R., Univ. Wisconsin, Bull. 450 (1911).
(7) Galegar, W. C., Stovall, W. B., and Huntington, R. L., Pipe Line Industry, **4,** 38 (1956).
(8) Hughmark, G. A., Ph.D. Thesis in Chem. Eng., Louisiana State Univ. (1959).
(9) Moore, T. V., and Wilde, H. D. Jr., Trans, Am.. Inst. Mining Met. Eng. Petrol Development and Technology, **92,** 296 (1931).
(10) Nowels, K. B., Trans. Am. Inst. Mining Met. Eng. Petrol Development and Technology, **98,** 401 (1932).
(11) Poettmann, F. H., and Carpenter, P. G., Drilling and Production Practice, A.P.I., 257 (1952).
(12) Uren, L. C., Gregory, P. P., Hancock, R. A., and Feskow, G. W., Trans. Am. Inst. Mining Met. Eng. Petrol Development and Technology, **86,** 209 (1930).
(13) Weiss, D. H., M.S. Thesis in Mech. Eng., Illinois Inst. Tech. (1952).
(14) Finnigan, J. W., Ph.D. Thesis in Chem. Eng., Oregon State Coll. (1958).
(15) Charles, M. E., M.Sc. Thesis in Chem. Eng., Univ. Alberta (1959).
(16) Charles, M. E., Govier, G. W., and Hodgson, G. W., "The Horizontal Pipeline Flow of Equal Density Oil-Water Mixtures", Can. J. Chem. Eng., **39** (1961).
(17) Russell, T. W. F., Hodgson, G. W., and Govier, G. W., Can. J. Chem. Eng., **37,** 9 (1959).
(18) Sullivan, G. A., M.Sc. Thesis in Chem. Eng., Univ. Alberta (1958).
(19) Wood, R. K., M.Sc. Thesis in Chem. Eng., Univ. Alberta (1960).

★ ★ ★

Some Rheological Parameters of Clays and Their Thixotropic Behavior[1]

A. S. YALCIN[2] and R. McINTOSH[3]

Rheological characteristics and thixotropic behavior of four clay minerals belonging to different types of morphology and lattice structure were investigated.

Clay-water samples were prepared at about their liquid limits and the testing was accomplished by unconfined compression applied at different rates of deformation.

From the stress to strain rate relationships the yield value was determined as an intercept on the stress axis at zero rate of strain, and the slope gave the viscosity coefficient.

Regain of strength or thixotropic character of the samples was evaluated in terms of the viscosity and yield values at various periods of aging.

The influence of temperature on the aging process was studied using attapulgite at three temperatures, 21°C., 36°C., 51°C.

The activation energy of the process of aging for attapulgite was calculated using both viscosity coefficients and ultimate yields. The values were within experimental uncertainty for the two sets of data and it was thereby concluded that changes of these parameters were due to a single reaction. The activation energy was found to be 9.4 kcal mole^{-1}, which suggests a physical rather than a chemical change.

The usual engineering method of establishing the 'strength' of a clay-water mixture is to determine its compressive or torsional shearing strength. The former is obtained by unconfined compression tests[(1)] and the latter by vane tests[(2)]. The basis of both methods is the application of a shearing stress at some arbitrary and constant rate of strain, so that strengths thus determined may be dependent upon the particular rate of strain chosen. One objective of this investigation was to obtain a more complete description of the systems than afforded by 'strength' tests, and this may be developed by studying the systems over a range of rates of strain. Such an examination also permits the evaluation of the viscosity coefficient and the yield value which form the basis of the rheological description of viscous fluids[(3)].

Sensitivity of a clay-water sample is normally defined as the ratio of its undisturbed and disturbed strengths ascertained under the arbitrary conditions of testing noted above. The reduction of strength is attributed to the destruction of bonds between clay particles or aggregates. It is also known that strength is regained on resting or aging the sample[(1)], and such materials are classified as thixotropic. Thus the evaluation of sensitivity should consider the factors of shear stress, the rate of strain and the rate of recovery of the strength. Regain of strength is of practical importance and is estimated by the 'inverted tube test'[(4)]. A preferred procedure would be one based upon the observation of the rate at which the system regains its strength, and until a more extensive knowledge of the behavior of the systems is available the best criteria for classifying the sensitivity of these materials can hardly be considered as established. A second objective of this work was therefore, to obtain data of viscosity and yield value in order to observe the regain of sensitivity more completely. The present investigation has involved the examination of attapulgite and to a lesser extent montmorillonite, illite and kaolinite by means of the unconfined tests employed using a variety of rates of strain. The thixotropic character of the clay mineral was assessed by following the rates of establishment of yield values and the rate of increase of the viscosity coefficient. The aging of the samples of attapulgite was carried out at three temperatures. All samples were of fixed water content corresponding approximately to the liquid limit.

The results immediately showed the influence of rate of strain, and have produced reliable values of viscosity coefficient and of yield value. The temperature coefficient of the rate of increase of viscosity coefficient and of yield have been determined and were the same within experimental error. Although the mechanism by which viscosity and yield increase has not been discovered thereby, it seems clear that the same process leads to the establishment of the value of both viscosity coefficient and yield. Evidence of the flow of free water during compression at low rates of strain has been obtained for freshly prepared samples.

Finally, comparisons are made of the behavior of the clays as ascertained by these more exhaustive tests and the behavior as assessed by the usual tests.

Materials

The clays were supplied by Ward's Natural Science Establishment, Rochester, New York. The properties of the clays were obtained from Project Report No. 49, American Petroleum Institute (1950). A brief description of their purity and the source from which they were obtained follows:

1. Kaolinite
   Purity: 95%
   Impurities: quartz, orthoclase, limonite
   Source: Macon, Georgia

2. Illite
   Purity: 90%
   Impurities: pyrite, quartz, plagioclase, calcite
   Source: Morris, Illinois

[1]*Manuscript received July 16, 1960; accepted November 11, 1960.*
[2]*Graduate student and holder of a research assistantship from the Ontario Joint Highway Research Program.*
[3]*Department of Chemistry, University of Toronto, Toronto, Ont.*
Based on a thesis by A. S. Yalcin in partial fulfillment of a Ph.D. degree. Joint contribution of the Departments of Civil Engineering and Chemistry, University of Toronto, Toronto, Ont.

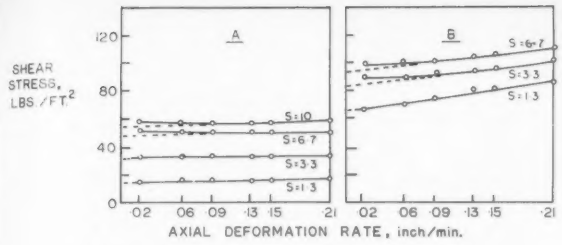

Figure 1—Relationship of stress and unconfined compressional deformation rate at room temperature.
A Kaolinite W = 49.0 ± .4
LL = 50.5 no aging
B Kaolinite W = 49.0 ± .4
LL = 50.5 14 days aging at room temperature.

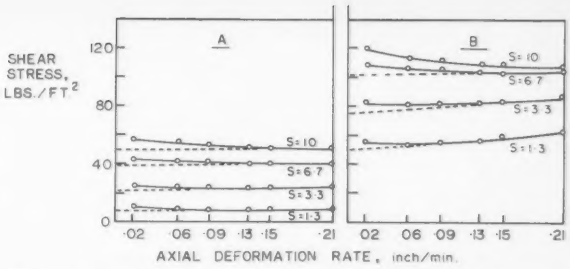

Figure 2—Relationship of stress and unconfined compressional deformation rate at room temperature.
A Illite W = 52.0 ± .4
LL = 58.0 no aging
B Illite W = 52.0 ± .4
LL = 58.0 14 days aging at room temperature.

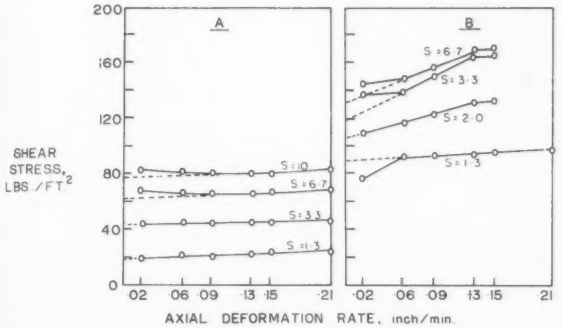

Figure 3—Relationship of stress and unconfined compressional deformation rate at room temperature.
A Montmorillonite W = 102.0 ± .5
LL = 103.5 no aging
B Montmorillonite W = 102.0 ± .5
LL = 103.5 14 days aging at room temperature.

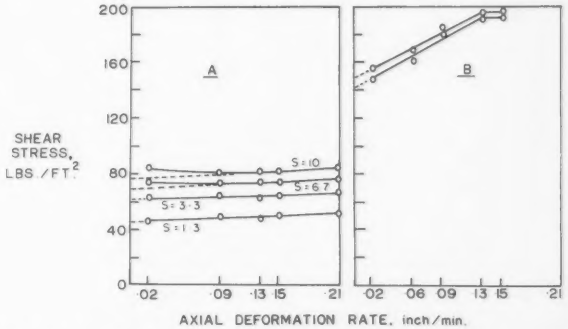

Figure 4—Relationship of stress and unconfined compressional deformation rate at room temperature.
A Attapulgite W = 163.0 ± .7
LL = 200 + no aging
B Attapulgite W = 163.0 ± .7
LL = 200 + 14 days aging at room temperature.

3. Montmorillonite
   Purity: 96%
   Impurities: ferro-magnesium minerals, quartz, sericite, carbonates
   Source: Chambers, Arizona
4. Attapulgite
   Purity: 99%
   Impurities: quartz, limonite
   Source: Attapulgus, Georgia
5. Asphaltic Mixture
   Source: Imperial Oil Limited, Sarnia, Ontario

Experimental

Unconfined Compression Test at Various Rates of Strain

A Karol-Warner standard unconfined compression machine was modified to permit its operation at constant rates between 0.01 in./min. and 0.21 in./min. A stress-strain curve was obtained for a given sample at some fixed rate of strain, and by repeating such tests on similar samples at various rates of strain, it was possible to synthesize plots of stress vs rate of strain for given values of strain or deformation. Strain, and hence rate of strain, had to be converted from axial strain to that along the shearing plane, which was taken to be at 45° from the direction of application of the stress. Assuming small strain and no volume change of the sample, rate of strain was found from the relation,

$$r = \frac{1}{2t}\left(\frac{\pi}{4} - \tan^{-1}\frac{2(1-S)}{2+S}\right)$$

where S is the axial strain and t the time in minutes.

The primary data of shear stress vs rate of axial strain are shown in Figures 1, 2, 3, 4. However, in order to obtain the values of the viscosity coefficient, the rate of strain along the slip plane must be known. The conversion of rate of axial strain to rate of strain along the shear plane was effected by means of the formula above. The assumption was also made that the shear stress could be taken as one half the axial stress. This is in conformity with the usual Mohr analysis relating shear stress to the principal stress. For the size of sample employed, namely 3.0 inches, the conversion factor to obtain viscosity co-efficient in poises from the slopes of such plots as Figures 1, 2, 3, 4 was 1.3×10^7.

From the slope of plots of stress vs rate of strain (for fixed strain) the viscosity coefficient of the sample was obtained. On extrapolation of such plots back to the stress axis at zero rate of strain, the yield value was obtained. As will be discussed more fully later, the yield value was a function of the strain, and reached a maximum value designated as the 'ultimate yield value' at a fairly large strain, for example, 5%.

The instrument was calibrated by using a sample of asphalt obtained from Imperial Oil Limited, Sarnia. It was designated as having a penetration between 85 and 100. Such asphaltic materials have been examined using other methods[5], and have viscosity coefficients of the order of 1×10^7 poises. The value obtained in the instrument used by us was 1.15×10^7 poises.

Preparation and Aging of the Clay Samples

The clay samples were prepared close to their 'liquid limit' consistency and placed in brass cylinders of 4.0 in. long and 1.4 in. in diameter. Each cylinder was closed at the ends by wax paper and rubber discs which were held in place by a wooden

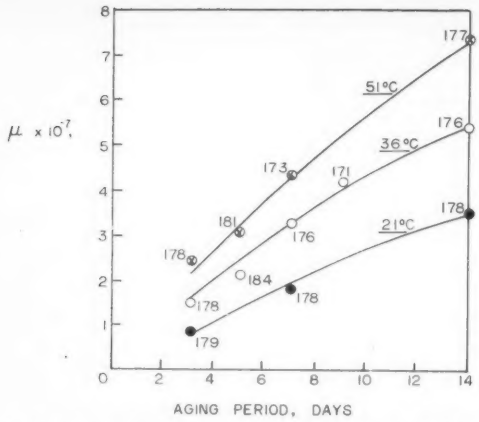

Figure 5—Variation with time of viscosity co-efficient of attapulgite aged at different temperatures. Figures indicate water/solid in % by weight.

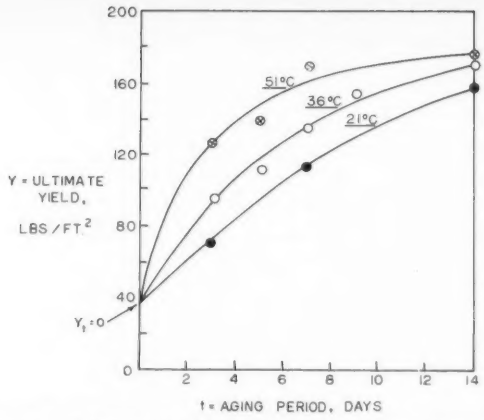

Figure 6—Ultimate yield values developed in attapulgite aged at different temperatures.

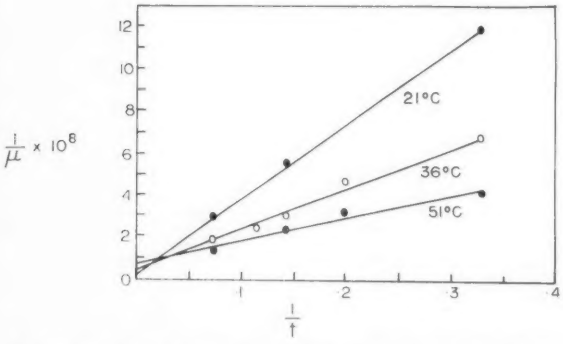

Figure 7—Plot of the reciprocal of viscosity co-efficient and reciprocal of time for attapulgite aged at different temperatures.

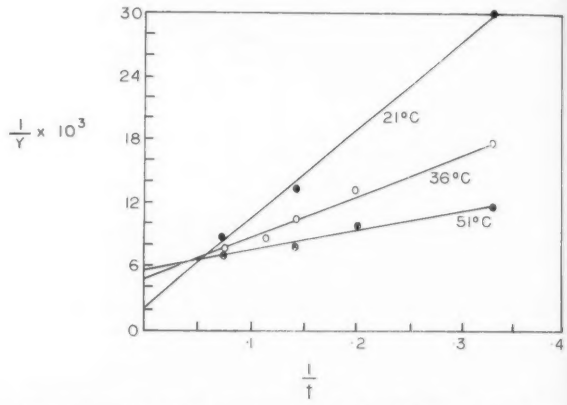

Figure 8—Plot of the reciprocal of the difference of yield value and reciprocal of time for attapulgite aged at different temperatures.

frame. Thus the water content of the samples remained constant. Storage was carried out at 21°C., 36°C., 51°C. for attapulgite. After storage and removal from the brass cylinders samples of the four types of mineral listed above were examined by the unconfined compression test, but the majority of the tests were performed using attapulgite. The temperature coefficient of the process of aging was studied adequately only for attapulgite. Water content of the samples was determined by oven drying after the compression tests were completed.

Results

Stress versus rate of strain plots for the four minerals are shown in Figures 1, 2, 3, 4. In each case a freshly prepared sample and a sample which has aged for 14 days are compared. In Figures 5 and 6 the viscosity and yield as functions of time are represented for aging at several temperatures in case of attapulgite. The yield values are dependent upon the strain, and ultimate yields are recorded. In order to obtain the initial rate of increase of viscosity at any given temperature, the reciprocal of viscosity was plotted against the reciprocal of time, and the linear plots so derived employed in an obvious manner to obtain the limiting value of $d\mu/dt$ at $t = 0$ (see Figure 7)*.

*Because different batches of the clays varied to some extent in water content, the scatter of the viscosity data was greater than the uncertainty of the physical measurement. This error was pronounced in unaged samples and made necessary the evaluation of the limiting slope at time = 0 from data obtained after a minimum period of aging of three days. Some of the scatter of Figure 5 is also to be attributed to this cause and moisture contents have been indicated on the plot for this reason.

The necessity of obtaining the initial value is discussed in a later paragraph dealing with the determination of the activation energy of the process. A somewhat similar treatment was accorded the data dealing with ultimate yield. Because yield values established due to the aging process alone were desired, the ultimate yield of a freshly prepared sample was subtracted from the ultimate yield value of the aged sample, and the difference of these values was employed to obtain the linear plots shown Figure 8. Again the rate of change of ultimate yield at $t = 0$ was obtained. A comparison of the behavior of the four minerals for an aging temperature of 21°C. and period of 14 days is given in Figure 9 in the form of yield vs axial strain plots.

The data summarized in these Figures and in Table 1 reveal the following facts:

(1) A viscosity coefficient which varies with time and temperature of aging of the sample may be deduced from the stress vs rate of strain curves and is independent of strain up to 4% strain. An exception to this statement for freshly prepared samples, low rates of strain, and large strains must be noted. In these circumstances a negative slope of the plot is revealed which we attribute to flow of free water. At higher rates of strain and after aging, the plots usually become normal, but longer periods of aging are necessary for this to occur with montmorillonite and illite. The difference in behavior of freshly prepared samples and aged samples confirms the finding of Day[6] on the changing state of the contained water with aging. The normal character of the curve at high rates of strain suggests that insufficient time is available for the drainage to occur at the higher rates of strain.

TABLE 1

TABLE SHOWING RANGE OF STRAIN GIVING CONSTANT VISCOSITY COEFFICIENT*

Aging Period	Mineral Type	Viscosity Coeff. (10^6)	Strains (%)							Average μ
			.67	1.33	2.00	2.67	3.33	4.00	6.67	
14-day	Kaolinite	μ		*8.5*	*9.0*	*9.5*	*9.5*	*9.0*	*9.0*	9.1
14-day	Illite	μ	*6.0*	*5.5*	*6.3*	*5.7*	*5.4*	2.9	2.0	5.8
14-day	Montmorillonite	μ			26.0	50.0	44.0		40.0	
14-day	Attapulgite	μ	*40.0*	*60.0*	*50.0*	*50.0*				50.0

*Italic figures show range of strain values for which μ is constant within experimental reproducibility.

(2) A yield value may be obtained by extrapolation of the plots to zero rate of strain. This yield value depends upon the strain to which the sample is subjected, and as Figure 9 shows, appears to have a zero value at zero strain. Yield values which show such variation with strain are well known for plastic materials[3] and can be attributed to rearrangements of the particles as strain is increased. The fact that curves of yield vs strain become steeper on aging shows that a smaller degree of rearrangement occurs for a given stress as the aging process continues, and that shearing of bonds and plastic flow occur at higher stresses and smaller strains.

(3) Differences of the behavior of the four types of mineral are shown in Figure 9. Among these may be noted the large gain of yield value in attapulgite and the fact that it is achieved for small values of strain. In contrast with attapulgite, illite does not develop an ultimate yield value even at 7% strain. These characteristic differences are undoubtedly connected with the shape of the mineral particles and the lattice structure, but no detailed speculation concerning this appears warranted at this time.

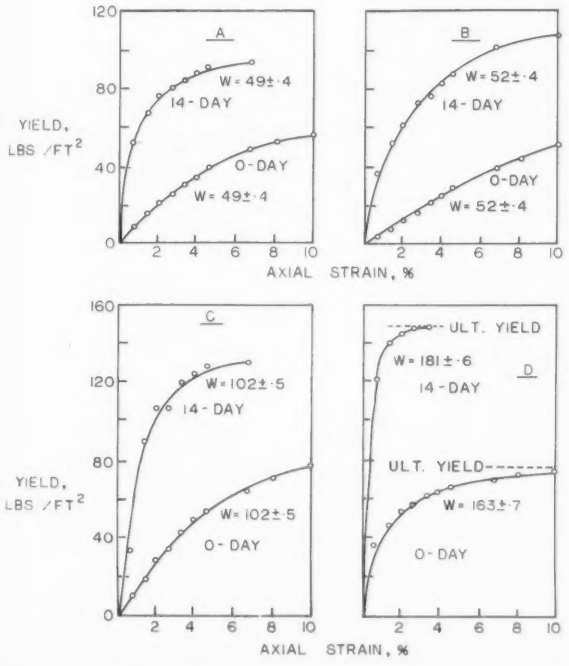

Figure 9—Effect of aging at 21°C. on the yield value as a function of axial strain.
A Kaolinite B Illite C Montmorillonite D Attapulgite.

(4) The rate of increase of viscosity coefficient of attapulgite is dependent upon the temperature. The final value of viscosity coefficient is perhaps dependent upon the temperature at which the aging was carried out, as is suggested by the different intercepts of the plots of Figure 7. The experimental accuracy is insufficient to state this with certainty, but the possibility is raised that aging at a low temperature may bring about a higher viscosity in the clay than is obtained by aging at higher temperatures.

(5) The rate of increase of ultimate yield is also a function of temperature and the remarks made concerning viscosity coefficient may be restated in connection with the yield values (see Figure 8).

The Activation Energy of the Aging Process

As was pointed out earlier, the initial rates of increase of viscosity coefficient and of yield were determined in order to find the activation energy of the process or processes which cause the variation of these properties. It was assumed in the treatment of the data that $d\mu/dt = k\pi C_i^j$ where k is the specific rate constant multiplied by a coefficient relating concentration of product with viscosity coefficient, π designates the product of the concentrations C_i of each species, and the overall order of the reaction would be given by sum of the j values. Since the concentrations and the powers of concentration were unknown, comparisons for different temperatures had to be made under identical conditions of concentration. This would only

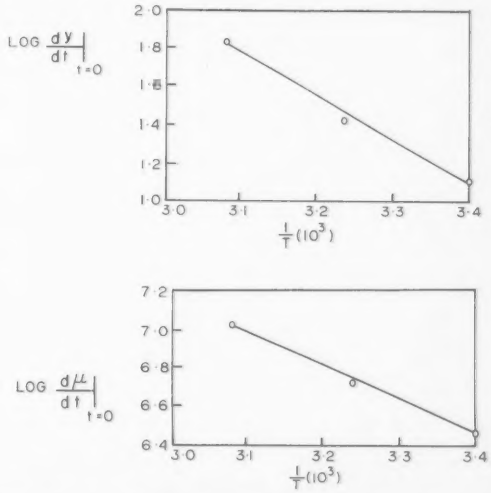

Figure 10—A Plot to obtain activation energy of process causing increased viscosity; B Plot to obtain activation energy of process causing increased yield.

be assured in a freshly prepared sample, so that the value of $(d\mu/dt)_{t=o}$ was required. On this basis,

$$\left.\frac{d\mu}{dt}\right|_{T_1=o} = k_{T_1}\pi C_i^j$$

$$\left.\frac{d\mu}{dt}\right|_{T=o} = k_T\pi C_i^j$$

Assuming the usual form $k_T = Ae^{-E}/RT$, and that the pre-exponential factor A is insensitive to temperature, one obtains,

$$ln\left.\frac{d\mu}{dt}\right|_{T_1=o} - ln\left.\frac{d\mu}{dt}\right|_{T=o} = -\frac{E}{R}\left[\frac{1}{T_1} - \frac{1}{T}\right]$$

It must be remembered here that the coefficient of viscosity inherent in the k's cancels, because viscosity coefficient is measured at the same temperature in each experiment. The activation energy is obtained from the slope of Figure 10(a) and amounts to 8.7 kcal mole^{-1}. An identical treatment was employed with the values of the ultimate yield at time t less the ultimate yield at time zero, and the activation energy of 10.0 kcal mole^{-1} follows from the slope of Figure 10(b). These two values do not differ in view of the limited data and the procedure used in evaluating the energy term. Thus the activation energy is assigned the mean value of 9.4 kcal mole^{-1}. Two conclusions may be derived, namely that there is only one process involved in the aging and it causes both increased viscosity and yield, and that no very strong bonds must be broken to bring about the reaction. This latter conclusion suggests a physical process (such as diffusion) rather than a chemical one.

Since this work was completed a very extensive and valuable paper by J. K. Mitchell has appeared in the Proceedings of the American Society of Civil Engineers[7]. Mitchell employed a mixture of 25% Wyoming bentonite and 75% sand with a water content of 24%. He determined the stress required to cause a given degree of strain after various times of aging at several temperatures. This stress was plotted against the logarithm of the time and the slope of the linear section was taken as a measure of the rate constant. On this basis, he reports an activation energy varying from 3900 to 1900 kcals mole^{-1}, and compares this with the activation energy for the viscous flow of water reported by Glasstone, Laidler and Eyring[8]. The activation energy obtained by us is considerably higher. The difference may be due to the fact that different systems were studied, but it may also be due to the very different procedures employed in analyzing the data. The treatment presented here is based upon the usual definition of a specific rate constant, and is therefore to be preferred.

Remarks Concerning Current Methods of Testing

It has been shown in this investigation that the properties of clay mixtures are dependent upon the rate of strain which is employed in the test. Thus the so called 'strength' and 'sensitivity' of the samples are arbitrary figures. Even for purposes of comparison among clays it is not sufficient to specify that a given rate of strain be employed, since the effect of this variable differs from one type of clay to another. On the other hand we have demonstrated that viscosity coefficient is independent of strain and rate of strain over wide limits. Using the viscosity attained at very long times in comparison with the value of a fresh sample provides a measure of regain of strength.

Yield values have been shown to be dependent upon the strain, but this disadvantage may be overcome by estimating the value of the ultimate yield. Ultimate yield can then be compared for freshly prepared and aged samples.

Finally, although reasonable hypotheses concerning the mechanism which bring about increased viscosity and strength in clays, e.g., Mitchell[7] have been put forward on several occasions, it seems that more experiments designed to measure clearly defined rheological properties such as yield or viscosity are needed before these hypotheses may be adequately tested.

Nomenclature

A = the usual pre-exponential factor multiplied by a coefficient relating concentration of product and viscosity coefficient. Dimensions as for k.
C_i = concentration of reactant i in moles litre^{-1}.
E = activation energy in calories mole^{-1}.
k = specific rate constant in appropriate concentration units and t^{-1}, multiplied by coefficient relating concentration of product and viscosity coefficient.
LL = liquid limit, ratio of weight water to weight dry solids x 100.
μ = viscosity coefficient in poises.
r = rate of strain along shear plane (t^{-1}).
R = gas constant, 1.987 calories mole^{-1} degree^{-1}.
S = axial strain.
t = time.
T = degrees Kelvin.
W = ratio of weight of water to weight of dry solids x 100.

Acknowledgement

We acknowledge with pleasure our indebtedness to W. L. Sagar of the Department of Civil Engineering for providing the facilities required for this investigation.

References

(1) Moretto, O., 'Effect of Natural Hardening on the Unconfined Compression Strength of Remolded Clays'. Proc. 2nd Intern. Conf. Soil Mech., Vol. 1, 1948.
(2) Skempton, A. W., Northey, R. D., 'The Sensitivity of Clays'. Geotechnique, Vol. 3, 1952.
(3) Scott-Blair, G. W., 'A Survey of General and Applied Rheology'. Pitman, London, 1945.
(4) Ackermann, E., 'Thixotropy and Flow Properties of Fine-Grained Soils'. Reprint from Geol. Runds., Vol. 36, 1948. (Trans. by H. A. G. Nathan, N.R.C., Ottawa, 1950).
(5) Pfeiffer, J. Th., 'The Properties of Asphaltic Bitumen'. Elsevier Publ. Co., 1950.
(6) Day, P. R., 'Effect of Shear on Water Tension in Satured Clay'. (As referred to by J. K. Mitchell). Annual Reports, I, II. Western Regional Res. Proj. W-30, 1954, 1955.
(7) Mitchell, J. K., 'Fundamental Aspects of Thixotropy in Soils'. Proc., Am. Soc. Civil Engrs. SM3, June 1960.
(8) Glasstone, S., Laidler, K., Eyring, H., 'Theory of Rate Processes'. McGraw-Hill, 1941.

★ ★ ★

Dynamic Behavior of a Continuous Stirred-Tank Reactor[1]

RICHARD I. KERMODE[2] *and WILLIAM F. STEVENS*[2]

Solution of the non-linear differential equations of a continuous flow stirred-tank reactor, with a first-order reacting system, has been accomplished by the use of the analog computer. The three common modes of control have been programmed on the computer and, while controlling temperature or composition by means of the adjustment of cooling water flow rate, the regions of stability have been determined for various values of the controller constants. These results have been compared to those obtained by applying the root-locus method to the linearized forms of the differential equations previously derived.

The general theory of a continuous flow stirred-tank reactor, which contains a material undergoing a reaction of the type A → Products, has been discussed by van Heerden[1] and others. Some work has been done using the analog computer to simultaneously solve linearized forms of the mass and heat balances and the reaction velocity constant equation and draw a phase plane plot of the system[2]. Recently the root-locus method has been applied to a hypothetical system, being controlled by the three normal modes of control, to determine its stability[3]. As a natural extension of the above, this paper reports the solution of the non-linear differential equations for a first order system, and the simulation of the system with various modes of control on the analog computer. The computer results are then compared with the theoretical limits of stability as predicted by the root-locus method.

System Equations

The differential equations for the heat and mass balances were written as follows:[4]

$$\frac{dT}{dt} = -\frac{kX\Delta H}{C_p} + \frac{Q(Ti - T)}{V} - \frac{UA\Delta T_m}{V\rho C_p} \quad \ldots\ldots(1)$$

$$\frac{dX}{dt} = \frac{Q}{v}(Xi - X) - kX \quad \ldots\ldots(2)$$

The reaction velocity constant k was assumed to be predicted by the Arrhenius equation.

$$k = A'e^{-E/RT} = f(T) \quad \ldots\ldots(3)$$

ΔTm was solved for by a heat balance on the heat exchanger, assuming an arithmetic mean ΔT. [4] In its final form it appears below.

$$\Delta Tm = \frac{T - T_c}{1 + 1/F} \quad \ldots\ldots(4)$$

where $\frac{1}{F} = \frac{UA}{2Q_c\rho_c C_c}$

Substitution of the assumed values for ΔH, Q etc. produced the final form of the differential Equations (5) and (6).

$$\frac{dX}{dt} = 18Xi - 18X - kX \quad \ldots\ldots(5)$$

$$\frac{dT}{dt} = 333kX + 18(Ti - T) + 8.333\theta(t)(T_c - T) \quad \ldots\ldots(6)$$

$$\theta(t) = \frac{1}{1 + 1/F}$$

Root-Locus Analysis

At this point the root-locus method for determining stability was applied. First all nonlinear terms were linearized using a Taylor expansion. As an example, the term $-.25f(T)X$ was linearized as follows:

$$-.25f(T)X = -.25\left\{f(T_s)X + \frac{X_s f(T_s)ET}{RT_s^2} - \frac{X_s f(T_s)E}{RT_s}\right\} \quad \ldots\ldots(7)$$

The units on Equations (5) and (6) are lb. moles/ft.^{3}hr., and it was decided to change the time units to seconds and then to speed up the machine solution by a factor of 36. Dividing both sides of the equation by 3600 converts the units to lb. moles/ft.^{3}sec. The substitution of $t = 36\tau$; $dt = 36d\tau$ into the equation speeds up the solution by a factor of 36. After linearization and conversion of units the Laplace transformed mass balance became:

$$25p\overline{X} = \alpha\overline{X} + \beta\overline{T} \quad \ldots\ldots(8)$$

where $\alpha = -\{4.5 + .25f(T_s)\}$

$$\beta = \frac{-.25X_s f(T_s)E}{RT_s^2}$$

Applying the same procedure to the heat balance produced

$$.1p\overline{T} = .333f(T_s)\overline{X} + R\overline{T} + H\overline{Q}_c$$

$$R = +1.333\beta - .018 - .00833\phi$$

$$H = 0.00833B(T_c - T_s)$$

$$B = (\delta - \phi\delta)$$

$$\phi = \frac{8.64Q_{cs}}{1 + 8.64Q_{cs}}$$

$$\delta = \frac{8.64}{1 + 8.64Q_{cs}}$$

[1]*Manuscript received June 15, 1960; accepted January 31, 1961.*
[2]*Northwestern University, Evanston, Ill., U.S.A.*

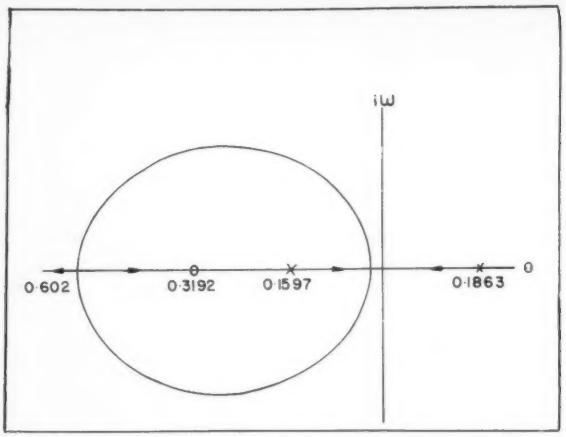

Figure 1—Proportional control on temperature.

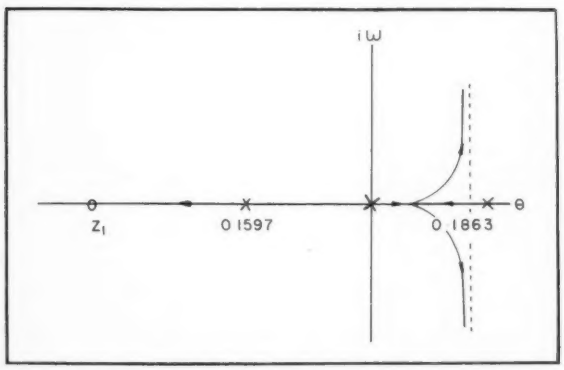

Figure 3—Proportional plus integral control on concentration.

Solving Equations (8) and (9) for $\overline{X}$ and $\overline{T}$ and substituting the values of Q_c, T_s, etc. at the unstable point gave the following results:

$$\overline{X} = \frac{.02541\overline{Q}_c}{(p - .18634)(p + .15970)} \quad \ldots\ldots(10)$$

$$\overline{T} = -\frac{(14.62p + 4.668)\overline{Q}_c}{(p - .18634)(p + .15970)} \quad \ldots\ldots(11)$$

The following is an example of the application of the root-locus method to the analysis of a control system. In this case, Q_c was adjusted by the output of a proportional controller, which was measuring and controlling the outlet temperature of the tank T. The open loop system transfer function was written as follows:

$$G_{pT} = \frac{\overline{T}}{\overline{Q}_c} = \frac{(14.62p + 4.668)}{(p - .18634)(p + .15970)} \quad \ldots\ldots(12)$$

Next the loop was closed and the transfer function below resulted:

$$\left(\frac{G}{1+G}\right)_{pT} = \frac{(14.62p + 4.668)K_p}{p^2 + (14.62K_p - .02664)p - .02976 + 4.668K_p} \quad \ldots(13)$$

The root-locus diagram corresponding to this expression is shown in Figure 1. This diagram indicates that the system should be stable for all $K_p > .00639$. Application of the same method to the case of proportional control with concentration as the controlled variable, indicated that this system was unstable for all values of K_p. This is apparent from Figure 2, the root-locus plot for this case.

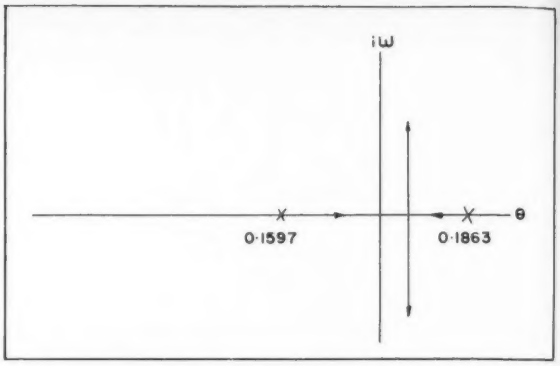

Figure 2—Proportional control on concentration.

Next, proportional plus integral control was considered with composition being controlled. The root-locus plot, Figure 3, shows that the system should be unstable for all values of K_p and K_I. Some comment should be made concerning this root-locus plot. Since the curve is a function of Z_1 the intersection of the vertical asymptote with the real axis will approach the breakaway point of root-locus line as Z_1 approaches 0.1597. With all three modes of control the root locus approach indicated that the system should be stable when composition was being controlled. The general criteria for stability, using all three modes of control simultaneously, are as follows. The system should be stable if $K_p > 1.171$, $K_R > 1.048$, and $K_I < .02541K_pK_R - .02664K_p - .02976K_p + .03120$. Addition of rate and integral modes when controlling on temperature will not change the stability, but will affect the response of the system to any given upset.

Analog Computer Simulation

One of the advantages of the analog computer simulation is that it need not be expressed in real time. It was decided to speed up the computer program by a factor of 36. This seemed to work out satisfactorily and saved essential time since less than two minutes of machine time were equivalent to one hour of actual process operation.

Generation of the exponential on the computer proved tedious, but it was finally accomplished. Several methods were available for expressing an exponential. The use of potentiometers to represent straight line approximations of the curve over the entire range has the advantage that it can be made almost as accurate as desired simply by using more potentiometers. It has the disadvantage that loading effects cannot be neglected, so the setting of the potentiometers at the proper voltages is difficult. Use of an $x - y$ plotter is also a good method. However, it was decided to attempt solution directly within the machine as follows:

$$\frac{dk}{dT} = \frac{Ek}{RT^2} \quad \ldots\ldots(14)$$

If dk/dT were available and could be integrated by the machine this would provide an acceptable method for producing k. The independent machine variable is time (t) not temperature (T), so the familiar transformation

$$\frac{dk}{dt} = \left(\frac{dk}{dT}\right)\left(\frac{dT}{dt}\right)$$

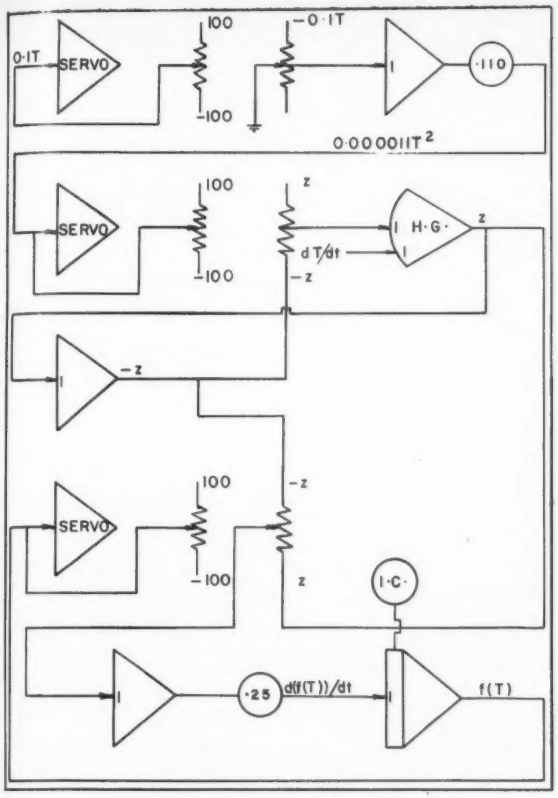

Figure 4—Exponential program.

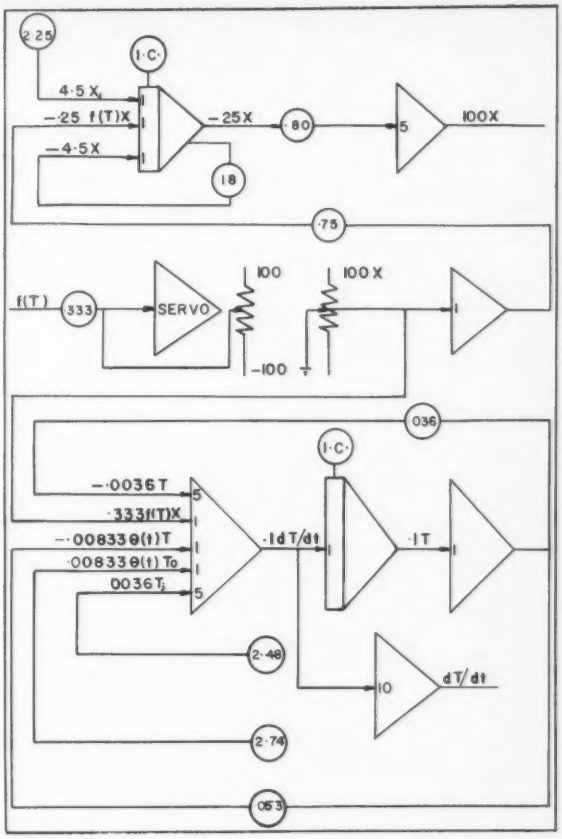

Figure 5—System equations program.

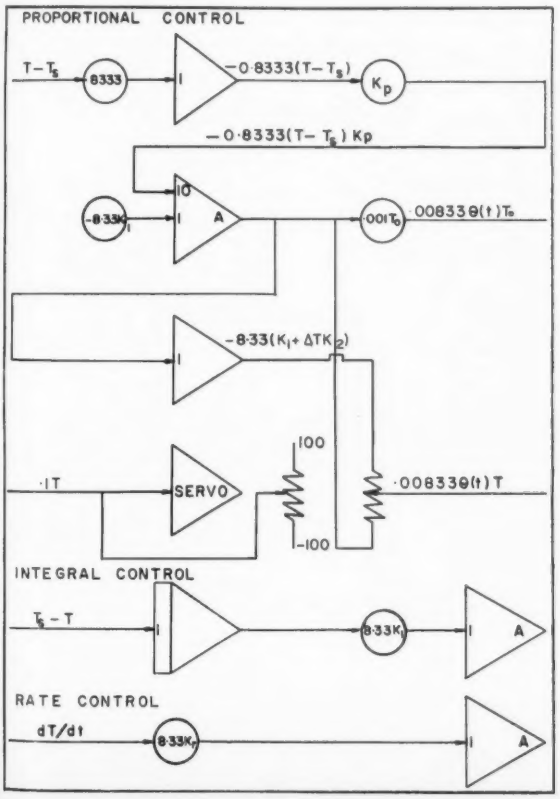

Figure 6—Controller programs.

was used. After substitution in Equation (14) the following equation resulted and was programmed on the computer:

$$\frac{dk}{dt} = \frac{Ek}{RT^2}\left(\frac{dT}{dt}\right) \quad \ldots\ldots\ldots\ldots\ldots\ldots (15)$$

This looked very straightforward since both T and dT/dt were readily available from other parts of the problem. The entire exponential program is shown in Figure 4. Many possible sources of trouble and error were seen in the proposed program, however. First, two multiplications and one division were necessary. This means that three mechanical servo multipliers in series were required. A servo driving a servo directly usually presents stability problems, and this program was no exception. Second, the division circuit used required a high gain amplifier which also produced noise, and was not very stable. Finally, the large range of values for k (0 to 1000) produced doubtful areas of accuracy. Since the amplifier outputs were limited to a maximum of 100 volts the k values could not be generated directly, but were scaled down by a factor of 10. Thus at k values near 1, the errors might exceed the value of k itself. For this reason it was decided to use two programs, one for k = 10 to 1000, and one for k = 0 to 100. These two have a good region of overlap in which they should agree if both programs are correct. The scaling voltages should be mentioned and are shown as follows:

1 volt = 1 lb. mole/ft.^{3} for X and Xi

1 volt = 1 hr.$^{-1}$ for k

1 volt = 1°R. for T and T_c

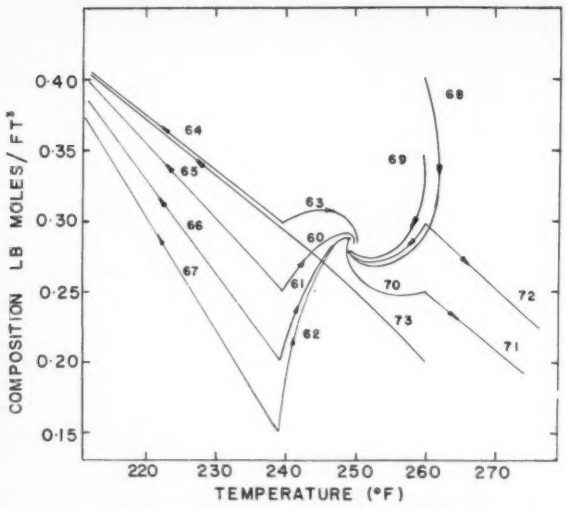

Figure 7 — Phase plane plot; proportional control on temperature.

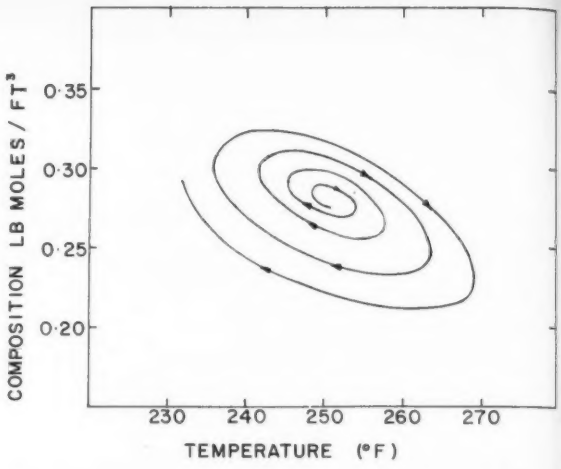

Figure 8 — Phase plane plot; proportional control on composition.

The final differential equations which were programmed for the computer are shown below.

$$25\frac{dX}{dt} = 4.5Xi - 4.5X - .25kX \quad \ldots\ldots\ldots\ldots (16)$$

$$.1\frac{dT}{dt} = .333kX + .018Ti - .018T - .00833\theta(t)T + .00833\theta(t)T_o \quad (17)$$

The analog program is presented in Figure 5. The three modes of control: proportional, integral, and rate were simulated on the computer and are presented in Figure 6. When integral or rate mode is added to the proportional controller, the lower circuits become additional inputs to amplifier A.

Computer Results

The phase plane plot of a first order irreversible system should indicate a maximum of two stable solutions and one unstable solution to the equations. These solutions can be determined exactly by trial and error from the original differential equations and are as follows:

	Temperature	Composition
stable	200.60°F.	0.465
unstable	250.91°F.	0.277
stable	307.38°F.	0.054

The three steady state solutions as indicated by the phase plane plot of the machine solution are tabulated below. These were used to evaluate the accuracy of the programs.

stable	203.5	0.453
unstable	251.5	0.280
stable	309.0	0.058

As a check of the root-locus diagrams by means of the analog computer, various values for the constants were assumed, and control was attempted near the unstable point ($X = 0.277$; $T = 250.9$°F.). Figure 7 shows the phase plane plot for the case in which the temperature of the outlet reactor stream was controlled and the rate of cooling water was manipulated by the output of a proportional controller. Lines 60 to 63, and 68 to 70 are with $K_p = 0.05$. The unstable point has been converted to a stable point by addition of proportional control. Lines 64 to 67 and 71 to 73 are for $K_p = 0.001$. This point is still an unstable point as was predicted by the root-locus plot with this value of K_p. The results of using the same proportional controller with composition as the controlled variable are shown in Figure 8. The system was started exactly at the unstable point ($X = 0.277$; $T = 250.91$°F.) and spiralled away as time increased.

One advantage of the root-locus method is apparent from these examples. It predicts the stability for all values of K_p, while the computer gives information only concerning one specific K_p.

For the case of proportional plus integral control with composition as the controlled variable, tests on the analog computer confirm the root-locus analysis of stability and indicate that the system is unstable for all values of K_p and K_I tested. Computer confirmation of the behavior of the system with all three modes of control was not attempted.

An attempt was made to find the optimum controller constants at the unstable point. By starting with $T = 245.9$°F. and $X = 0.277$ and measuring the time required for the system to reach steady state, the response of the system to a 5° step in temperature could be determined with any mode of control and at various values of controller constants. The results of this are presented in Table 1.

Obviously, a minimum change in ΔX, ΔT and Δt is desirable. Not all of these are a minimum for any given set of K values, however the table shows that some choices are distinctly better than others. II provides rapid response, but the final value of ΔX is quite large, while V combines both a short time with a smaller

TABLE 1

Control Mode				SS Time	$\Delta X_{min.}$	ΔX_{final}
	K_p	K_I	K_R			
I	0.03	—	—	12.0 min.	0.0225	0.0125
II	0.05	—	—	6.2 min.	0.0160	0.0125
III	0.07	—	—	10.4 min.	0.0125	0.0068
IV	0.05	0.02	—	10.8 min.	0.0112	0.0050
V	0.05	0.02	0.02	9.0 min.	0.0093	0.0050
VI	0.03	0.03	—	19.0 min.	0.0135	0.0060
VII	0.03	0.03	0.01	17.1 min.	0.0119	0.0070
VIII	0.03	0.01	0.01	12.7 min.	0.0155	0.0090

ΔX. The offset (ΔX) in all instances is less than 4%. If this deviation in composition can be tolerated, then the best of controller constants tried would be V.

Summary

After checking the accuracy of the analog computer program by means of a phase plane plot, the program was used to check the results of the root-locus analysis. All three modes of control were simulated on the analog computer, singly and combined. Both X and T were controlled and the stability of the system checked for various combinations of controller constants. Finally, optimization of the controller constants brought out the value of each mode of control. In all cases the linearized root-locus equations produced results that agreed very well with the nonlinear form of the differential equations solved on the computer.

Nomenclature

A = heat transfer, ft.^{2}
A' = frequency factor in Arrhenius Equation, sec.$^{-1}$
C_c = heat capacity of coolant, B.t.u./lb.$-$°R.
C_p = heat capacity of reactant mix, B.t.u./lb.$-$°R.
E = activation energy, B.t.u./lb. mole
F = heat transfer parameter, dimensionless
G = transfer function
ΔH = enthalpy change of reaction, B.t.u./lb. mole
k = reaction rate constant, sec.$^{-1}$
K_p, K_I, K_R = controller constants, dimensionally consistent
p = Laplace transform operator, sec.$^{-1}$
Q = feed rate, ft.^{3}/sec.
Q_c = coolant feed rate, ft.^{3}/sec.
R = gas constant, B.t.u./lb. mol.$-$°R.
t = time, sec.
T = reactor temperature, °R.
T_i = feed temperature, °R.
T_c = coolant temperature, °R.
ΔT_m = mean ΔT across heat exchanger, °R.
U = heat transfer coefficient, B.t.u./hr.$-$°F.$-$ft.^{2}
V = reactor volume, ft.^{3}
X = reactor composition, lb. mole/ft.^{3}
X_i = feed composition, lb. mole/ft.^{3}
θ = heat transfer function, dimensionless
ρ = reactant mix density, lb./ft.^{3}
ρ_c = coolant density, lb./ft.^{3}
subscript s = steady-state values
super $^-$ = Laplace transformed variables

References

(1) Van Heerden, C., Ind. Eng. Chem., **45,** 1242 (1953).
(2) Bilous, O., and Amundson, N. R., A.I.Ch.E. Journal, **1,** 513 (1955), and A.I.Ch.E. Journal, **2,** 117 (1956).
(3) Ellingsen, W. R., and Ceaglske, N. H., A.I.Ch.E. Journal, **5,** 30 (1959).
(4) Kermode, R. I., M.S. Thesis, Northwestern Univ. (1959).

★ ★ ★

Non-Filmwise Condensation of Binary Vapors of Miscible Liquids[1]

V. V. MIRKOVICH and R. W. MISSEN
Department of Chemical Engineering,
University of Toronto

When two substances condense from a mixture of their vapors to form one liquid phase, the condensation is expected to be filmwise[1]. While measuring heat transfer coefficients for such systems, however, we have encountered non-filmwise condensation. Since this does not appear to have been reported previously, we present some photographs to illustrate the phenomenon.

Total condensation of saturated vapor mixtures was studied at 750 mm. Hg on the outside, vertical surface of a cylindrical nickel plate, 40 mm. high and 150 mm. in diameter, contained in a glass apparatus. The systems studied were pentane-hexane and the three pairs formed from methyl alcohol, pentane and methylene dichloride. Non-filmwise condensation occurred at certain temperatures and compositions in two systems: pentane-methanol and pentane-methylene dichloride. It consisted of a transition from filmwise to dropwise condensation as the temperature difference between the vapor and the nickel surface (Δt_{vs}) decreased, with streaks occurring between these two extremes.

The behavior for pentane-methylene dichloride mixtures is shown in Figures 1 to 3 for a mole fraction of 0.14 of pentane (x_p). Condensation was filmwise at this composition for $\Delta t_{vs} > 15$°C. At $\Delta t_{vs} = 14.3$°C., the film began to streak in an irregular pattern at the top of the condensing surface, as shown in Figure 1. At $\Delta t_{vs} = 12.8$°C., the irregular pattern covered the surface (Figure 2). At lower values of Δt_{vs}, condensation became partly dropwise, and at 4.4°C. it was

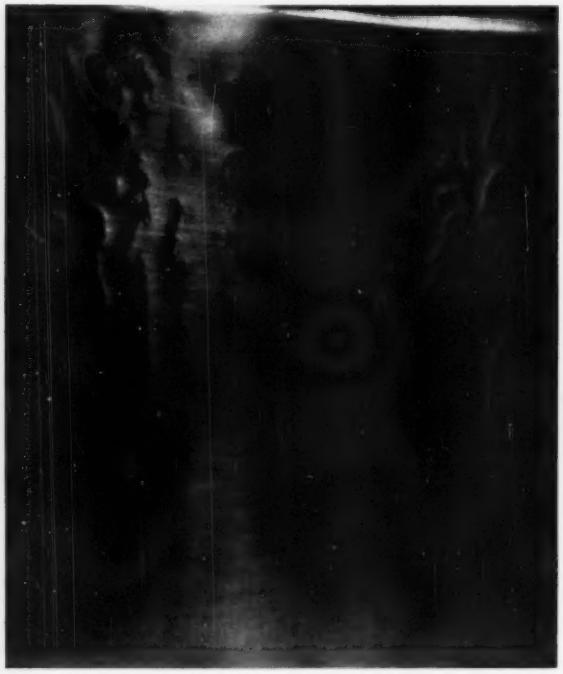

Figure 1—C_5H_{12} – CH_2Cl_2 System.
First formation of streaks; $\Delta t_{vs} = 14.3$°C.; $x_p = 0.14$.

Figure 2—C_5H_{12} – CH_2Cl_2 System.
Irregular, streaky pattern over entire surface
$\Delta t_{vs} = 12.8$°C.; $x_p = 0.14$.

Figure 3—C_5H_{12} — CH_2Cl_2 System.
Dropwise condensation; $\Delta t_{vs} = 4.4°C.$; $x_p = 0.14$.

Figure 4—C_5H_{12} — CH_3OH System.
Dropwise condensation; $\Delta t_{vs} = 30.2°C.$; $x_p = 0.19$.

almost entirely dropwise (Figure 3). Similar behavior occurred at a mole fraction of 0.26 for $\Delta t_{vs} < 9°C.$, but at mole fractions of 0.52, 0.65 and 0.82, the condensation was filmwise.

Non-filmwise behavior was also found for the pentane-methyl alcohol system at a mole fraction of 0.19 of pentane. The eventual dropwise condensation is shown in Figure 4 for $\Delta t_{vs} = 30.2°C.$ There was some indication of non-filmwise condensation at a mole fraction of 0.36, but at higher mole fractions it was entirely filmwise.

The heat transfer and liquid-vapor equilibrium characteristics of these systems will be reported in full later.

Acknowledgement

This work has been assisted by financial grants from the National Research Council and the Ontario Research Foundation.

Reference

(1) McAdams, W. H., Heat Transmission, McGraw-Hill, New York, 3rd ed., 1954, p. 352.

★ ★ ★

The Application of the Copper Oxide-Alumina Catalyst for Air Pollution Control[1]

S. SOURIRAJAN[2] and MAURO A. ACCOMAZZO[3]

The catalytic combustion of 1-hexene present in diluent nitrogen in the concentrations of 1170 p.p.m. and 3000 p.p.m. by excess oxygen, has been studied in the presence of the CuO-Al_2O_3 (1:1) catalyst in the temperature range 242° to 424°C. and gas space velocity in the range 4000-16,000 hr.$^{-1}$. The experimental data on the kinetics of the reaction were found to fit an empirical half-order law with respect to the 1-hexene concentration. The presence of water vapor in the reactants was found to have no effect on the efficiency of the catalyst at temperatures higher than 400°C. The above results were similar to those obtained for the catalytic oxidation of n-hexane studied earlier.

The possible use of the above copper oxide-alumina catalyst for the simultaneous removal of hydrocarbons and carbon monoxide present in the auto exhaust gases has been tested, making use of a 1955 six-cylinder Chevrolet engine run on leaded gasoline fuel. The hydrocarbon and carbon monoxide concentrations encountered in these studies varied in the range 170-16,000 p.p.m. and 1-7% respectively. It was found that the minimum initial temperature of the catalyst bed required for the complete removal of both hydrocarbons and carbon monoxide, simultaneously, was 226°C. under no load condition, 342°C. under an engine load of 2.5 h.p., 400°C. under an engine load of 5.1 h.p. or higher, and 236°C. under deceleration conditions. The catalyst showed no deterioration in performance even after 100 hours of continuous service in conjunction with the above auto exhaust gases.

The catalytic combustion of hydrocarbons and carbon monoxide present in low concentrations in the exhaust gases escaping into the atmosphere from various sources, is of particular interest as a possible method of air pollution control. The kinetics of the catalytic oxidation reactions of n-hexane and carbon monoxide have already been studied in the presence of the copper oxide-alumina (1:1) catalyst.[1,2] The object of this investigation is two-fold. The first one is to study the kinetics of the catalytic oxidation of 1-hexane present in low concentrations; this study is significant from the point of view of the mechanism of heterogeneous combustion of hydrocarbons because of the fact that the formation of olefins is a general phenomenon in the oxidation of paraffins. The other object of this study is to test the efficiency of the copper oxide-alumina (1:1) catalyst for the simultaneous removal of both hydrocarbons and carbon monoxide present in auto exhaust gases, by total oxidation; this part of the study is indeed one of practical significance since it is now recognized that the automobile remains the largest uncontrolled source of air polluting gases[3].

[1]*Manuscript received October 7, 1960; accepted December 7, 1960.*
[2]*Institute of Geophysics, University of California, Los Angeles, Calif.*
[3]*Department of Engineering, University of California, Los Angeles, Calif.*
Contribution from the Department of Engineering, University of California, Los Angeles, Calif.

Experimental Details

The apparatus used was similar to the one described earlier[1]. It consisted essentially of a gas sample tank containing 1-hexene in diluent nitrogen, a vycor glass preheater and reactor tube, 90 cm. long and 2 cm. diameter, enclosed in a furnace and a combustibles-analyzer. The gas flow rates were measured by appropriate flow meters which were initially calibrated. The lower section of the vycor tube, filled with porcelain beads, served as a preheater for the reactant gases. The temperature of the catalyst bed was measured by means of a thermocouple. The gases flowing through the preheater and reactor tube could be sampled both immediately before and after passing through the catalyst bed. The combustibles-analyzer used was that developed by Miller[4]. It consisted essentially of two cells constituting the two arms of a Wheatstone Bridge arrangement; the combustion of the gas sample material took place on the surface of the hot platinum wire in one of the cells, and the resistance change, resulting from the increase in temperature due to the combustion, measured the concentration of the combustibles in the gas mixture entering or leaving the catalyst bed. The instrument, coupled to an automatic recorder, was initially calibrated for different concentrations of 1-hexene, and the data on the extent of the catalytic oxidation of the hydrocarbon were obtained in terms of the total combustibles expressed in 1-hexene equivalents. The analyzer gave results reproducible within 1%. Though the above method of expressing the extent of catalytic oxidation of the hydrocarbon was not an exact one (except when the hydrocarbon was either totally oxidized or not oxidized at all), it was considered sufficiently indicative for the purpose of evaluating the performance of the catalyst.

1-Hexene concentrations of 1170 p.p.m. and 3000 p.p.m. in diluent nitrogen, premixed with 3-3.5 times the stoichiometric amount of oxygen needed for complete combustion were used in these experiments. The temperature of the catalyst bed was varied from 242° to 424°C. and the gas space velocities (volume of gas at 25°C./hour/volume of catalyst) ranged from 4000-16,000 hr.$^{-1}$. During the reaction, the furnace controls were set so that the temperature gradient across the different parts of the catalyst bed was less than 10°C. Under steady state conditions, the highest temperature of the catalyst bed (taken as the reaction

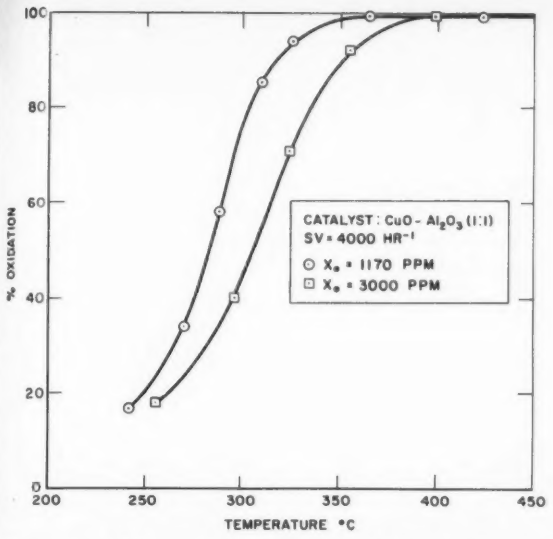

Figure 1 — Effect of concentration and temperature on catalytic oxidation of 1-hexene.

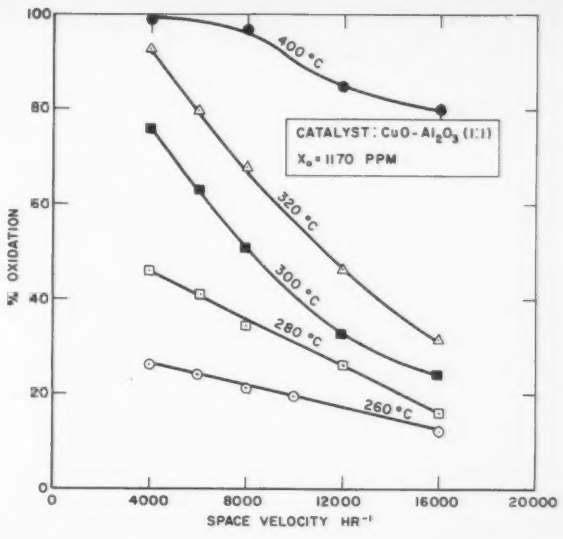

Figure 2 — Effect of space velocity and temperature on catalytic oxidation of 1-hexene.

temperature), the gas flow rate and the concentrations of the combustibles in terms of 1-hexene equivalents in the gases entering and leaving the catalyst bed were recorded, and the efficiency of the catalyst for the total oxidation of 1-hexene was evaluated.

The catalyst was prepared as follows. Copper hydroxide was precipitated on the alumina carrier from a hot dilute aqueous solution of copper nitrate by the addition of an excess of sodium hydroxide. The precipitate was then filtered and washed free of alkali. The wet solid mass was then extruded, dried and pelleted. The composition of the catalyst was CuO: Al_2O_3 = 1:1. The catalyst material was heated in the reactor at 450°C. for a period of 12 hours in a current of air before use in the experiments. The surface area of the catalyst, as determined by the B.E.T. method was 128 sq. m./gm., and its pore volume, as determined by the helium-mercury method, was 0.56 cu. cm./gm. The mean radius of the pores in the catalyst, as calculated from its known surface area and pore volume measurements assuming cylindrical pores, was 87°A. Twenty-five cubic centimeters of the catalyst material was used in all these experiments.

Experimental Results and Discussion

Efficiency of the Catalyst. The experimental results obtained on the combustion of 1-hexene present in diluent nitrogen, in the concentrations of 1170 p.p.m. and 3000 p.p.m. by excess oxygen in the presence of the copper oxide-alumina catalyst described above are given in Figures 1 and 2 which show the effect of temperature and gas space velocity, respectively, on the extent of oxidation.* The results showed (1) the percentage oxidation of 1-hexene at a given temperature was dependent on its initial concentration, the extent of oxidation increasing with the decrease in the concentration of the hydrocarbon in the feed, and (2) at 400°C., more than 90% of 1-hexene was removed by total oxidation at all gas space velocities up to 10,000 $hr.^{-1}$. The above results are similar to those obtained for the oxidation of n-hexane studied earlier[1]. It is, however, significant to note that the combustion of 1-hexene was somewhat less readily achieved than that of n-hexane under otherwise identical experimental conditions.

*The experimental data on the catalytic combustion of 1-hexene are given in Tables 2 and 3 in the Appendix of this paper, which has been deposited as Document No. 6537 with the ADI Auxiliary Publications Project, Photoduplication Service, Library of Congress, Washington 25, D.C. A copy may be obtained by citing the Document No. and by remitting $5.00 for photoprints, or $2.25 for 35 mm. microfilm. Advance payment is required. Make cheques or money orders payable to: Chief, Photoduplication Service, Library of Congress.

Kinetics of 1-Hexene Oxidation. An empirical rate equation for the catalytic combustion of 1-hexene by excess air can be derived as follows to fit the experimental data reported above. For flow reactors,

$$\frac{V_R}{F} = \int_0^Z \frac{dZ}{r} \quad \ldots\ldots(1)$$

$$r = -\frac{dC}{d\theta} = kC^n C_{o_2}^m \quad \ldots\ldots(2)$$

When the oxygen concentration is much in excess,

$$kC_{o_2}^m \approx k' = f(T) \quad \ldots\ldots(3)$$

$$\therefore \frac{V_R}{F} = \int_0^Z \frac{dZ}{k'C^n} \quad \ldots\ldots(4)$$

At any point in the reactor where a conversion of fraction Z has taken place, the concentration of 1-hexene can be written as:

$$C = C_0(1 - Z) \quad \ldots\ldots(5)$$

Hence, at constant temperature,

$$\frac{V_R}{F} = \frac{1}{k'C_0^n} \int_0^Z \frac{dZ}{(1 - Z)^n} \quad \ldots\ldots(6)$$

For $n \neq 1$,

$$\frac{V_R}{F} = \frac{1}{k'C_0^n} \left[\frac{1 - (1 - Z)^{1-n}}{1 - n}\right] \quad \ldots\ldots(7)$$

$$X_0 = C_0 V_m 10^6 = C_0 \frac{RT}{P} 10^6 \quad \ldots\ldots(8)$$

$$F = QC_0 \frac{T}{T_1} \quad \ldots\ldots(9)$$

$$\therefore \frac{V_R}{Q} = \left[\frac{X_0 P 10^{-6}}{R}\right]^{1-n} \frac{T^n}{T_1 k'(1 - n)} [1 - (1 - Z)^{1-n}] \quad \ldots\ldots(10)$$

The relative positions of the graphs shown in Figure 1 on the effect of concentration and temperature on the catalytic oxidation of 1-hexene, indicates that n is less than one. For $n = 1/2$,

$$\frac{V_R}{Q} = \left[\frac{X_0 P 10^{-6}}{R}\right]^{1/2} \frac{2T^{1/2}}{T_1 k'} [1 - (1 - Z)^{1/2}] \quad \ldots\ldots(11)$$

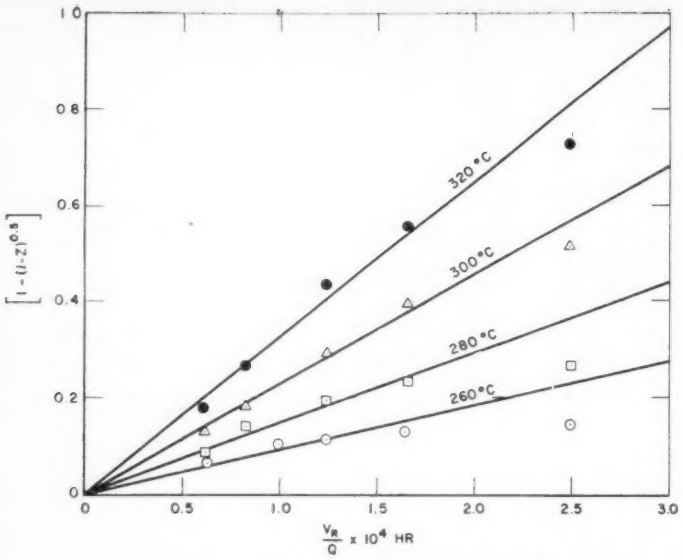

Figure 3—Apparent half-order plot for the catalytic oxidation of 1-hexene present in low concentrations.

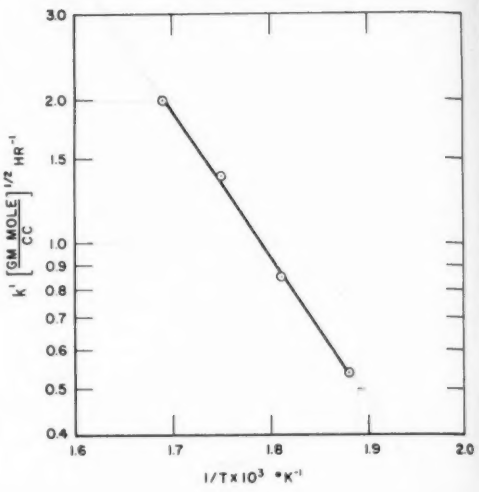

Figure 4—Variation of reaction-rate constant with temperature.

At constant temperature, a plot of V_R/Q vs. $[1-(1-Z)^{1/2}]$ should be a straight line passing through the origin with slope = $\frac{T_k k' R^{1/2}\ 10^3}{2\ (X_0 P T)^{1/2}}$. Such plots are shown in Figure 3, and the graphs obtained are seen to be nearly straight lines except for the low space velocity runs in which pore diffusion appears to have a controlling influence on the reaction rate.

Assuming $k' = f(T) = Ae^{-E/RT}$ .....(12)

the plot of $ln\ k'$ vs. $1/T$ should be a straight line with slope = $-E/R$. Such a plot is shown in Figure 4 which is also seen to be nearly a straight line giving an apparent activation energy of 14 k cal./g. mole with A = $3.0 \times 10^5 \left[\frac{\text{g. mole}}{\text{cc.}}\right]^{1/2}$ hr.$^{-1}$.

Thus, $r = Ae^{-E/RT}\ C^{1/2}$ .....(13)

appears to be a satisfactory empirical rate equation for the catalytic combustion of low concentrations of 1-hexene by excess oxygen.

Mechanism of the Heterogeneous Combustion of Hydrocarbons. It is generally recognized that the formation, propagation and termination of free radical chains are involved both in the pyrolysis and the oxidation of higher hydrocarbons. Though the combustion of the paraffins and that of olefins show the general characteristics of a degenerately branching chain, the ready oxidizability of the paraffins compared to that of the corresponding olefins is attributed to the formation of the relatively stable allyl radicals[5,6]. Based on a chain reaction mechanism involving the generation of free radicals suitable as chain carriers, Bolland deduced a relation showing that the rate of the oxidation reaction was proportional to the square root of the rate of formation of chain carriers[7]. The experimental data on the catalytic combustion of n-hexane reported earlier[1], and of 1-hexene reported in this paper appear to be consistent with the mechanism of the combustion process stated above.

Experiments with Water Vapor in Reactants. The presence of water vapor is known to reduce the activity of the catalyst in the oxidation of carbon monoxide at lower temperatures[2]; and water is also known to be a poison for the destruction of hydrogen atoms on a glass surface[8]. Hence, it was of interest to study the effect of water vapor on the efficiency of the above $CuO - Al_2O_3$ catalyst for the oxidation of 1-hexene. With 1170 p.p.m. of 1-hexene in diluent nitrogen saturated with water vapor at the laboratory temperature (i.e., with water vapor in the feed = 3.0%), experiments were carried out on the effect of temperature on the extent of oxidation at a gas space velocity of 4000 hr.$^{-1}$ using 3-3.5 times excess oxygen. The results obtained are given in Figure 5. It was found that the presence of water vapor did retard the rate of reaction at lower temperatures, but it had no effect at temperatures higher than 400°C. when the hydrocarbon was completely removed by total oxidation.

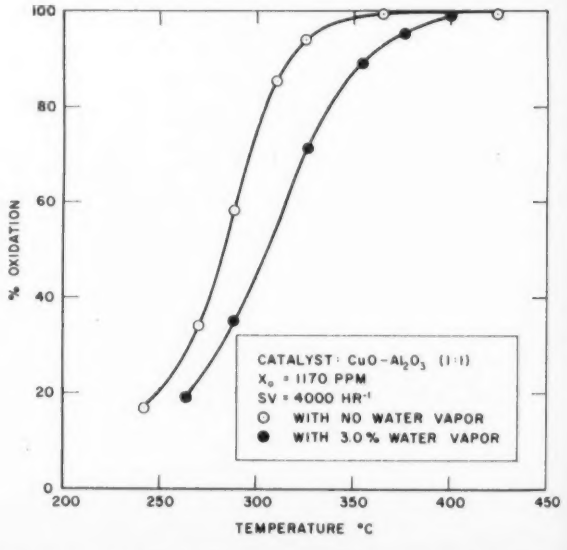

Figure 5—Effect of water vapor and temperature on catalytic oxidation of 1-hexene.

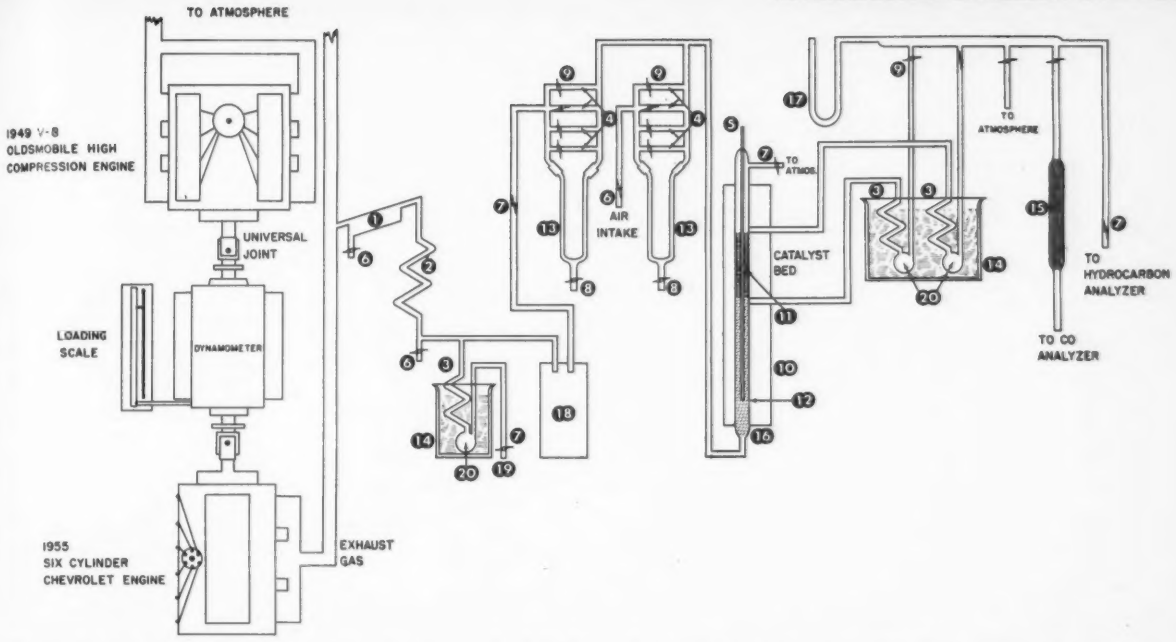

Figure 6—Catalyst testing system for the removal of hydro-carbons and carbon monoxide from auto exhaust gases. APPARATUS: (1) coarse particle trap; (2) air cooled tube; (3) water cooled tube; (4) capillary tubes (5) thermocouple tube; (6) brass valves; (7) pinch clamp; (8) glass stopcocks; (9) Teflon stopcocks; (10) furnace; (11) catalyst; (12) ceramic beads; (13) flow meters; (14) water bath; (15) calcium chloride; (16) Vycor pre-heater and reactor tube; (17) water monometer; (18) 10,000 cc. surge tank; (19) to Orsat analyzer or air-fuel analyzer; (20) water traps.

Experiments with Auto Exhaust Gases. The copper oxide-alumina (1:1) catalyst has thus been shown to be efficient for the total oxidation of n-hexane, 1-hexene and carbon monoxide present in low concentrations[1,2]. The object of this part of the experimental program was to test the practical possibility of the application of the above catalyst for the simultaneous removal of both hydrocarbons and carbon monoxide present in auto exhaust gases. For this purpose, a 1955 six-cylinder Chevrolet engine coupled to an eddy current dynamometer was used. Deceleration runs were simulated by driving the above engine with a 1949 Oldsmobile V-8 engine coupled to the dynamometer. The engine was run on leaded gasoline fuel. The performance of the catalyst was evaluated in terms of the percentage removal of both hydrocarbons and carbon monoxide from the auto exhaust gases when passed through the catalyst bed under different operating conditions. A schematic drawing of the catalyst testing system used in these experiments is shown in Figure 6.

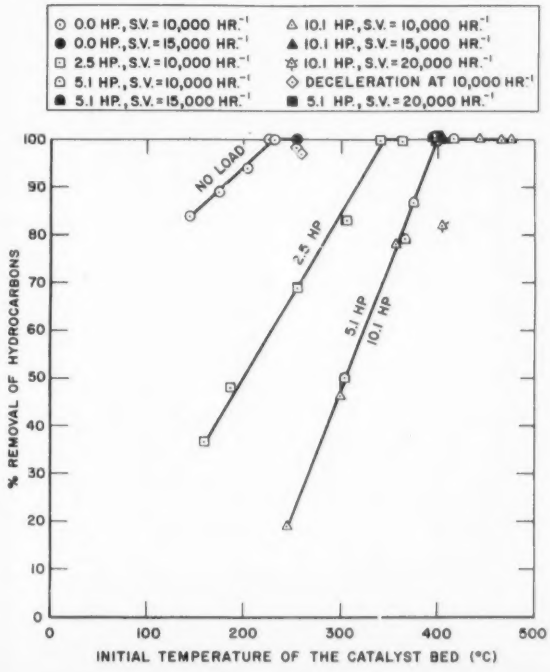

Figure 7—Efficiency of the copper oxide-alumina catalyst for the removal of hydrocarbons present in auto exhaust gases.

The air/fuel ratio in the engine was determined by a Du Mont type 932 exhaust gas analyzer. Part of the exhaust gases from the engine was cooled to room temperature, mixed with 2 to 3 times the air needed for complete combustion and then passed through the hot catalyst bed at a gas space velocity of 10,000 hr.$^{-1}$ at 25°C. The amount of carbon monoxide present in the engine exhaust gases was determined by orsat analysis, and that present in the gases leaving the catalyst bed was determined by means of a Mines Safety Appliance carbon monoxide indicator (using hopcalite catalyst) capable of analyzing CO within 50 p.p.m. A Beckman Model 15A infrared analyzer was used for hydrocarbon analysis and the results were obtained in terms of n-hexane equivalents. The performance of the catalyst was tested under different engine load conditions and initial temperatures of the catalyst bed. As soon as the air-mixed exhaust gases from the engine entered the reactor, the temperature of the catalyst bed increased rapidly due to the reaction and attained steady state conditions within 15 minutes; under the steady state operating conditions, the concentrations of hydrocarbons and carbon monoxide in the engine exhaust gases and in the gases entering and leaving the catalyst bed, together with the maximum temperature of the catalyst bed,

TABLE 1

DATA ON THE USE OF THE CuO–Al_2O_3 (1:1) CATALYST FOR THE SIMULTANEOUS REMOVAL OF HYDROCARBONS AND CARBON MONOXIDE PRESENT IN AUTO ENGINE EXHAUST GASES.

	Engine Conditions						Reactor Conditions and Catalyst Performance							
Expt. No.	RPM	Cylinder vacuum in. of Hg	H.P.	Air/fuel ratio	Hydrocarbon in exhaust p.p.m.	Carbon monoxide in exhaust %	Hydrocarbon in entering gas p.p.m.	Carbon monoxide in entering gas p.p.m.	SV $hr.^{-1}$	Stoichiometric air factor	Initial temperature of catalyst bed °C.	Maximum temperature of catalyst bed °C.	Extent removal of hydrocarbons %	Extent removal of carbon monoxide %
1	500	20.0	0.0	11.2	580	5.0	390	38,000	10,000	2.07	230	708	100	100
2	500	19.8	0.0	11.1	650	5.0	440	38,000	10,000	2.03	174	708	89	100
3	500	20.0	0.0	11.1	720	7.0	500	47,500	10,000	1.86	145	518	84	100
4*	500	18.5	0.0	10.7	1300	5.0	810	34,000	10,000	2.18	204	458	94	100
5	500	19.0	0.0	10.7	1300	5.0	730	36,000	10,000	2.08	254	770	100	100
6*	500	19.0	0.0	10.7	1300	5.0	880	36,000	15,000	2.09	226	878	100	100
7	1000	19.5	2.5	13.3	400	4.0	240	30,400	10,000	2.78	160	380	37	99
8	1000	19.7	2.5	13.4	420	4.0	240	30,400	10,000	2.63	188	426	46	100
9	1000	19.7	2.5	12.9	420	4.0	240	30,400	10,000	2.63	308	510	83	100
10*	1000	19.8	2.5	13.3	440	3.6	260	28,800	10,000	2.27	342	536	100	100
11	1000	18.5	2.5	13.2	620	4.0	420	30,400	10,000	2.45	254	466	69	99
12	1000	19.8	2.5	12.6	530	4.0	330	30,400	10,000	2.53	364	622	100	100
13	1350	18.5	5.1	14.1	240	2.0	190	16,800	10,000	3.10	360	476	79	100
14	1350	18.7	5.1	14.1	320	2.0	210	16,800	10,000	2.92	416	494	100	100
15*	1350	18.4	5.1	13.8	360	2.0	250	16,800	10,000	2.84	398	484	100	100
16	1350	18.2	5.1	13.9	340	2.0	250	16,800	10,000	3.47	374	466	86	100
17	1350	18.2	5.1	13.6	370	2.0	240	16,800	10,000	2.82	304	434	50	100
18*	1350	18.0	5.1	13.3	350	3.0	220	24,000	15,000	2.55	400	562	100	100
19*	1350	18.0	5.1	13.3	360	2.0	220	16,800	20,000	2.86	400	540	100	100
20	1550	16.5	10.1	14.4	240	2.0	160	17,000	10,000	3.00	406	496	100	100
21	1550	16.5	10.1	14.4	210	2.0	160	17,000	10,000	3.07	466	530	100	100
22	1600	17.0	10.1	14.3	190	1.2	130	11,000	10,000	2.56	398	442	100	100
23	1550	16.2	10.1	14.3	230	1.0	130	9,000	10,000	3.12	358	470	78	100
24	1550	16.2	10.1	14.3	230	1.0	140	9,000	10,000	3.12	408	490	100	100
25	1550	17.2	10.1	14.3	170	1.0	130	9,550	10,000	1.39	446	448	100	100
26	1550	17.0	10.1	14.5	170	1.0	130	9,550	10,000	1.39	478	484	100	100
27	1550	15.8	10.1	14.3	260	1.0	210	9,000	10,000	2.97	248	360	19	100
28*	1550	15.5	10.1	14.5	270	1.0	160	9,500	15,000	2.71	400	480	100	100
29	1550	15.5	10.1	14.4	270	1.0	170	9,200	20,000	2.29	404	498	82	100
30*	1550	15.5	10.1	14.4	260	1.0	160	9,000	10,000	2.91	404	498	100	100
31	1550	16.2	10.1	14.4	220	1.0	140	9,000	10,000	3.12	302	432	46	99
32*	1400	24.5	DEC	11.7	16000	4.0	4800	12,800	10,000	2.48	252	822	99	100
33	850	24.0	DEC	11.3	11000	5.5	2900	17,500	10,000	3.21	258	828	97	100
34*	850	24.2	DEC	11.4	11000	5.5	2900	17,500	10,000	3.21	236	740	99	100

*This experiment was repeated after the 100 hour test period; the results obtained were identical with those reported herein.

were determined. The experimental results obtained are given in Table 1.

In the above experiments, the concentrations of carbon monoxide in the engine exhaust gases varied in the ranges 5-7%, 3.6-4%, 2-3%, 1-2% and 4-5.5% under the engine load conditions of 0 h.p., 2.5 h.p., 5.1 h.p., 10.1 h.p. and deceleration respectively; the corresponding hydrocarbon concentrations varied in the ranges 580-1300 p.p.m., 400-620 p.p.m., 240-370 p.p.m., 170-270 p.p.m. and 11,000-16,000 p.p.m. under the respective engine load conditions stated above; and, the initial temperature of the catalyst bed was varied from 145° to 478°C. At all conditions of engine operation tested above, it was found that carbon monoxide in the exhaust gas was completely removed by oxidation. The extent of removal of hydrocarbons from the exhaust gases was found to depend on the initial temperature of the catalyst bed and the engine load condition. The experimental data obtained on the extent of removal of hydrocarbons are shown in Figure 7. It was found that the minimum initial temperature of the catalyst bed required for the complete removal of both hydrocarbons and carbon monoxide simultaneously by total oxidation was 226°C. under no load condition, 342°C. under an engine load of 2.5 h.p., 400°C. under an engine load of 5.1 h.p. or higher, and 236°C. under deceleration conditions.

In order to test the continued efficiency of the catalyst under service conditions, the engine was run on leaded gasoline fuel for 50 hours under 2.5 h.p. load, and for another 50 hours under 5.1 h.p. load, and part of the exhaust gases from the engine was led through the catalyst bed at a gas space velocity of 10,000 $hr.^{-1}$ at 25°C. throughout this entire period of 100 hours. The analysis of the gases leaving the catalyst bed was carried out every eight hours, and the results showed the complete removal of hydrocarbons and carbon monoxide from the exhaust gases throughout the above test period. Again, experiment numbers 4, 6, 10, 15, 18, 19, 28, 30, 32 and 34 were repeated, and the results obtained were identical with those found before the above 100-hour test period.

Conclusion

Thus, the copper oxide-alumina (1:1) catalyst developed in this program of investigations has been found to be efficient for the continuous and simultaneous removal of both hydrocarbons and carbon monoxide present in auto exhaust gases. The catalyst showed no deterioration in performance even after 100 hours of continuous service in conjunction with exhaust gases from an auto engine run on leaded gasoline fuel. It is realized that a successful 100 hour run does not constitute a life test on the catalyst, but it does indicate the potential applicability of the catalyst in air pollution control devices. The engineering design of the suitable converter for any particular practical application of the catalyst should naturally take into account the heat liberated during oxidation. Instantaneous catalyst temperatures of the order of 900°C. have been encountered in this work with no deleterious effect on the subsequent effectiveness of the cat-

alyst. It is considered that, by proper choice of the converter design, the heat liberated during the reaction can be advantageously used to maintain the full effectiveness of the catalyst under all conditions of engine operation encountered in normal practice.

In conclusion, it may be stated that aside from the successful experiments with the auto exhaust gases reported above, the copper oxide-alumina catalyst developed in this work has possible application in any air pollution control device concerned with the removal of hydrocarbons and/or carbon monoxide present in low concentrations, by oxidation. For every particular practical application, one would certainly expect to be able to improve the physico-chemical nature of the above catalyst by a suitable modification of the method of its preparation and also by the inclusion of appropriate carriers, promoters and poison resistants in the catalyst matrix.

Acknowledgements

This investigation forms part of the catalysis studies in the air pollution research program being supported by the State of California. The authors are grateful to L. M. K. Boelter, W. C. Hurty and J. M. English for their continued support and encouragement to this work. Our thanks are due to David Cahn for his valuable assistance in this project and to Delmar J. Albright who fabricated the glass apparatus.

Nomenclature

A = constant
C = concentration of 1-hexene at any time θ, in mole/cc.
C_0 = concentration of 1-hexene in the gas entering the catalyst bed in mole/cc.
C_{o_2} = concentration of oxygen at any time θ, in mole/cc.
DEC = deceleration engine condition
E = apparent activation energy in cal./g. mole
F = 1-hexene feed rate, in mole/hr.
H.P. = engine load in horse power
k = constant
k' = constant
m = order of reaction with respect to oxygen
n = order of reaction with respect to 1-hexene
P = total pressure (1 atmosphere)
p.p.m. = parts per million
Q = gas flow rate at laboratory temperature in liters/hour
r = reaction rate in mole/hr. cc.
R = universal gas constant cal./g. mole °K.
RPM = engine revolutions per minute
S.V. = space velocity, $hr.^{-1}$ at 25°C.
T = temperature in °K.
T_l = laboratory temperature in °K.
V_m = molar volume
V_R = volume of catalyst bed
X_0 = concentration of 1-hexene in the gas entering the catalyst bed in p.p.m.
Z = fraction oxidation of 1-hexene

References

(1) Sourirajan, S., Accomazzo, M. A., and Ken Nobe. Proc. Congr. Catalysis, 2nd, Paris, Paper 130 (1960).
(2) Sourirajan, S. and Accomazzo, M. A., Can. J. Chem., **38,** 1990 (1960).
(3) Faith, W. L., Chem. Eng. Progr., **52,** 342 (1956).
(4) Miller, J., "The Measurement of Combustibles by a Hot Wire Method", M.S. Thesis, Department of Engineering, Univ. of Calif., Los Angeles (1958).
(5) Von Elbe, G., Fifth Symposium (International) on Combustion, pp. 79-85. Reinhold Publ. Corp., New York (1955).
(6) Bawn, C. E. H. and G. Skirrow, *ibid.*, pp. 521-529.
(7) Bolland, J. L., Quart. Rev., **3,** 1 (1949).
(8) Steiner, W., Trans. Faraday Soc., **31,** 962 (1935).

★ ★ ★

Spherical Agglomeration of Solids in Liquid Suspension[1]

J. R. FARNAND[2], H. M. SMITH[3] and I. E. PUDDINGTON[2]

The process of spherical agglomeration provides a method for making rapid and efficient separations of solids from liquid suspensions. Because preferential wetting of the solid surface by a second liquid, which acts as a bridging agent between the particles, is a basic requirement of the operation, a novel method for the separation of multi-component solids becomes available. The procedure is also useful in the breaking of emulsions through the addition of a finely divided solid, the surface of which is repellent to the continuous phase and wetted by the emulsified phase. The process operates equally well in aqueous or in organic media. A number of illustrative examples are given.

The rapid and clean separation of finely divided solids from liquids in which they are suspended is a frequent industrial requirement. Except where the products are particularly valuable, gravity settling is the most practical procedure. Since the rate of fall of a solid particle through a liquid medium is approximately proportional to the square of the particle diameter, flocculating agents are commonly added to increase the rate of sedimentation. This procedure is a compromise because the interstitial volume of the settled material is increased, often by as much as 100%, owing to the structure of the flocs and, at the same time, the effective density difference between the solid and liquid is reduced. Hence, completeness of segregation is sacrificed to achieve a more rapid operation. The desirability of producing densified flocs is obvious and it will be shown that in many instances this is possible through a combined chemical and mechanical treatment of the suspension. This operation leaves the flocculated solid in the form of small, dense spheres which settle very rapidly to a volume substantially less than that found at equilibrium in the unflocculated material. It will be demonstrated that the procedure is also applicable to the selective separation and recovery of one or more of the constituents of a multi-component suspension.

The formation of spherical aggregates of 0.5 — 1.0 mm. in diameter was reported by Stock[(1)] when dried barium sulphate was agitated with dry benzene. Subsequently it has been shown[(2)] that spheres can be formed from barium sulphate suspended in a number of organic liquids but only in the presence of a second liquid such as water. Apparently the second liquid is selectively adsorbed on the surface of the solid thereby partially displacing the suspension medium and, when two or more of the suspended particles collide, adhesion results owing to the formation of liquid bridges between the particles. Although the adhesive forces depend initially on the free energy at the interface of the adsorbed liquid and the suspending medium, some recrystallization may eventually occur between the points of contact of the solid particles to produce a stronger bond, particularly if the adsorbed liquid possesses some solvent power for the surfaces with which it is in contact. Random collisions obviously will produce a voluminous floc. However, if sufficient of the second liquid component is available to form multiple junctions, provided appropriate physical contact is made between the adjacent particles, suitable mechanical action will produce compact spheres from which much of the original suspending liquid has been ejected and much of the original adsorbed solvent displaced. The process is somewhat similar to the conventional granulation of solids where water provides the initial interparticle bond. In the present case, however, the whole process takes place in a liquid medium instead of in air. If the ultimate particles are considered as uniform diameter spheres, it will be apparent that the number of junctions associated with an individual particle will vary from a minimum of about 2 if the flocs form chain structures only to a maximum of 12 within the body of an hexagonally packed structure. It is therefore not surprising that a rather well-defined minimum quantity of bridging liquid is required to produce the dense spheres. Smaller amounts form only voluminous flocs, while quantities in excess of the minimum requirement give spheres of greater diameter. Eventually, if too much bridging liquid is added, the large spheres become soft and tend to smear and the wetted solid is essentially "extracted" from the suspension by the second liquid phase. Spheres of a centimeter or more in diameter are not uncommon and these are sufficiently strong to withstand ordinary manipulation. The increased number of inter-particle junctions in the larger spheres approximately accounts for the increased percentage of bridging liquid required for their formation. Settling of these larger spheres is virtually instantaneous. It will be apparent that the amount of bridging liquid required for the densified flocculation will depend on the geometry of the particles. Flat surfaces in contact require very little to produce a very strong adhesive bond while cylindrical and spherical surfaces require considerably more. The maximum requirement will probably occur when the ultimate particles are flexible fibres or porous bodies. Interstitial volume in the flocs, much of which will be filled eventually by the bridging liquid will also vary considerably. Some appreciation of this variation can be obtained by considering the packing characteristics of uniform size solid bodies of various shapes. Actually the volume percentage of bridging liquid based on the solid recovered required for spherical agglomeration to take place

[1]*Manuscript received May 14, 1960; accepted December 12, 1960.*
[2]*Division of Applied Chemistry, National Research Council, Ottawa, Ont.*
[3]*N.R.C. Postdoctorate Fellow, 1957-59, National Research Council, Ottawa, Ont.*
Contribution from the Division of Applied Chemistry, National Research Council, Ottawa, Ont. Issued as N.R.C. No. 6211.

under the experimental conditions used when perhaps 20 different solids were investigated varied from about 1% for barium sulphate suspended in benzene to nearly 200% for a highly solvated solid suspended in water.

Since preferential wetting of a solid surface by a second liquid phase is a critical feature in the formation of interparticle bonds, application of the principle would normally be limited by the ability of available liquids that are immiscible with or sparingly soluble in the suspending medium to displace it from the surface of the suspended solid. A stable suspension implies considerable interaction between disperse phase and dispersion medium and the wetting requirement can therefore be a serious limitation indeed. However, the scope of the procedure becomes virtually unlimited if the wetting properties of the solid phase can be changed appropriately through the selective adsorption of suitable reagents. Thus it has been possible to desolvate semi-lyophilic materials in the presence of the solvating liquid and selectively to granulate one or more constituents from a multiple solid component suspension by altering the normal surface properties of the solids involved. Although they are by no means restricting, the following experiments are recorded to demonstrate the scope of the process on a laboratory scale and to suggest its possibilities for industrial use. No particular attempt was made to use minimal quantities of reagents. These are undoubtedly related to the type and degree of agitation used to distribute the immiscible liquid as well as the surface area of the solid involved and the mutual solubility of the various ingredients of the systems. Mainly because of its convenience, horizontal, reciprocal shaking of the entire system was used in most of the work. The horizontal displacement of the shaker was 6 cm. and it was operated at 4 cycles per second. Simple rolling or tumbling in a cylindrical container, following high shear dispersal of the bridging liquid in a waring blendor or its equivalent, generally produced larger spheres probably owing to the low shear stresses imparted by this form of agitation.

Experimental

Coagulation of a Single Solid Component Suspension

Although the previous work was confined to the spherical agglomeration of barium sulphate in hydrophobic organic liquids, it is not difficult to extend the process to other solids suspended in organic liquids. It requires only that the surface of the solid be rendered repellent to the liquid suspending medium and attractive to the additive, if it is not already in that condition. For suspensions in many organic liquids, water or aqueous solutions are the most convenient coagulants and a number of solids such as silica, calcium carbonate, barium sulphate and the like, the surfaces of which are naturally hydrophilic, are readily coagulated into spheres with no further conditioning.

If, however, graphite, carbon black or other solids which have hydrophobic surfaces are suspended in liquids such as Varsol or toluene, water alone does not preferentially wet the solid surface and conditioning is necessary. Coagulation results rapidly, however, if water containing tannic acid or chlorophyl is used as the coagulant. In a specific case a 10 weight percent suspension of finely divided graphite in varsol produced excellent spheres when the suspension was shaken with 5% of a 5% aqueous tannic acid solution.

If water is the suspending medium, a similar set of conditions prevails. In this case the most suitable bridging liquids will be organic compounds that are sparingly soluble in water. Typical examples include nitrobenzene, toluene, kerosene, fuel oil and chlorinated hydrocarbons. For agglomeration to occur with no conditioning, the surface of the solid must be hydrophobic. Table 1 records the behavior of a suspension of graphite in water which fulfils this condition. The flocculation characteristics and sedimentation volumes indicated are typical of all of the systems that have been studied. With successive small additions of nitrobenzene, the sedimentation volume of the graphite increases to a maximum that is followed by a pronounced decrease coincident with the onset of granulation.

TABLE 1

AGGLOMERATION RESULTS WITH WATER/GRAPHITE
1 gm. Acheson graphite powder Grade 38
10 ml. water

Added nitrobenzene gm.	Comparable sediment volume ml.	Agglomerating effect
0	3.5	Not flocced
0.03	5.5	Flocced graphite
0.09	6.5	
0.15	5.6	
0.21	5.6	
0.30	3.3	Flocced with some agglomerates apparent
0.45	2.4	
0.51	1.7	Spherical agglomerates formed
0.60	–	
0.66	3 spheres	
0.69	2 spheres	
0.75	1 sphere	
0.90	1 sphere	
1.05	1 sphere	

Following the initial granulation further quantities of bridging liquid increase the size of the spheres. With the small quantities used in the experiment, little observable change in the sedimentation volume takes place as fewer spheres with larger diameters form.

Aqueous suspensions of solids having hydrophilic surfaces are probably the most common type encountered in practice. Typical of these are many of the insoluble salts of the common metals. In this type of suspension surface conditioning is required before granulation of the solid constituent will take place. Conditioning consists essentially in causing a suitable heterpolar molecule to be physically or chemically adsorbed at the solid-liquid interface. The conditioner will usually have a balanced hydrophilic-hydrophobic molecular character and should be adsorbed with the hydrophobic portion of the molecule oriented outward thus allowing the solid to be wetted by the water insoluble liquid. Suitable conditioners may be selected frequently from a knowledge of the sorptive properties of the solid to be conditioned. Information of this kind is usually contained in standard text-books on surface chemistry and general rules of adsorption have been formulated. Usually strong adsorption occurs with compounds that form complexes with or that hydrogen bond to the surface atoms of the solid. Thus acids, or xanthates and their soluble salts, alcohols and amines that contain a sufficiently large hydrocarbon nucleus will be suitable for rendering the surfaces of many metals, and metal salts and their hydrates hydrophobic. Conditioning of metal surfaces particularly may be done step-wise, i.e., the surface atoms may be changed to make adsorption of the conditioner easier. Solids having hydroxylated surfaces such as silica, and carbohydrates can frequently be conditioned with organic amines to make them wettable by organic liquids in the presence of water. Sometimes improved results are obtained when mixtures of conditioning agents are used. This is especially true with naturally occurring products and this effect is possibly owing to the existence of different types of adsorption sites on the surface of the solid. Thus greater total adsorption is obtained from the wider variety of conditioners than could be obtained from a single species. Reverse considerations apply if it is desired to make a hydrophobic surface hydrophilic.

Virtually any water insoluble liquid is suitable for a bridging agent in an aqueous suspension. Low viscosity and slight solubility favor its easy distribution by agitation to the solid to be flocculated. Volatility favors its removal from the granulated

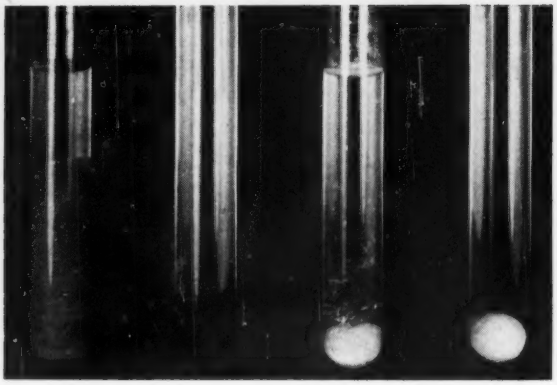

Figure 1—Portion of an aqueous suspension containing 10% each of graphite, zinc sulphide and calcium carbonate along with the separated constituents.

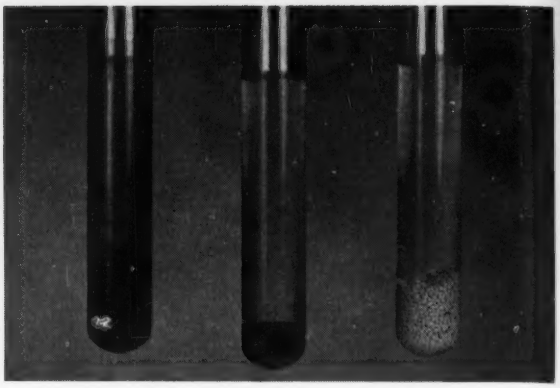

Figure 2—Portion of a Varsol suspension containing 10% each of graphite and powdered sulphur along with the separated components.

solid after its separation. Density greater than 1 reduces the possibility of the flocs floating to the surface of the liquid suspending medium. In a practical operation economic considerations would be of importance. Not infrequently the conditioner may also be used as the bridging liquid. This is true of a number of liquid fatty acids, amines, esters and alcohols. It is sometimes possible also for the bridging liquid to contain enough polar impurity to act as a conditioner. This sometimes occurs with partially oxidized liquid hydrocarbons. Care should be exercised to avoid excess of conditioner which may result in two layer adsorption leaving the solid surface hydrophilic[3]

While the amounts of conditioner and bridging agent required obviously will depend on a number of factors, the following examples are illustrative: a 10% suspension of precipitated calcium carbonate required the addition of 0.5% of oleic acid as a conditioner and 3% of nitrobenzene as a bridging agent to give on mechanical agitation spherical agglomerates of about 2 mm. diameter.

The solids in a slurry of hydrated lime prepared by slaking calcium carbide and containing 20% of calcium hydroxide were converted into quite uniform spheres of about a millimeter diameter by agitating the slurry for one minute with 15% of tall oil and 27% of domestic furnace oil based on the solids content. Eight percent of naphthenic acid and 22% of a low viscosity lubricating oil also behaved satisfactorily. Further agitation caused the spheres to grow, in some cases to balls about 1 inch in diameter. This phenomenon appeared to be caused by sufficient oil becoming available on the surface of the small spheres during further agitation to allow them to flocculate in turn to larger units. There was some indication that the agglomeration was stepwise and the larger units in turn eventually exuded sufficient oil to cause them to adhere strongly to a neighbour. Further agitation converted the dumbell, triangular or pyramidal shape depending on whether two, three or four spheres mutually adhered, to a new larger sphere. Since the large spheres require more oil than small sizes the growing processes eventually must stop unless further additions of bridging liquid are made. The fact that it occurrs in the first place probably indicates a considerably improved packing of the solid with continued agitation. Collapse of structure as more associated water is displaced from the flocculated solid surface may also contribute to the phenomenon. It is interesting to note that although a cake from the original slurry contained 40% of water after exhaustive suction filtration, only 15% of water remained in a large sphere immediately following its removal from the aqueous medium and allowing the water to drain from its surface.

The dewatering effect was even more apparent when the treatment was applied to a sample of natural peat. This sample in its native state contained only about 11% of solids and was obviously highly hydrated since little free water separated from the system. When the sample was agitated with octyl amine, tall oil and low viscosity hydrocarbon oil sufficient water exuded so that 60% of the original water content could be decanted. The final dry product which was a free flowing granulated solid had a particle diameter of 1-2 mm. It contained 33% solids and 16, 8 and 42% of the respective additives.

Separations of Multi-solid Component Suspensions

The application of the technique to separations of selected solids from multi solid component suspensions will depend on the ability of these particular solids to be conditioned selectively. It has been possible to do this readily with a number of prepared mixtures. For example, the graphite was selectively spheronized, virtually quantitatively, from an aqueous suspension containing 10% of graphite and 10% of precipitated chalk by agitating the mixture directly with 5% of nitrobenzene followed by a simple straining operation. The calcium carbonate could then be granulated by the procedure previously outlined, viz. by adding 0.5% of oleic acid, a further 5% of nitrobenzene and agitating a second time. Flame photometric analysis of the separated graphite showed that only 0.8% of calcium carbonate had been occluded in the separation, indicating remarkably good segregation of the constituents.

A three component system containing 10% of zinc sulphide in addition to graphite and calcium carbonate was separated by a similar procedure. For this suspension it was necessary to remove the zinc sulphide as the second step in the process. Otherwise, since oleic acid is adsorbed on this compound as well as on the calcium carbonate, co-conditioning would result from its use. The zinc sulphide surface was therefore selectively treated following the removal of the graphite by the addition of 2.5% of copper sulphate and 0.6% of secondary butyl xanthate based on the solid to be removed and adjusting the pH of the system to 7-8. It was then readily granulated and removed with the usual 5% addition of nitrobenzene and sufficient agitation to form spheres. Following this the calcium carbonate was removed as previously described. Figure 1 shows a portion of the original suspension and the separated constituents. In this instance the zinc sulphide and calcium carbonate have been collected into single balls.

Mixed solids suspended in organic liquids may be separated similarly. For example, from a suspension containing 10% of

graphite and 10% of powdered sulphur in Varsol, the graphite was easily granulated and removed using water as the bridging agent along with tannic acid as a conditioner. The sulphur was then agglomerated with a dilute solution of sodium hydroxide after it had been conditioned with Aerofloat 15 (an aryl dithio phosphoric acid preparation supplied by the American Cyanamid Co.). This separation is illustrated in Figure 2.

When the graphite of the previous example was substituted with silica flour, water alone selectively removed the silica and the sulphur could then be granulated by the above procedure.

It is apparent therefore that similar procedures may be used to separate the constituents of multicomponent solid suspensions in either aqueous or non-aqueous media.

Possible Applications

The experiments described in the preceding sections suggest a number of possible uses for the phenomenon of spherical agglomeration. For example, individual constituents of ore bodies might be concentrated and separated. Finely divided solids may be pelletized or granulated directly from suspension to give reduced packing volume and dust[4, 5]. Dispersible pigments might be prepared in granulated form where a portion of the future vehicle acts as the bridging agent. Metal powders are particularly susceptible to the treatment and a variety of catalysts may be prepared in a pelletized condition. Direct granulation of polymers with plasticizers to produce molding powders is also possible. Breaking of oil in water and water in oil emulsions may be accomplished by the addition of a suitable amount of a finely divided solid for which the emulsified liquid will act as a bridging agent. Very substantial improvement in the density of the sediment of a number of industrial suspensions is also possible where improved separation is desired.

While each suspension must be considered individually, the number of possible applications make the wet granulation process described an attractive procedure.

References

(1) Stock, D. I., Nature, **170,** 423 (1952).
(2) Smith, H. M., and Puddington, I. E., Can. J. Chem. **38,** 1911 (1960).
(3) Cuming, B. D., and Schulman, J. H., Australian J. Chem. **12,** 413 (1959).
(4) Rumf, H., Chem. Ing. Tech., **30,** 144 (1958); ibid, **30,** 146 (1958); ibid, **30,** 329 (1958).
(5) Peck, W. C., Chem. & Ind., 1674 (1958).

★ ★ ★